Coded-OFDM based PLC Channel for SISO and MIMO Smart Grid Systems

Shirui Zhang

Newcastle University

Newcastle upon Tyne, U.K.

A thesis submitted for the degree of

Doctor of Philosophy

September 2021

Abstract

The electricity demand is increasing due to the people's living standards is in the increase. Many countries began to shift their attention to Smart Grid (SG) systems instead of the traditional Gird. Communication technology in the SG has gradually become the most popular core issue in recent years.The PLC, which uses the existing power grid to propagation medium in grid communication system with the low cost and easy to set up, can replace the wireless SG communication system – like optical Fiber. In this thesis, new receiver technology in Single Input and Single Output (SISO) PLC system and new channel estimation method in the MIMO PLC system has been investigated to optimize the Bit Error-Rate (BER) performance of the PLC system with real-valued Orthogonal Frequency-Division Multiplexing (OFDM) input.

The novel contributions in this thesis are presented in three sections. First of all, we consider PLC for the SG in the presence of impulse noise modelled using the Symmetric α-stable (SαS) distribution. The proposed system utilizes coded OFDM with a real-valued output signal implemented using Hermitian symmetry of the modulated symbols in the frequency domain. In this part, we compare the BER performance of both Low-Density Parity-Check (LDPC) code and Polar code in the PLC channel to choose the better error correction method about PLC system. In the receiver part, we introduce a novel Maximal Ratio Combining (MRC) technique that exploits the Hermitian symmetry inherent in the real-valued OFDM symbol and compare its performance to the Zero Forcing (ZF) equalizer and Minimum Mean Square Error (MMSE) equalizer that are used to remove the effect of the Intersymbol interference (ISI). The presented simulation results included in the investigation demonstrate that in the PLC channel, the performance of the proposed MRC approach using LDPC codes outperforms the polar codes consis-

tently for Quadrature Amplitude Modulation (QAM) of orders M = 16 and M = 256.

Secondly, to investigate the channel estimation method utilised in the MIMO-PLC system, the comb pilot and the block pilot design methods are presented to estimate the ideal PLC channel and compared the BER performance of the two estimate pilot methods. As both pilot methods' performance is affected by Additive White Gaussian Noise (AWGN), an averaging process method is introduced to reduce the effects of AWGN and Mean Square Error (MSE) metric is used to assess the quality of the channel estimation. The value of the estimated PLC channel in each averaging time (frame) is different. Meanwhile, they are affected by the value of the previous averaging times. The BER performance in the estimated channel system becomes better after the averaging procession. Moreover, the performance of the averaging approach in pilot design method is affected by the different weight factors and the averaging times, In this part, the thesis focuses on analysing the averaging pilot design and provides the best choice of the value of the weight factors and the averaging times.

Finally, We investigate a 2×2 MIMO-OFDM system and propose a novel Nonzero-comb Pilot (NZCP) design for channel estimation that can cope with pilot contamination without the zero data insertion in adjacent channels. The BER performance vs. E_b/N_0 is demonstrated using numerical simulations for uncoded and coded systems using LDPC error correcting codes. The performance is compared with conventional comb and the block pilot methods through the frequency-selective multipath PLC channels and in the presence of AWGN. The numerical results presented demonstrate that the NZCP approach using averaging outperforms all the methods considered, e.g. for the uncoded system at a BER of 10^{-5} an improvement in E_b/N_0 of 3.6 and 4 dB against block and comb approaches, respectively. In contrast, in the coded system, the coding gain is of the order of 20 dB compared to the uncoded cases with the NZCP proposed method outperforming all the other considered approaches by at least 0.5 dB.

In conclusion, the work presented in this thesis provides the MRC detector to optimize the performance of the SISO-PLC system. Furthermore, it also introduces and compares different types of channel estimation pilot technology. The averaging approach and NZCP method have been utilized in MIMO-PLC to optimize the BER performance based on the traditional pilot design.

Acknowledgements

I would like to express my sincerest gratitude to my supervisor Dr. Charalampos Tsimenidis, for his advice and guidance during my four-year study in Newcastle university. His experience and enthusiasm inspired me to work on Equalizer investigation and PLC channel estimation, which is the focus of the thesis. I am very grateful to his brilliant ideas and many hours spent on me discussing my research and proofreading my papers. I would also like to thank my second supervisor Dr. Said Boussakta for his encouragement and valuable suggestions during my PhD. Furthermore, I would like to thank my panels Dr. Martin Jhonston and Dr. Paul Haigh for their suggestions on error correction coding and MIMO system. I have learnt a lot from him.

I would like to acknowledge my friends and colleagues Huan Cao, Yang Sun, Zeyu Fu, Safaa Nash'At Awny and Jummah Abdulwali for their help and friendship during the past four years in the UK.

I would like to thank medical workers and people who are actively resist COVID-19 to give me a healthy environment to finish my PhD research when the virus is raging around the world.

Finally, I would like to express my deepest love and gratitude to my family. I really thank my parents for their encouragement and support in innumerable ways throughout my study in the UK. No words are enough to express my appreciation for them. Especially, I am grateful to my wife, Xunyao Xu. She gives me a chance to be father. We have our own child in my final year of PhD. I am so excited about the brith of the baby. My wife and my baby inspired me to work very hard and finished the thesis possible.

Contents

List of Figures

List of Tables

Chapter 1

Introduction

1.1 Introduction

According to the international standard (IEEE1901), [4], which was adopted in 2010, Power-line Communication (PLC) uses the existing power grid as propagation medium and has become the most popular wired communication channel in the field of information transmission in Smart Grid (SG). The low cost characteristics due to utilizing existing infrastructure make every country pay more and more attention to PLC [5]. In recent years, the performance of PLC under different channel coding systems with varying noise channels has been investigated in the literature [6, 7]. However, the PLC channel coded system with real-valued Orthogonal Frequency-Division Multiplexing (OFDM) input signal over Symmetric α-stable (SαS) distribution noise channel has not been investigated yet. Besides, the proposed Maximum Ratio Combining (MRC) equalizer has been used to reduce the impact of the Inter-Symbol Interference (ISI) in the PLC system. Moreover, the channel estimation method has been optimized and utilized in the OFDM system and gave a better performance than the traditional channel estimation technology [8–11].

1.2 Motivation and Challenges

Nowadays, the SG system gradually shifted the investigation focus from wireless communication to PLC channel with existing wiring to reduce the cost of the communication equipment. With Multiple-Input Multiple-Output (MIMO)-OFDM and the new channel estimation method, the channel's capacity and the system's accu-

racy can be significantly optimized. The SαS distributions noise, which arises from Radio Frequency Interference (RFI) in laptops, personal computers, and background noise in power-line communications [12–15], will be utilized in the PLC channel system to investigate the impact of the impulsive noise on PLC. Meanwhile, the simulation will give a Bit Error-Rate (BER) performance contrast between Additive White Gaussian Noise (AWGN) and SαS noise channel system. More and more investigations about communication technologies are focused on the two principal error correction codes - Low-density parity-check (LDPC) and polar code in recent years. However, there is no prior research work about these error control coding methods used in the PLC channel with real-valued OFDM signal waveforms under the impulsive noise environment. In this thesis, the performance of these two types of coding methods in Single-Input and Single-Output (SISO) PLC systems will be investigated.

Moreover, channel estimation, which refers to methods that identify the communication Channel Impulse Response (CIR) and Channel Frequency Response (CFR), has been utilized in the MIMO-PLC channel system. There are many research works in the literature about the channel estimation methods, especially related to the comb pilot and the block pilot approaches. This thesis two novel pilot correlation methods are proposed to obtain more accurate estimated CFR and improve the BER performance of the standard pilot methods. These are, the averaging approach and the Nonzero Comb Pilot (NZCP) channel estimation methods.

1.3 Aim and Objectives

The thesis proposes an MRC equalizer to optimize the performance of the SISO-PLC with SαS noise and real-valued OFDM signal input. Moreover, the NZCP with the averaging method can give a better BER performance than other pilot methods. The objectives of this thesis are to investigate the BER performance of:

- Real-valued OFDM using the MRC equalizer in the SISO-PLC channel with SαS noise.
- LDPC and polar codes using different M-ary Quadrature Amplitude Modulation (QAM) in PLC channels.

- Comb and block pilot with the averaging method in the MIMO-PLC channel system.
- NZCP instead of the zero-comb pilot in the MIMO-PLC channel system.
- NZCP with the averaging method in the MIMO-PLC channel system.

1.4 Novel Contributions of the Thesis

The contributions of this thesis are focused on the proposed MRC equalizer over SISO-PLC with SαS noise channel and the optimizztion of channel estimation method over MIMO-PLC channel system. The novelty of the thesis is described as follows:

In Chapter 4, the uncoded SISO-PLC system with real-valued OFDM input signal under SαS distribution noise is derived. Moreover, two types of error correction methods - LDPC codes and polar codes have been utilized to avoid the impact of the impulsive noise. Furthermore, the novel MRC equalizer is derived in the receiver part and demonstrated a better BER performance than the Zero Forcing (ZF) and Minimum Mean Square Error (MMSE) equalizer. Finally, the contrast between LDPC and polar performance in different order QAM systems have been simulated.

In Chapter 5, the 2×2 MIMO-PLC, which is constructed by four SISO-PLC channels with different multipath and parameters, has been proposed. The channel estimation methods - the block pilot and the comb pilot, have been used in the MIMO-PLC system. To optimize the different types of pilot design, the novel averaging approach will be utilized to averaging the estimated CFR, narrowing the difference between estimated CFR and original CFR and improving the BER performance.

In Chapter 6, to reduce the number of transmitting pilots of the zero-comb pilot method, a new pilot design called NZCP has been proposed to instead of the zero-comb pilot approach and utilized in the MIMO-PLC channel. The novel technique can increase the channel transmission capacity and optimize the BER performance over estiamted MIMO-PLC system. Moreover, the averaging method has been combined with the NZCP approach for the further optimization of the estimated system. Finally, the NZCP method has been applied in the different order QAM system to show whether each QAM system's property has the same

optimization by using the averaging NZCP model or not.

1.5 Orgnization of the thesis

This thesis is orgnized as follow:

In Chapter 2, the literature survey of PLC channel is provided to overview past PLC research during these last decade. Moreover, the background and application cases of LDPC codes and polar codes are exhibited as well. Finally, the Hermitian Symmetry, which can construct the real-valued OFDM symbols, has been described.

In Chapter 3, the multipath PLC model and the MIMO-PLC model are presented in this chapter. In terms of the error correction method, the theoretical background of LDPC and polar codes are introduced. Furthermore, the generation and the parameter of the impulsive SαS distribution noise model are provided. In addition, the background of traditional channel estimation is presented, including the comb pilot and block pilot models over the SISO-PLC channel system.

In Chapter 4, the performance contrast between the AWGN channel and SαS distribution noise channel under uncoded SISO-PLC with real-valued OFDM input symbols is investigated. Besides, the LDPC and polar codes are utilized in the SISO-PLC to give a comparison to examine the performance of these two types of error correction codes. Furthermore, this thesis presented the MRC equalizer with higher performance than the ZF and MMSE equalizers modelled in the SISO-PLC system. At the end of this chapter, the MRC equalizer is utilized in the different order QAM simulations and both AWGN and SαS noise channel to demonstrate the properties of the MRC equalizer over these circumstances.

In Chapter 5, the performance of MIMO-PLC with the zero-comb pilot and the block pilot methods are derived. The averaging approach is utilized in the channel estimation system as well. With the different number of frames and the value of the weight factor, the BER performance by using the averaging approach has a dramatic difference. Hence, the various characteristics of averaging block pilot are derived and used in the 16-QAM model to give the BER performance contrast between different conditions. This proposed method has been utilized in the 16-QAM, 64-QAM, 256-QAM and 1024-QAM systems to investigate the performance of the averaging approach over different conditions of MIMO-PLC channel.

In Chapter 6, as the zero-comb pilot cannot perform well, the NZCP method

is proposed. Half of the pilots can be saved to transmit the information data with a better performance of the zero-comb pilot. With the averaging process, the estimated CFR of the NZCP is presented, and the BER performance is almost the same as that of the standard MIMO-PLC channel system.

In Chapter 7, the conclusion of this whole thesis has been provided. Furthermore, future research and optimized scheme are listed in this field as well.

1.6 Publications Related to the Thesis

1. **S. Zhang**, C. Tsimenidis, H. Cao, and S. Boussakta, "Coded OFDM in PLC Channels with SaS distribution Impulsive Noise using MRC detector," 2019 UK/ China Emerging Technologies (UCET), 2019.

2. **S. Zhang**, C. Tsimenidis, "Optimized Block/Comb Pilot Channel Estimation over MIMO-PLC System," IEEE Access.

Chapter 2

The literature survey of Coded-OFDM signal over PLC channel

2.1 Introduction

This chapter will focus on the survey of the main points of this thesis, such as the PLC channel, the utilized error correction codes, OFDM and the Hermitian symmetry. Initially, the PLC channel is introduced including definition, application and development. Furthermore, two principal popular error correction code methods - LDPC code and Polar code, which are used in the Fifth generation communication technology, are presented to optimize the BER performance in the PLC channel system. The construction and the brief historical evolution of each type of code are discussed in this chapter. Finally, the real-valued OFDM signal is discussed, which is created by Hermitian symmetry and has been utilized as the input signal in the PLC system.

2.2 Power line communication

Power line communication is a unique communication channel that uses high voltage (110 kV long transmission line), medium voltage (66 or33 kV sub-transmission line) or low voltage distribution line (380/220 V user line) as an information transmission medium to transmit voice or data [16]. Compared to other communication methods

such as coaxial, twisted-pair and fibre-optic cables, PLC has the characteristics of a fast transmission rate. The cost of the electric equipments is much lower than that of either wireless module or fibre cable. The PLC system's principle is to modulate the information data as the input signal, load the high-frequency signal into the electrical power line. The modulated signal is taken out through the filter at the receiving end and demodulated to get the original signal.

2.2.1 Development history of Power Line Communication

Power line communication technology appeared in the early 1920s. The earliest example of using a power line to transmit a signal is the power line telephone. Its application scope is to filter the electrical signal from the power line within the power supply line of the same transformer [4]. Even if many countries are committed to investigating the PLC system, PLC still cannot be applied on a large scale. Firstly, the distribution transformer has a blocking effect on the power carrier signal so that the power carrier signal can only be transmitted in a distribution transformer area. Secondly, the power line has its impulse interference. Compared to AWGN, impulsive noise generated by impulse interference is more challenging to eliminate. Finally, due to the different quality of power lines in other regions, each area's influence on signal transmission is distinct. It is more difficult to estimate the channel frequency response similar to the original channel at the receiver part of the system, which dramatically reduces the accuracy of channel transmission.

2.2.2 Future of Power Line Communication

Traditional PLC mainly uses a high-voltage transmission line as the transmission channel of high-frequency signals, which is only limited to the transmission of voice and remote control signals. The application range is narrow and low transmission rate, which can not meet users' requirements. However, due to the maturity of intelligent home systems, PLC is developing in large capacity and high speed. Meanwhile, it turns to a low-voltage distribution network for carrier communication. In the smart home system, Personal Computer (PC), as the core, can connect all intelligent electronic devices in the room through Homeplug to control and monitor. Compared to the wireless channel, PLC can solve the problems of many obstacles caused by indoor layout, which affect the quality of wireless transmission. So that

the cost of a home transmission signal is reduced, the transmission speed and accuracy can be increased as well. Besides, the Remote Automatic Meter Reading system (AMR) [17], and Remote monitoring system of street lamp [18] are also two systems applying PLC. Nowadays, the application mode of PLC systems is not simple point-to-point data transmission but plays an essential role in the open information network structure.

2.3 Error Correction

The process of detecting errors in transmission information and reconstructing original error free data in communication channel is called error correction. Error correction code encodes effective information with redundant information. This method allows a limited number of errors and corrects them by decoding without retransmission. During the decoding process, the received signal must be the same as the symbol in the sequence. Otherwise, it is said that the information has an error in the transmission to proceed to correct the error symbol [19]. As long as appropriate error correction codes are used, the error rate can be arbitrarily low when transmitting messages on multiple types of channels. The channel capacity, channel bandwidth and Signal-noise Ratio (SNR) have an optimal limit which is called Shannon limitation [20]. Two types of coded methods - LDPC and Polar code have been introduced in this thesis. LDPC has good performance close to the Shannon limit and low decoding complexity and flexible structure. The polar code is theoretically proven to reach the Shannon limit. This thesis will focus on these two types of codes investigation and utilisation in the PLC system.

2.3.1 Low-Density Parity-Check code

LDPC code is a linear block code with a realizable hardware decoder. Moreover, the performance of this coding method is close to the channel capacity in many data transmission and data storage channels. Gallager first wrote LDPC codes in his doctoral dissertation in 1960 [21]. In the last 35 years, people almost forgot LDPC code until Tanner popularized LDPC code and introduced the graphical representation of LDPC code, now called Tanner graph, that LDPC code was once again proposed for further research [22]. Mackay, Luby and others discovered the advantages of linear

block codes with sparse parity check matrix in the mid-1990s [23–26]. Meanwhile, the Binary-LDPC codes in 1/2 rate with random construction can achieve BER performance of 10^{-6} within 0.0045 dB SNR away from the Shannon limitation in the AWGN channel [27–29]. Nowadays, LDPC codes have been adopted in many modern applications such as Digital Video Broadcasting - Satellite - Second Generation (DVB-S2/T2), WiFi 802.11 standard and International Telecommunication Union (ITU)-T G.hn standard. Meanwhile, It was also adopted in the proposed standard for PLC (G.hn/G.9960) [30], DVB-S2 standard [31] and the 10 Gigabit Ethernet [32].

There are some literature works about the PLC system research by using LDPC code as well. In 2007, Nikoleta compared the BER performance over the PLC system between LDPC code, Reed–Solomon code and convolutional code. The research uses different code rates, which is the ratio of information bits and code length, of LDPC compare to other types of the code methods to investigate the impact of the PLC channel system. According to the results of the simulation, LDPC code can give a better BER performance than other types of code methods under all different conditions in the paper [33]. In 2013, the short-LDPC code was utilized in the Narrow-band PLC system with varying types of noise like AWGN and impulsive noise. LDPC also can give the better BER performance with seven different code length which is the number of the coded signal [34]. Turbo code is one of the most popular coding methods for PLC research as well. Due to the patent fees of the turbo code, researchers had to find other methods to improve the performance of the LDPC code instead of the turbo code. In 2014 [6], Gautham proposed that the performance of LDPC code can be similar to that of Turbo code with higher code lengthon the channel with a typical and realistic PLC system when the packet length is optimized.

Moreover, using Quasi-Cyclic LDPC (QC-LDPC) code can reduce the additional complexity associated with the increase of code length [6]. With the indoor broadband PLC channel, Yasin gives an optimization method to improve the BER performance of the PLC system by using LDPC code in 2013 [35]. Compared to uncoded OFDM system, LDPC coding scheme has considerable coding gain and low coding complexity in the whole channel [36, 37]. In addition to comparing other coding methods, the literature also provides many approaches for reducing the impact of different types of noise. In 2017, Ghanim presented a new receiver method by com-

puting the Log-Likelihood Ratios (LLRs) required for soft decoding based on the derived probability density functions using in the LDPC-PLC system. The BER performance gives a significant improvement compared with the conventional receiver and other traditional receivers [38]. There are also many investigations on the different types of noise reduction effects of LDPC in other channels [39–41].

2.3.2 Polar code

In 2008, Erdal Arikan, who is from Turkey, proposed channel polarization for the first time. Based on this theory, he proposed the first channel coding method that can be strictly proved to reach the channel capacity and named it polar code. The core of the polar code construction is to process the channel polarization and adopt a method on the coding side to make each subchannel present different reliability. When the code length continues to increase, some channels tend to be perfect channels with a capacity close to 1, and the other channels tend to be pure noise channels with a capacity close to 0. On this basis, the channel with a capacity close to 1 is chosen to transmit information directly to approach the channel capacity [42]. According to [43], The performance of polar code depends on the construction. With the different types of noise, the coding construction is completely different. In other words, the premise of the good performance of the polar code system is the type of noise channel known before constructing the polar code. There are some other methods about polar code construction in the literature [43–49]. In this thesis, we construct the polar code by using Arıkan's method [44].

As the good performance of the polar code use in the wireless channel, the wired PLC channel can be investigated with polar code as well. As can be seen in Ammar's research, the polar code has been utilized in the PLC-OFDM system with the Middleton Class-A Noise, which is a typical non-Gaussian noise model [50]. The BER performance of the system has been increased rapidly, even better than the LDPC codes. The same conclusion appears in Jin's research [51]. However, there is no literature on the PLC channel with real-valued OFDM input signal with either AWGN or impulsive noise channel. Hence, this thesis will carry out a comparative investigation of LDPC and polar code.

2.4 Orthogonal Frequency Division Multiplexing

OFDM is a multi-carrier transmission method. It divides the frequency band into several subcarriers to transmit data in parallel. In other words, the OFDM modulator divides one high-speed data stream into several parallel low-speed data streams. It is then modulated to the subcarriers of each channel for transmission. Because the frequency spectrum can be divided into separate parts to mitigate frequency selective channels, the OFDM can eliminate the interference between channel waveforms and achieve the purpose of combating multipath fading.

OFDM is a standard modulation method of PLC [52] because OFDM can ensure the stable and complete transmission of data in the communication environment of severe electromagnetic interference. The specification of Homeplug 1.0 covers the communication frequency band of $4-21MHZ$, in which 84 OFDM communication channels are divided [53]. The principle of OFDM is that several communication channels are frequency-divided according to the 90 degree phase. When a channel waveform crosses zero, the waveform of adjacent channels has the maximum amplitude. Under this circumstance, the channels will not overlap and crosstalk due to external interference.

In general, if the input signal is not preprocessed, the OFDM signal formed after the signal passes through Inverse Fast Fourier Transform (IFFT) is a complex signal in the Matlab simulation system. In this thesis, OFDM can only transmit real-valued signals in baseband transmission in the PLC system. Hermitian symmetry is utilized to create a real-valued OFDM input signal in the PLC system.

2.4.1 Hermitian symmetry

Hermitian symmetry is based on the Hermitian matrix, which is a self conjugate matrix [54]. In this matrix, every element of the i-th row and j-th column equals the conjugate of the elements of the j-th row and i-th column. The features on the main diagonal of the Hermitian matrix are all real numbers, and their eigenvalues are also real numbers. Many authors utilized Hermitian symmetry to create the real-valued OFDM signal to investigate the PLC system during these years. In 2016, Filbert used real-valued OFDM symbols as the input signal to examine the effect of the impulsive noise in the PLC system [55]. Another author called Minkyu presented a novel Discrete Fourier transform (DFT)-precoded Coherent Optical OFDM

(CO-OFDM) combined with a Hermitian symmetry system to mitigate fibre non-linearities for the CO-OFDM systems in 2012 [7]. Minkyu's system can also be implemented using a Fast Fourier transform (FFT) instead of DFT. In this thesis, the real-valued OFDM symbols are also created by the Hermitian symmetry after the M-ary QAM to evaluate for the baseband transmission over PLC channel system.

2.5 Summary of the Chapter

In this chapter, the general PLC survey and the development has been introduced. Besides, as the product and popularization of intelligent home systems and the Internet of things (IoT), PLC will stand out in many communication technologies with its characteristics based on the existing power line to transmit data. Furthermore, the LDPC codes and polar codes have been utilized to optimize the BER performance in the PLC system. The literature about the coded-PLC system during these years has been list as well. At the end of this chapter, the real-valued OFDM signal, which is created by Hermitian symmetry, is presented as the input signal in the PLC system. The investigation of this thesis will focus on the optimization of coded PLC systems with real-valued OFDM input signals.

Chapter 3

Preliminaries of PLC model, coded model, SαS distribution noise model and channel estimation model

3.1 Introduction

This chapter provided the main models of the communication system of this thesis. The multipath PLC channel models with SISO and MIMO systems are presented, including the primary factors and parameters. The details of the construction of LDPC code and polar code are provided in this chapter as well. In addition, the SαS distribution impulsive noise is explained. Finally, the background of channel estimation, the detailed explanations on the block pilot and the comb pilot design under the SISO system have been concluded. These are the essential prerequisite material for the novel work presented in chapters 4, 5 and 6.

3.2 PLC model

Nowadays, many models such as the Zimmermann and Dostert model [1], Philipps model [2] and the Anatory model [56] utilized to construct the PLC model. Compared to all these models, to adopt in this thesis, all the PLC model constructions depend on the Zimmermann model.

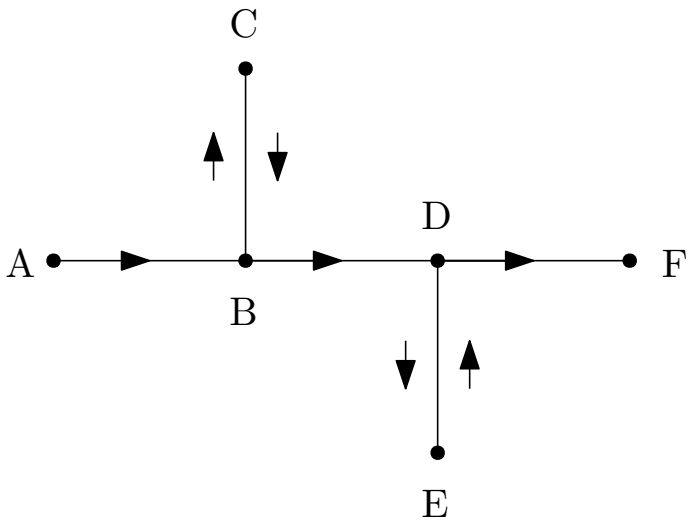

Figure 3.1: Multipath signal propagation in one tap cables.

3.2.1 SISO multipath PLC channel model

The multipath PLC channel utilized in this thesis is shown in Fig. 3.1 [57, 58]. The OFDM signal is transmitted from point A to the receiver end at point F. However, due to multipath propagation, several possible paths are established, i.e. $A \to B \to D \to F, A \to B \to C \to B \to D \to F, A \to B \to D \to E \to D \to F, A \to B \to C \to B \to D \to E \to D \to F$. The channel frequency response (CFR) for this channel can be given as [1]

$$H(f) = \sum_{i=1}^{L} \underbrace{g_i}_{\text{weighting factor}} \underbrace{e^{-(a_0+a_1 f^q)d_i}}_{\text{attenuation}} \underbrace{e^{-j2\pi f \frac{d_i}{v_p}}}_{\text{delay}}, \tag{3.1}$$

where f is the frequency of each subcarrier, L is the number of multipaths, l denotes the index of multipaths, a_0 and a_1 are the attenuation parameters, q is the exponent of attenuation factor and d_i is the length of the cable. Furthermore, v_p is the phase velocity given as

$$v_p = \frac{c_o}{\sqrt{\varepsilon_r}}, \tag{3.2}$$

where c_0 denotes the speed of light which is 3.0×10^8 m/s and $\varepsilon_r = 4$ is the dielectric constant of the polyethylene, which is a kind of insulation material using in the power line transmission system. The CIR of the PLC channel is obtained by using the inverse Fourier transform of Fig. 3.2. For $q = 1$, we consider first the attenuation portion of the PLC CFR, which corresponds to the following analytic

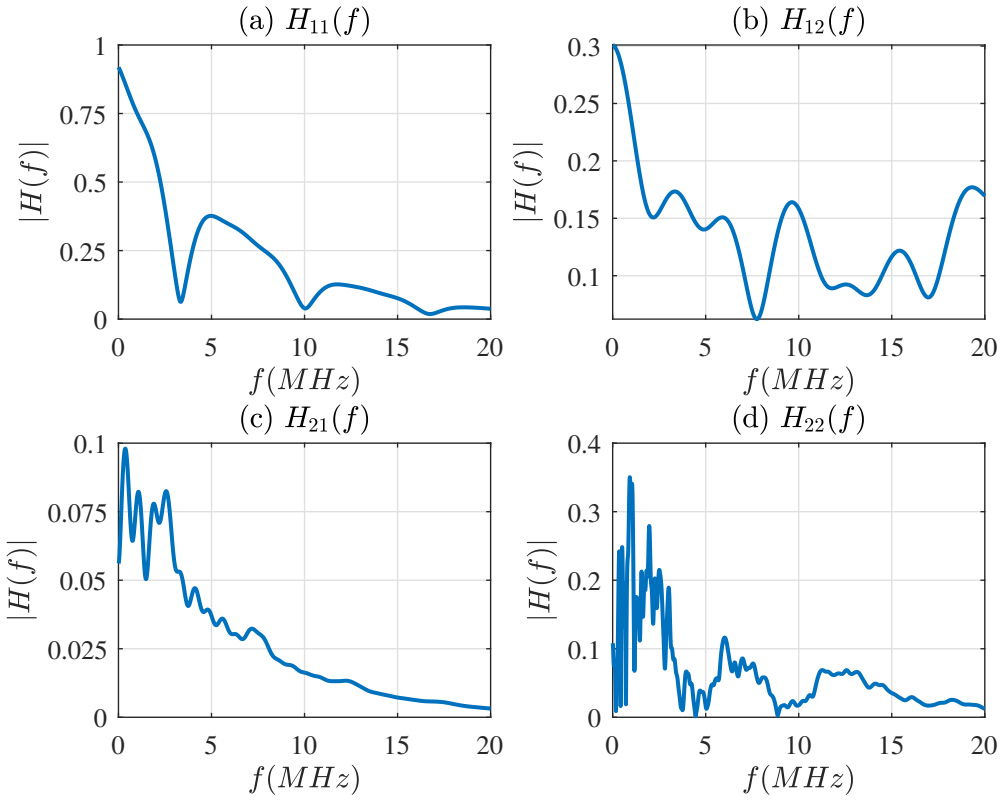

Figure 3.2: The magnitude of Channel Frequency Response of MIMO-PLC.

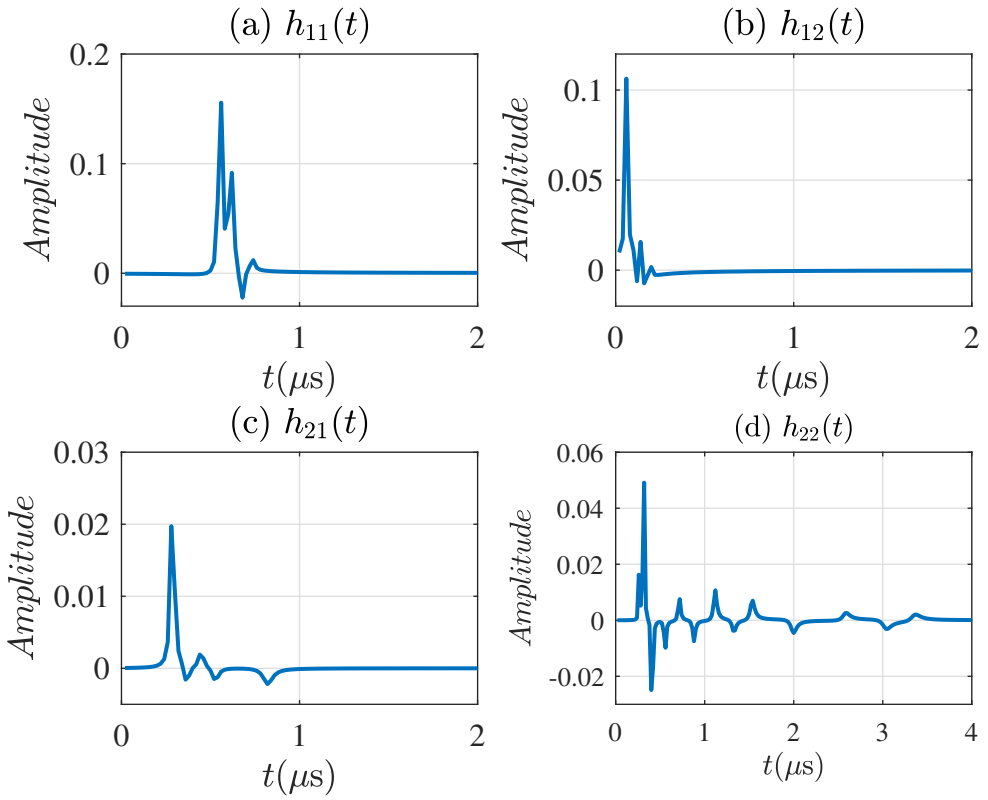

Figure 3.3: The Channel Impulse Response of MIMO-PLC.

and bandlimited frequency response, i.e. $A(f) = 0, \forall f < 0$, and

$$A(f) = e^{-a_0 d_i} e^{-a_1 d_i f}, \text{ with } 0 \leq f \leq B$$

The inverse Fourier transform (FT) of $A(f)$ is computed as [59]

$$\begin{aligned} a(t) &= \int_{-\infty}^{\infty} A(f) e^{j2\pi ft} df \\ &= \int_{0}^{B} e^{-a_0 d_i} e^{-a_1 d_i f} e^{j2\pi ft} df \\ &= e^{-a_0 d_i} \int_{0}^{B} e^{-(a_1 d_i - j2\pi t)f} df \\ &= e^{-a_0 d_i} \frac{e^{-(a_1 d_i - j2\pi t)f}}{a_1 d_i - j2\pi t} \Bigg|_{B}^{0} \\ &= \frac{1}{a_1 d_i - j2\pi t} \left(1 - e^{-a_1 d_i B} e^{e^{-j2\pi Bt}}\right) \\ &= \frac{e^{-j \tan^{-1}\left(\frac{2\pi t}{a_1 d_i}\right)}}{\sqrt{(a_1 d_i)^2 + (2\pi t)^2}} \left(1 - e^{-a_1 d_i B} e^{-j2\pi Bt}\right) \end{aligned} \tag{3.3}$$

It is worth noting that t here denotes the multipath delay spread of the PLC channel rather than time. We proceed to define $t_i = \frac{d_i}{v_p}$, then using the time-shift property of the FT [59], we can write

$$\begin{aligned} a(t - t_i)u(t - t_i) &= \int_{0}^{B} A(f) e^{-j2\pi ft_i} e^{j2\pi ft} df \\ &= \frac{e^{-j \tan^{-1}\left(\frac{2\pi (t - t_i)}{a_1 d_i}\right)}}{\sqrt{(a_1 d_i)^2 + [2\pi (t - t_i)]^2}} \left(1 - e^{-a_1 d_i B} e^{-j2\pi B(t - t_i)}\right) \end{aligned} \tag{3.4}$$

where $u(t - t_i)$ is the Heaviside function delayed by t_i. The PLC CFR is analytic too and is given as

$$H_a(f) = \sum_{i=1}^{L} g_l e^{-a_0 d_i} e^{-a_1 f^k d_i} e^{-j2\pi ft_i} \tag{3.5}$$

The analytic CIR is obtained by taking the inverse FT of $H_a(f)$ as

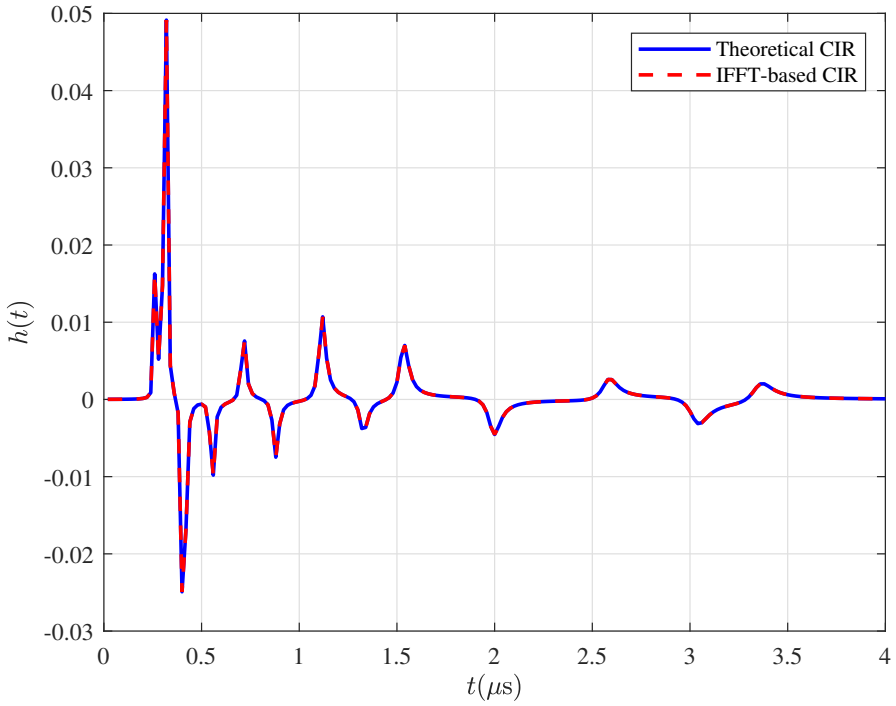

Figure 3.4: Theoretical and numerical CIR vs. multipath delay spread for a 15-path PLC multipath channel truncated to 200 samples.

$$\begin{aligned} h_a(t) &= \int_{-\infty}^{\infty} H_a(f) e^{j2\pi ft} df \\ &= \int_{-\infty}^{\infty} \sum_{i=1}^{L} g_l e^{-a_0 d_i} e^{-a_1 f d_i} e^{-j2\pi f t_i} e^{j2\pi ft} df \\ &= \sum_{i=1}^{L} g_l e^{-a_0 d_i} \int_0^B e^{-a_1 f d_i} e^{-j2\pi f t_i} e^{j2\pi ft} df \\ &= \sum_{i=1}^{L} g_l e^{-a_0 d_i} a(t-t_i) u(t-t_i) \end{aligned} \tag{3.6}$$

The PLC CIR is obtained by taking the real part of $h_a(t)$, i.e.

$$\begin{aligned} h(t) &= \mathrm{Re}\{h_a(t)\} \\ &= \sum_{i=1}^{L} g_l e^{-a_0 d_i} u(t-t_i) \times \\ &\frac{\cos(\phi_i)[1 - e^{-a_1 d_i B}\cos(\theta_i)] + e^{-a_1 d_i B}\sin(\phi_i)\sin(\theta_i)}{\sqrt{(a_1 d_i)^2 + [2\pi(t-t_i)]^2}} \end{aligned} \tag{3.7}$$

where B is the signal bandwidth, $\phi_i = \tan^{-1}\left(\frac{2\pi(t-t_i)}{a_1 d_i}\right)$ and $\theta_i = 2\pi B(t-t_i)$. The truncated and energy-normalized CIR is illustrated in Fig. 3.3. Truncation is performed to remove trailing zeros as the CIR values become very small after $L =$

200. Furthermore, it is worth noting that the variable t denotes the multipath delay spread of the PLC channel in units of seconds, and that the multipath amplitudes have been normalized so that $\sum_{t=0}^{L-1} |h(t)|^2 = 1$.

Fig. 3.4 shows the theoretical energy-normalized CIR along with the one obtained by taking the inverse FT of the analytical CFR. Evidently, there is a very good agreement between the theoretical and numerically computed CIR. It is worth noting that closed-form solution may not exist for arbitrary values of q.

3.2.2 MIMO-PLC model

Over the past ten years, MIMO-BPL techniques have been considered and researched extensively for the PLC channel to increase transmission speeds closer to the available channel capacity [60–68].

MIMO is the primary technology in the fourth and fifth-generation (4G/5G) of wireless communication [69]. In the PLC channel, the domestic electrical wiring includes three types of wires: Phase (P), Neutral (N) and Protective Earth (PE). In SISO systems, the communication signals are transmitted via the P and N wires using Time-division Multiple Access (TDMA) and Carrier-Sense Multiple Access with Collision Avoidance (CSMA/CA). However, voltage differences between PE, P and N as well can be utilized to establish MIMO communications using the three ports: P-PE, PE-N and P-N, to implement 3×3 MIMO system, implying three transmitters and three receivers per terminal [65]. The advantages and problems of MIMO-PLC systems have been discussed extensively in [70, 71], where appropriate communication methods have been proposed and investigated.

In this thesis, as can be seen in Fig. 3.5, four PLC channels with different value of multipaths and parameter values have been utilized to simulate a 2×2 MIMO-OFDM PLC-based system. The magnitude of four CFRs and four CIRs of the MIMO-PLC channels are illustrated in Fig. 3.3 and Fig. 3.2. Four PLC channel parameters can be found in Table. 3.1, Table. 3.2, Table. 3.3, Table. 3.4:

After Cyclic Prefix (CP) removal and FFT operation, the received signal at the n_{fft}-th subcarrier can be given as

$$\mathbf{Y} = \mathbf{HX} + \mathbf{W_S} \tag{3.8}$$

where $\mathbf{Y} \in \mathbb{C}^{2\times 1}$ is the received signal vector, $\mathbf{H} \in \mathbb{C}^{2\times 2}$ is the frequency-domain,

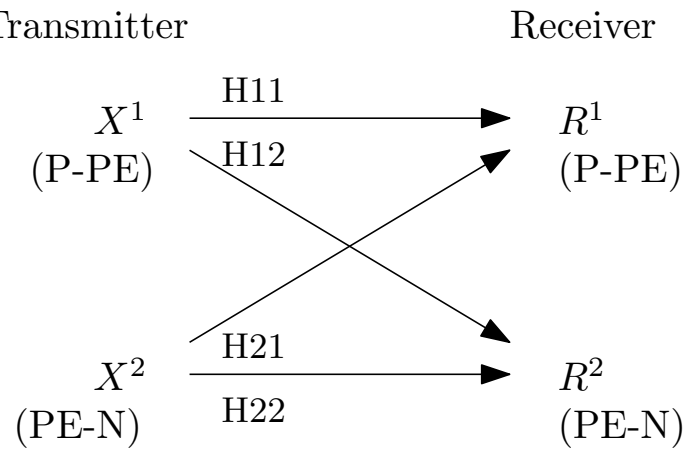

Figure 3.5: 2×2 MIMO-PLC Model.

Table 3.1: the weight factor and parameters of 4-path PLC (H11:$X^1 \rightarrow R^1$) [1].

Attenuation parameters: $a_0 = 0$; $a_1 = 7.8 * 10^{-10}; q = 1$						
Path parameters:						
l	g_i	d_i		l	g_i	d_i
1	0.64	200		3	-0.15	411
2	0.38	222.4		4	0.05	490

Table 3.2: the weight factor and parameters of 5-path PLC (H12:$X^1 \rightarrow R^2$) [2].

Attenuation parameters: $a_0 = 0$; $a_1 = 7.8 * 10^{-10}; q = 1$						
Path parameters:						
l	g_i	d_i		l	g_i	d_i
1	0.151	16.5		4	0.041	46.65
2	0.047	23.1		5	0.033	64.05
3	0.029	30.75				

Table 3.3: the weight factor and parameters of 5-path PLC (H21:$X^2 \rightarrow R^1$) [3].

Attenuation parameters: $a_0 = 0$; $a_1 = 1.65 * 10^{-9}; q = 1$						
Path parameters:						
l	g_i	d_i		l	g_i	d_i
1	0.09	100		4	-0.012	190
2	-0.012	130		5	-0.022	300
3	0.012	160				

Table 3.4: the weight factor and parameters of 5-path PLC (H22:$X^2 \rightarrow R^2$) [1].

Attenuation parameters: $a_0 = 0$; $a_1 = 2.5 * 10^{-9}; q = 1$						
Path parameters:						
l	g_i	d_i		l	g_i	d_i
1	0.029	90		9	0.071	411
2	0.043	102		10	-0.035	490
3	0.103	113		11	0.065	567
4	-0.058	143		12	-0.055	740
5	-0.045	148		13	0.042	960
6	-0.04	200		14	-0.059	1130
7	0.038	260		15	0.049	1250
8	-0.038	322				

channel coefficient matrix, and $\mathbf{W_S}^{2\times1}$ is the vector of the zero-mean, additive white Gaussian noise samples with variance $\sigma^2_{W_S}$, i.e. $\mathcal{N}(0, 2\sigma^2_{W_S})$.

3.3 Polar code

Polar code, which is the basis of establishing Channel polarization, divides into two-channel operations: channel combining and channel splitting. Before the polar code description, two main channel parameters of the Binary-input Discrete Memoryless Channel (B-DMLC) - the symmetric capacity $I(W)$, which is the highest rate of reliable communication at the same frequency using the input of B-DMC (W), is defined as

$$I(W) \triangleq \sum_{y\in[0,1]} \sum_{x\in[0,1]} \frac{1}{2} W(y|x) \log_2 \frac{W(y|x)}{\frac{1}{2}W(y|0) + \frac{1}{2}W(y|1)}, \tag{3.9}$$

and Bhattacharyya parameter $Z(W)$, which is the bound probability when W is only transmit 0 or 1, is derived as [72]

$$Z(W) \triangleq \sum_{y\in[0,1]} \sqrt{W(y|0)W(y|1)}, \tag{3.10}$$

where x, y denote the value of the input and output, respectively. Apparently from (3.9) and (3.10), $I(W)$ and $Z(W)$ take the values in [0,1], meanwhile, the

relationship between two parameters can be demonstrated as [42]

$$I(W) \geq \log_2 \frac{2}{1 + Z(W)}, \tag{3.11}$$

$$I(W) \leq \sqrt{1 - Z(W)^2}. \tag{3.12}$$

3.3.1 Channel Combining and Splitting

3.3.1.1 Channel Combining

In order to achieve the combination of N channels, the system transforms N independent channels W into one channel W_n through recursive process. Each recursive process changes N channels into $\frac{N}{2}$ small channel aggregations. For a single channel W, the channel transition probability is $W(y|x)$. Meanwhile, the transition probability of the W_n with is $W_n(y_1^N|x_1^N)$. Replace x_1^N into $u_1^N G_N$, the transition probability is defined as

$$W_N(y_1^N|x_1^N) = W^N(y_1^N|u_1^N G_N), \tag{3.13}$$

where W^N denotes the number of N independent channel W and the G_N represents the generator matrix which will give the detail in the polar code construction part. The recursive process can be seen in Fig. 3.6 [51] and the transition probability can be demonstrated as

$$W^2(y_1^2|u_1^2) = W(y_1|u_1 \oplus u_2)W(y_1|u_2), \tag{3.14}$$

$$\begin{aligned} W^4(y_1^4|u_1^4) &= W_2(y_1^2|u_1 \oplus u_2, u_3 \oplus u_4)W_2(y_3^4|u_2, u_4), \\ &= W(y_1|u_1 \oplus u_2 \oplus u_3 \oplus u_4)W(y_2|u_3 \oplus u_4) \\ &\quad W(y_3|u_2 \oplus u_4)W(y_4|u_4). \end{aligned} \tag{3.15}$$

3.3.1.2 Channel Splitting

The channel splitting process is to divide the composite channel W_N, which is created by channel combining, into the number of N coordinate channels W_N^i were $1 \leq i \leq$

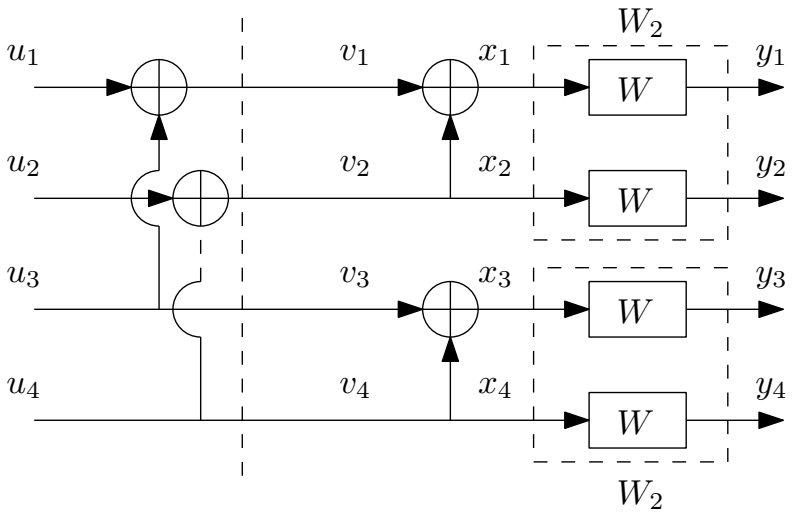

Figure 3.6: The recursive construction of W_4.

N. The transition probability can be defined as

$$W_N^i(y_1^N, u_1^{i-1}|u_i) \triangleq \sum_{u_{i+1}^N \in X^{N-i}} \frac{1}{2^{N-1}} W_N(y_1^N|u_1^N), \tag{3.16}$$

where u_i denotes the input and the output is (y_1^N, u_1^{i-1}). The relationship between each channel capacity can be difined as

$$I(W^{2i}) = 2 \times I(W^i) - I(W^i)^2, \tag{3.17}$$

$$I(W^{2i-1}) = I(W^i)^2. \tag{3.18}$$

Fig. 3.7 plots the description of the polarization phenomenon under $N = 2^{11} = 2048$ with different value of erasure probability $0 < \epsilon < 1$.

3.3.2 Polar code construction

The main point of the polar code construction is to create the generator matrix G_N [73]. Assume that the position of information bits are $|A|$ and $|A^f|$ are the position of frozen bits. The kernel matrix $F = \begin{bmatrix} 1 & 0 \\ 1 & 1 \end{bmatrix}$ has been proposed to construct the generator matrix G_N of this codes system that can be defined as

$$G_N = BF^{\otimes v}, \tag{3.19}$$

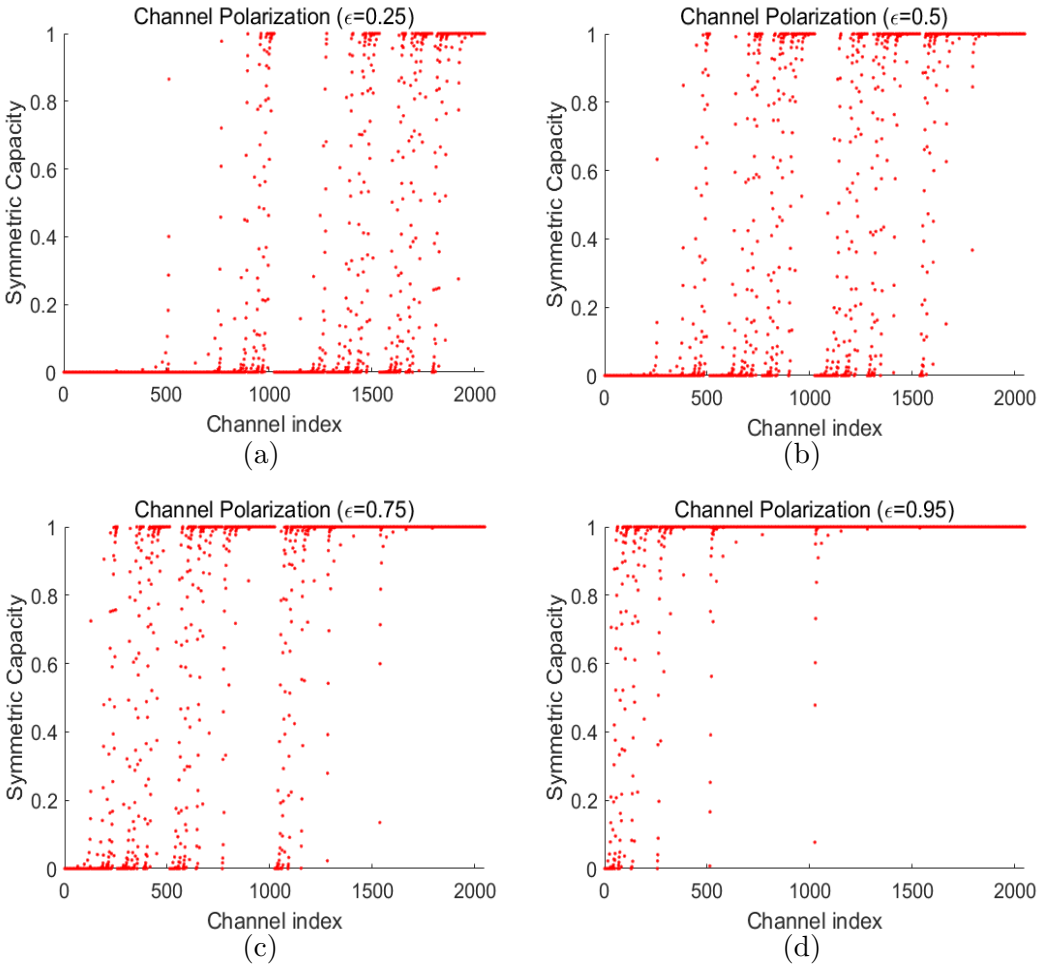

Figure 3.7: The $I(W)$ capacity verse $i = 1, ..., N = 2^{11}$ with (a) $\epsilon = 0.25$, (b)$\epsilon = 0.5$, (c)$\epsilon = 0.75$, (d)$\epsilon = 0.95$.

where B is bit revesal, $\otimes$ is the Kronecker product given as

$$F^{\otimes v} = F^{\otimes v-1} \otimes F. \tag{3.20}$$

The coded input signal can be written as

$$x^N = u_A G_N(A) \oplus u_{A^f} G_N(A^f), \tag{3.21}$$

where u_A is the information bits, and u_{A^f} is the frozen bits.

3.3.3 Successive Cancellation Decoder

The successive cancellation decoder decides $\hat{u}_i$ as follow [74–76]

$$\hat{u}_i = \begin{cases} u_i, & if\ i \in A^f \\ h_i(y_1^N, \hat{u}_i). & if\ i \in A \end{cases}$$

LLR can be utilized in the decision part as follow

$$h_i(y_1^N) = \begin{cases} 0, & if\ \ln \frac{Pr(y_i^N, \hat{u}_1^{i-1}|0)}{Pr(y_i^N, \hat{u}_1^{i-1}|1)} \geq 1 \\ 1. & if\ \ln \frac{Pr(y_i^N, \hat{u}_1^{i-1}|0)}{Pr(y_i^N, \hat{u}_1^{i-1}|1)} \leq 1 \end{cases}$$

Assume that the length of polar code is 2 with $\Pr(U_1, U_2, Y_1, Y_2)$, the LLR of U_1 should be defined as

$$\begin{aligned} \ln \frac{Pr(Y_1Y_2|U_1=0)}{Pr(Y_1Y_2|U_1=1)} &= \ln \frac{\sum_{U_2\in 0,1} Pr(Y_1|U_2)Pr(Y_2|U_2)}{\sum_{U_2\in 0,1} Pr(Y_1|1\oplus U_2)Pr(Y_2|U_2)} \\ &= \ln \frac{Pr(Y_1|0)Pr(Y_2|0) + Pr(Y_1|1)Pr(Y_2|1)}{Pr(Y_1|1)Pr(Y_2|0) + Pr(Y_1|0)Pr(Y_2|1)} \\ &= \ln \frac{\frac{Pr(Y_1|0)Pr(Y_2|0)}{Pr(Y_1|1)Pr(Y_2|1)} + 1}{\frac{Pr(Y_2|0)}{Pr(Y_2|1)} + \frac{Pr(Y_1|0)}{Pr(Y_1|1)}} \\ &= \ln \frac{1 + e^{L_1+L_2}}{e^{L_1} + e^{L_2}}, \end{aligned} \tag{3.22}$$

where Y_1, Y_2 are the to received symbols, U_1, U_2 are the input symbols, L_1, L_2 denote the LLR of two output symbols. The result of (3.22) can be approximate to

$$\ln \frac{1 + e^{L_1+L_2}}{e^{L_1} + e^{L_2}} \approx \text{sign}(L_1)\text{sign}(L_2) \min(|L_1|, |L_2|). \tag{3.23}$$

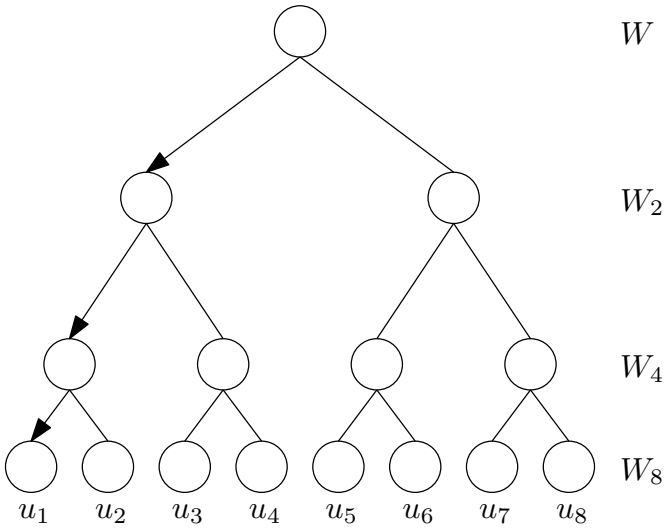

Figure 3.8: The Binary graph of SC decoder.

For LLR of U_2, the equation can be calculated by using U_1 as follow

$$\begin{aligned} \ln \frac{Pr(Y_1Y_2U_1|U_2=0)}{Pr(Y_1Y_2U_1|U_2=1)} &= \ln \frac{Pr(Y_1|U_1)Pr(Y_2|0)}{Pr(Y_1|1\oplus U_1)Pr(Y_2|1)} \\ &= \ln \frac{Pr(Y_1|U_1)}{Pr(Y_1|1\oplus U_1)} + \ln Pr(Y_2|0)Pr(Y_2|1) \\ &= (1-2U_1)L_1 + L_2, \end{aligned} \tag{3.24}$$

The Successive Cancellation (SC) decoding of the polarization code of length 2^N is just made up of 2^{N-1} 2×2 basic polarization code modules which can be shown in Fig 3.8.

According to the arrowhead indication, each node is judged step by step. After the result of u_1 is obtained, the SC decoder start to judge u_2 and so on.

3.4 LDPC code

LDPC code is a block code whose check matrix contains only a few non-zero elements. The sparsity of parity check matrix ensures that the decoding complexity and minimum code distance only increase linearly with the code length [77, 78]. LDPC code is the same as any other block code except that the check matrix is sparse. The design of the code starts with constructing a check matrix, then determines a generating matrix for the encoder. The decoding of LDPC codes is based on the image representation of its check matrix H_{LDPC}. Thus the design of the LDPC code is based on the characteristics of the check matrix.

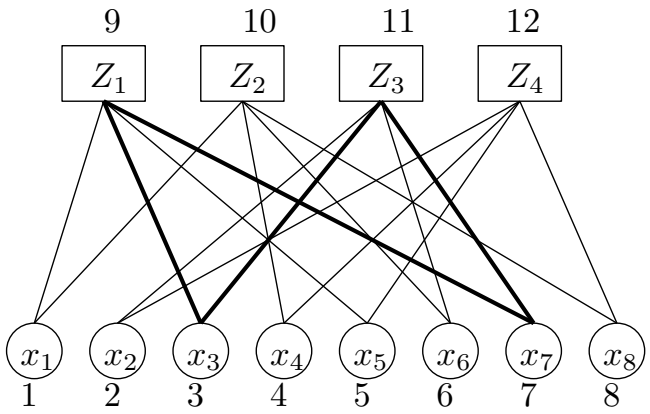

Figure 3.9: The Tanner graph of H (8,2,4).

3.4.1 Tanner graph

The essential tool to describe LDPC code is a bipartite graph, an undirected graph. Tanner graph is the concretization of bipartite graph which has two types of nodes - information bits nodes and check nodes [79]. Fig. 3.9 plots the tanner graph of the regular check matrix

$$H_{LDPC} = \begin{bmatrix} 1 & 0 & 1 & 0 & 1 & 0 & 1 & 0 \\ 1 & 0 & 0 & 1 & 0 & 1 & 0 & 1 \\ 0 & 1 & 1 & 0 & 0 & 1 & 1 & 0 \\ 0 & 1 & 0 & 1 & 1 & 0 & 0 & 1 \end{bmatrix}, \tag{3.25}$$

where (n,p,q)=(8,2,4), n is the length of code, p denotes column weight and q denotes row weight.

In the Tanner graph, the minimum length of a cycle with the same node as its starting point and ending point is the number of lines contained in the cycle. In Fig. 3.9, $3 \rightarrow 11 \rightarrow 7 \rightarrow 9 \rightarrow 3$ is a cycle with 4 of minimum cycle length.

3.4.2 LDPC construction and encoder

The LDPC code construction is utilized the diagonal method to construct the check matrix $H_{LDPC}(A|B)$. Assume that H_{LDPC} is a regular LDPC code check matrix with the size $(K \times N)$, where K is the length of information bits and N is the code length. A is a matrix with fixed row weight and column weight constructed by the traditional Gallager random construction method and the size is $(N-K) \times K$ as the information bit matrix. B is a Bi-diagonal matrix with the size of $(K \times K)$ as

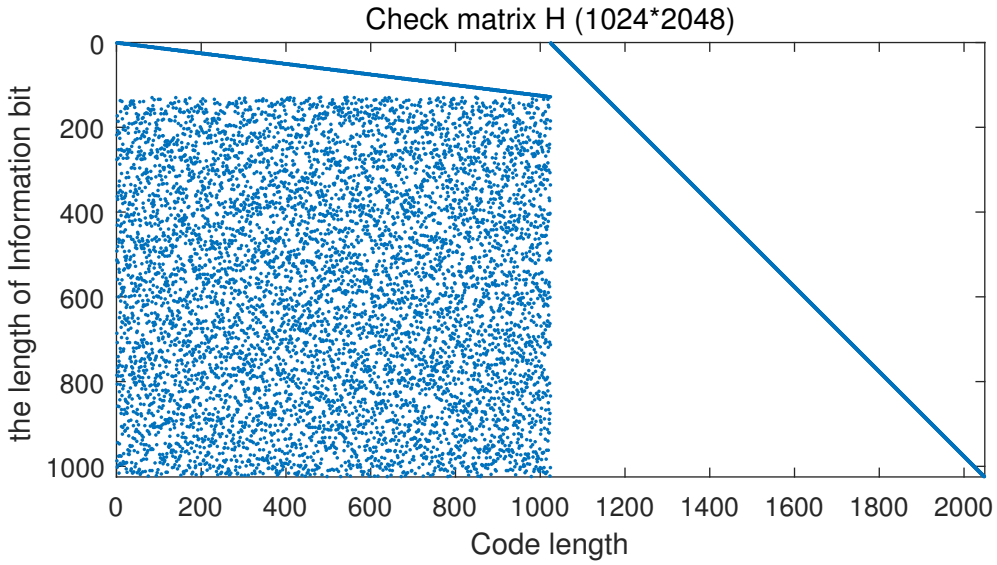

Figure 3.10: The Check matrix graph with diagonal method (1024 × 2048).

the check bit matrix. Fig. 3.10 plots the check matrix graph by using the diagonal method in Matlab.

As LDPC code is a kind of linear block code. Except the sparse matrix construction, the encoder is same as the normal linear block code. After Gaussian elimination, the sparse matrix changes to $H_{spa} = [P^T I]$, where I is the unit matrix. the generation matrix G should follow the condition that

$$GH_{LDPC}^{T} = 0, \tag{3.26}$$

in other word,

$$G = [IP]. \tag{3.27}$$

Thus, the output of encoder $\mathbf{c}$ is defined as

$$\mathbf{c} = \mathbf{u}G, \tag{3.28}$$

where $\mathbf{u}$ denotes the matrix of information bits.

3.4.3 Belief propagation soft decision decoding

3.4.3.1 Preliminary work

Except for the sparse matrix construction, the encoder is the same as the standard linear block code. After Gaussian elimination, the sparse matrix changes to $H_{spa} = [P^T I]$. The generation matrix G should follow the condition that

Theorem 1. A binary sequence of length N, where the probability of bit i being 1 is P_i^1, thus the probability of the whole sequence containing even 1 is defined as

$$\frac{1}{2} + \frac{1}{2}\prod_{i=1}^{N}(1 - 2P_i^1), \tag{3.29}$$

and the probability of the whole sequence containing odd 1 is defined as

$$\frac{1}{2} - \frac{1}{2}\prod_{i=1}^{N}(1 - 2P_i^1). \tag{3.30}$$

Theorem 2. If $y_i = x_i + n_i$, $n_i \in \mathcal{N}(0, \sigma^2)$, x_i denotes the BPSK signal, moreover, $Pr(x_i = 1) = Pr(x_i = -1) = 0,5$. Thus, the Pr over AWGN noise channel system can be defined as

$$Pr(x_i = 1|y_i) = \frac{1}{1 + e^{\frac{2y_i}{\sigma^2}}} \tag{3.31}$$

3.4.3.2 Decoding process

The decoding processing can be saparated into four steps [80–82].

Step 1. Initially,

$$\begin{aligned} L(c_n) &= \ln \frac{Pr(c_n = 0|y_n)}{Pr(c_n = 1|y_n)} \\ &= \frac{2}{\sigma^2} y_n, \end{aligned} \tag{3.32}$$

$$\theta_{n\to k} = L(c_n), \tag{3.33}$$

$$\lambda_{k\to n} = 0, \tag{3.34}$$

where $L(*)$ denotes the LLR of the signal, $n = 1, 2, ..., N$ is the index of the code length, $k = 1, 2, ..., K$ is the index of the length of information data, $\lambda_{k\to n}$ denotes

the information from check node k to variable node n, $\theta_{n\to k}$ means the information from variable node n to check node k.

Step 2. Updating check node, each $k, n \in X(k)$ can be calculated as

$$\lambda_{k\to n} = 2\tanh^{-1} \prod_{n`\in X(k)\setminus n} \tanh[\frac{\theta_{n`\to k}}{2}], \tag{3.35}$$

where $X(k)$ represents aggregate of all variable nodes connected to check node k and $X(k) \setminus n$ denotes the aggregate of $X(k)$ except n.

Step 3. Updating variable node, each $n, k \in Z(n)$ can be calculated as

$$\theta_{n\to k} = L(c_n) + \sum_{k`\in Z(n)\setminus k} \lambda_{k`\to n}, \tag{3.36}$$

$$\varphi_n = L(c_n) + \sum_{k\in Z(n)} \lambda_{k\to n}, \tag{3.37}$$

where $Z(n)$ represents aggregate of all check node connected to variable nodes n and $Z(n) \setminus k$ denotes the aggregate of $Z(n)$ except k.

Step 4. φ_n is decided in decoder. When $\varphi_n \geq 0$, $\hat{c}_n = 1$; when $\varphi_n < 0$, $\hat{c}_n = 0$, the estimated code data $\hat{\mathbf{c}} = (\hat{c_1}, ..., \hat{c_N})$ is calculated. The decoder is stopped when the system reach the maximum number of iterations. Otherwise, the decoder process back to step 2.

3.5 SαS distribution noise model

3.5.1 Impulsive noise

Impulse noise is a discontinuous noise composed of irregular pulses or noise spikes with short duration and large amplitude. The reason for the impulsive noise development can be separated into two types: Natural impulsive noise produced by the electromagnetic pulse radiation of thunder and man-made noise by using electrical equipments such as Middleton class A distribution noise [83, 84]. Some popular impulsive noise models are reviewed, such as the Middleton Class A and α-stable

distribution models.

There are three statistics-physical models of non-Gaussian noise proposed by Middleton, which are the crucial models that are to express the statistical features in the PLC channel system, especially the Middleton Class A model [85–88]. The Probability Density Function (PDF) of Middleton Class A with an infinite number of the normal distribution is defined as

$$p(x) = \sum_{n=1}^{\infty} \frac{A^n e^{-A}}{n! \pi \sigma_n^2} \exp(-\frac{|x|^2}{\sigma_n^2}), \tag{3.38}$$

where

$$\sigma_n^2 = \sigma_I^2 \frac{n}{A} + \sigma_g^2, \tag{3.39}$$

A denote the impulsive density, σ_I is the standard deviation of the AWGN noise and σ_g is the standard deviation of the impulsive noise.

Stable distribution is a special case of Gaussian distribution. Compared with other impulsive noise models, with the characteristics of strong flexibility and high accuracy, this model is usually utilized to investigate the underwater acoustic communication system and PLC channel system [15,89]. According to [90], the α-stable noise model has been utilized over the PLC channel system in the industrial environment. In this thesis, we chose the SαS distribution noise to module the impulse noise in the PLC system. The characteristic function of α-stable distributions can be demonstrated as [91, 92]

$$\varphi(t) = \exp(j\delta t - \mid \gamma t \mid^{\alpha} (1 - j\beta \text{sign}(t)\omega(t, \alpha))), \tag{3.40}$$

where

$$\omega(t, \alpha) = \begin{cases} \tan(\pi\alpha/2), & \alpha \neq 1, \\ -2/\pi \log |t|, & \alpha = 1, \end{cases}$$

where α denotes the characteristic exponent ($0 < \alpha \leq 2$) which controls the heaviness of the tail of the pdf and indicates the impulsiveness of the channel [13], β denotes the skewness of the pdf, δ is location parameter which indicates the mean of the pdf. γ, called the dispersion, measures the spread of the SαS pdf with a similar value to the variance of a Gaussian distribution.

3.5.2 Symmetric α-stable noise

The SαS distribution is the normal α-stable distribution with 0 value of skewness parameter β. Hence the function can be defined as

$$\varphi(t) = \exp\left(j\delta t - \gamma^{\alpha} \mid t \mid^{\alpha}\right). \tag{3.41}$$

Hence the PDF of the SαS distribution noise model can be defined as [93]

$$p_{\alpha}(x;\delta;\gamma) = \frac{1}{2\pi}\int_{-\infty}^{\infty} \exp(j\delta t - \gamma^{\alpha}|t|^{\alpha})e^{-jtx}dt. \tag{3.42}$$

As $0 < \alpha \leq 2$, when $\alpha = 1$, the distribution is Cauchy and the pdf is given as

$$f_1(x;\delta,\gamma) = \frac{1}{\pi}\frac{\gamma}{\gamma^2 + (x-\delta)^2}, \tag{3.43}$$

when $\alpha = 2$, the distribution is Gaussian and the standard pdf is

$$f_2(x;\delta,\gamma) = \frac{1}{2\sqrt{\pi}\gamma}\exp\left[-\frac{(x-\delta)^2}{4\gamma^2}\right], \tag{3.44}$$

because the SαS noise is a kind of Gaussian distribution noise,the relationship between variance and dispersion is $\sigma^2 = 2\gamma^2$. The dispersion γ can be defined as

$$\gamma = \sqrt{\frac{E_s C_g}{4C_g^{\frac{2}{\alpha}} R_c \log_2(M)\frac{E_b}{N_0}}}, \tag{3.45}$$

where $C_g = 1.78$ is the exponential of the Euler constant, $\frac{E_b}{N_0}$ is the SNR. Fig 3.11 demonstrated the PDF of SαS noise model with different α values. Moreover, when α decreases, the tail of the pdf becomes thicker. When $\alpha = 2$, the trend of the impulsive noise is the same as the AWGN noise trend. The properties of SαS can be defined as [13].

3.6 Channel estimation

Channel estimation refers to methods that identify the communications channel's channel impulse and frequency responses. For OFDM systems, two methods are widely used, i.e., the comb and block pilot approaches [8], which are considered

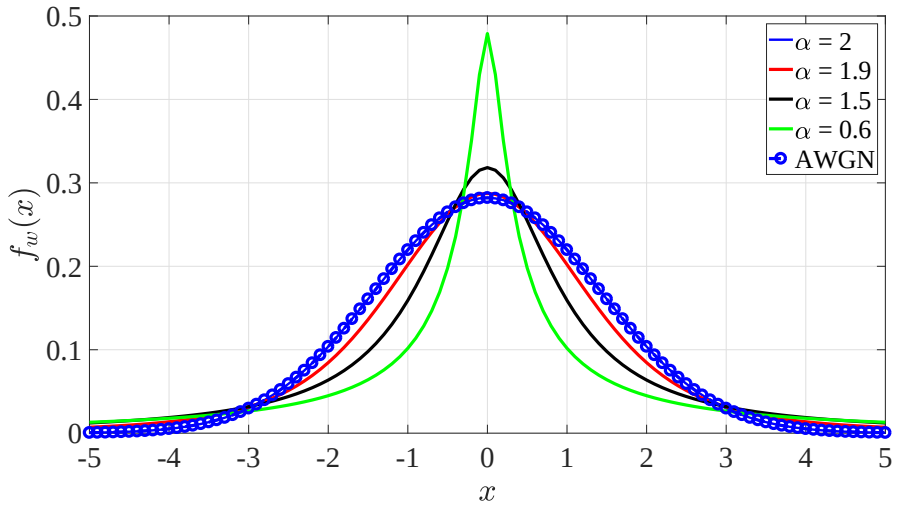

Figure 3.11: The PDFs of SαS noise with different value of α and AWGN.

as non-blind estimation methods as they utilize a reference signal. Although the pilots occupy information bits and waste the channel capacity, non-blind estimation is used widely because of its excellent performance compared to blind methods and their low-complexity of operation [9].

3.6.1 Block pilot approach in SISO system

Assume that the Ratio of the number of the Pilot to the number of Information Data (P-I ratio) is $\frac{1}{8}$. In other words, the length of the OFDM data block, $N_b = 9$ can be considered in nine OFDM symbols - one OFDM symbol is full of pilots and eight OFDM symbols are the information data, which can be expressed in Fig. 3.12 (a) [10, 11]. N_m denotes the number of OFDM symbols with a multiple of eight of size in this thesis and N_{fft} denotes the total subcarriers of the OFDM symbols. The transmitter can send one pilot symbol in each OFDM data block as the tracking data in all OFDM subcarriers to the receiver to calculate the estimated channel frequency response in the SISO-PLC system. For instance, the total number of the OFDM input symbols should be $\frac{9}{8}N_m$.

3.6.2 Comb pilot approach in SISO system

Under the exact circumstance of the block pilot approach, in every nine subcarriers ($N_c = 9$), we use one subcarrier to transmit pilot to make the P-I ratio is $\frac{1}{8}$, which shows in Fig. 3.12 (b) [10,94]. The total length of the subcarriers should be included

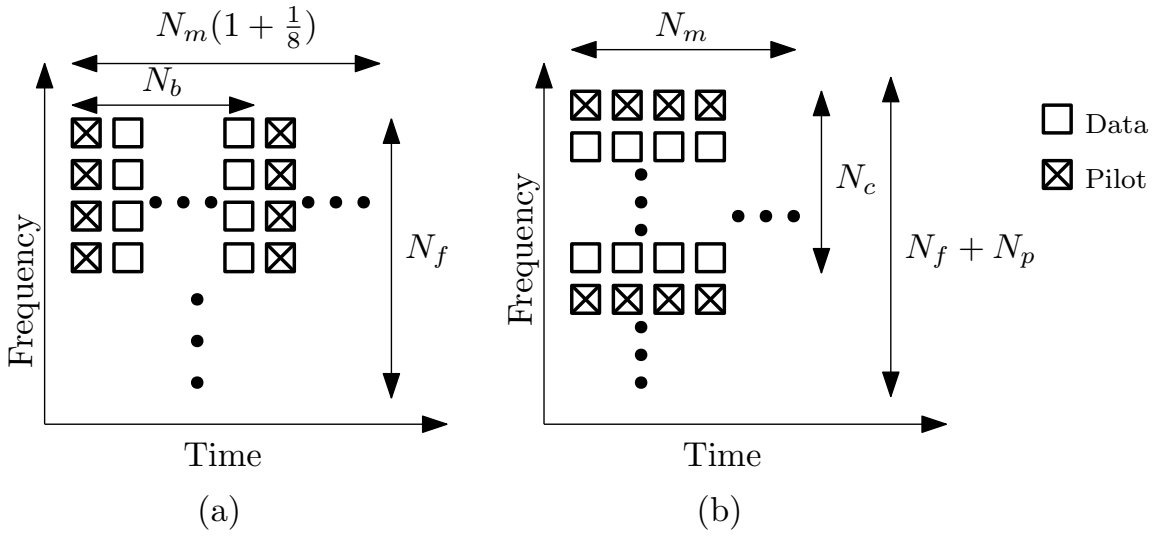

Figure 3.12: Types of SISO channel estimation: (a) Block Pilot, (b) Comb Pilot.

in both the original number of subcarriers ($N_{fft} = 4096$) and the pilot ($N_p = \frac{N_{fft}}{8} = 512$). At the receiver end, the estimated CFR in pilot position subcarriers can be calculated. Moreover, the rest of the remaining subcarriers' estimated CFR can be calculated accurately by using the interpolation algorithm [95]. To be more concrete, the interpolation cubic spline model, which is described in [96], has been constructed to create the estimated CFR in both zero-comb and NZCP approaches.

3.7 Summary of the Chapter

In this Chapter, the main SISO/MIMO -PLC models have been described, including the construction of CIR and CFR and the principle of the MIMO-PLC. All the parameters of each different path of PLC channels have been listed. Furthermore, another type of error correction code - LDPC has been described in detail, including the Tanner graph, the structure of the sparse matrix, the encoding and the soft decision process. The channel combining and splitting, the polar code construction and the successive cancellation decoder methods have been introduced in this chapter as well. Moreover, the PDF function of SαS distribution impulsive noise is given. Because the stable distribution is one of the Gaussian distribution, the PDF of SαS is the same as the PDF of AWGN when $\alpha = 2$. Finally, the channel estimation methods - the block pilot and the comb pilot in the SISO system are introduced. In a word, all these theoretical backgrounds are the basic principle architecture of the following chapters.

Chapter 4

MRC in uncoded/coded SISO-Multipath PLC channel with AWGN and SαS noise

4.1 Introduction

In this Chapter, the different multipath PLC system models with varying noise channels and distinct equalizers has been introduced. Firstly, the Chapter examines the construction of real-valued OFDM input signal by using Hermitian symmetry. Secondly, the three different types of equalizers - ZF, MMSE and the proposed MRC are derived for the PLC channel and their performance is investigated for uncoded and coded (polar and LDPC codes) systems. Furthermore, the SαS distribution based impulsive noise is utilized in the SISO-PLC channel to investigate its impact on the system performance by using different values of α and different types of the equalizers, and error correcting codes. Finally, for higher order QAM systesm, the impulsive noise impact and the optimization of the proposed MRC equalizer are investigated over both uncoded and coded systems too.

4.2 System model

We consider a multipath SISO-PLC system with information binary of length K bits. The code rate is set to $1/2$ with codeword of length $N = 2 \times K$. The codeword is mapped to a 16-QAM constellation to generate a hexadecimal input signal. Af-

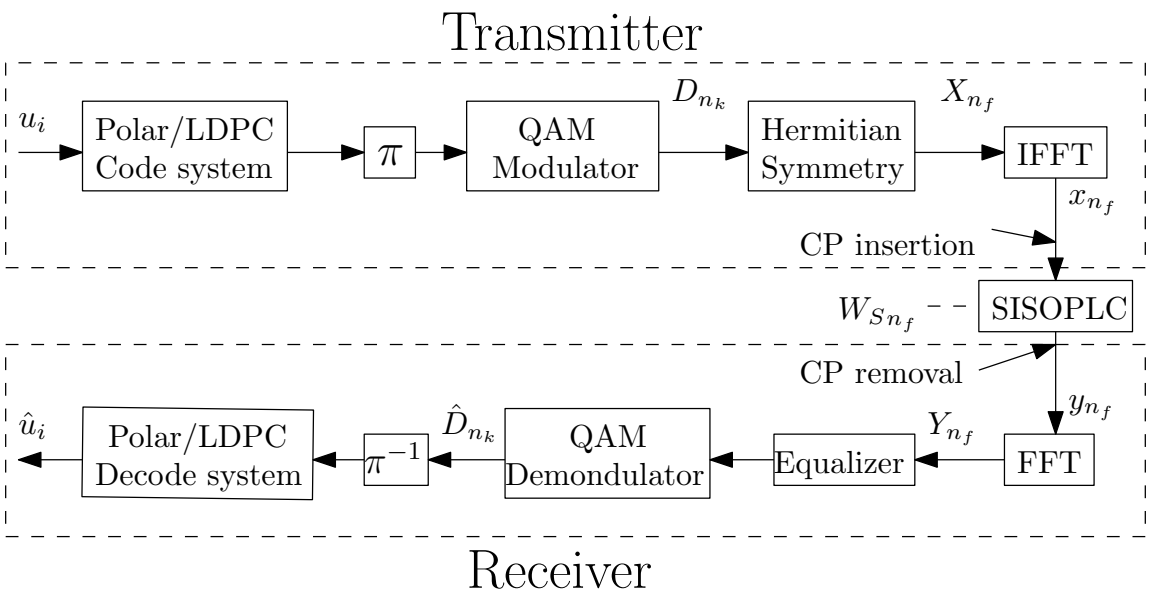

Figure 4.1: SISO-PLC channel model.

ter the Hermitian symmetry and OFDM modulation, the input real-valued OFDM transmitted signal with a length of N_f subcarriers went through the multipath PLC with noise channel. The system modeling can be seen in Fig. 4.1, where π denotes the interleaver and π^{-1} denotes the de-interleaver. The channel interleaver rearranges the encoded symbols in order to disperse the continuous symbols from each other as much as possible, which breaks the burst error of the continuous symbols with time correlation. [97]

4.3 Transmitter with real-valued OFDM signal

The Hermitian symmetry in the transmitted signal processing has been shown in (4.1)

$$X_{n_f} = [\mathrm{Re}(D_0),\ D_1, \ldots, D_{N_k-1}\ \mathrm{Im}(D_0),\ D^{\dagger}_{N_f-N_k+1}, \ldots, D^{\dagger}_{N_f-1}], \tag{4.1}$$

where D_k is the input of OFDM, which is also the output signal after the mapping of M-ary input to the Gray-encoded constellation vector C, N_k is the length of the QAM signal and the index $n_k = 0, 1, \ldots, N_k - 1$. N_f is the double length of N_k. $(*)^{\dagger}$ denotes the conjugate of the matrix. Thus, the real-valued time domain of the OFDM output signal can be implemented using the IFFT as [55]

$$x_{n_f} = \frac{1}{\sqrt{N_f}} \sum_{n_f=0}^{N_f-1} X_{n_f} e^{\frac{j2n_f n_f}{N_f}}, \tag{4.2}$$

where x_{n_f} is the OFDM signal in time domain, $n_f = 0, 1, 2, ..., N_f - 1$ denotes the index of the N_f.

To avoid the Inter-Symbol Interference (ISI) introduced by the multipath delay spread, the CP is inserted in each OFDM symbol at the start of the OFDM signal in time domain. The CP length should be larger than the maximum delay spread of the PLC channel to avoid ISI and preventing the previous OFDM multipath from interfering with the present OFDM symbol. The CP is filled in the blank transmission period because the content of CP can implement cyclic convolution. In other words, it can effectively guarantee the loss of orthogonality caused by frequency offset and effectively suppress Inter-Channel Interference (ICI). The input signal before the PLC channel in this system can be expressed as

$$x_{cp} = [x_{N_f - N_{cp}}, \ldots, x_{N_f - 1}, x_0, \ldots, x_{N_f - 1}], \tag{4.3}$$

where N_{cp} is the length of the cyclic prefix, x_{cp} is the time domain of OFDM signal added cyclic prefix.

4.4 Receiver of SISO-PLC channel

In a multipath fading channel, the relationship between input and output in the frequency domain can be defined as

$$Y_{n_f} = X_{n_f} H_{n_f} + W_{Sn_f}, \tag{4.4}$$

where Y_{n_f} is the received symbols, X_{n_f} is the input symbols, H_{n_f} is the channel frequency response and W_{Sn_f} denotes the noise channel.

4.4.1 Zero Forcing Equalizer

In systems with complex-valued base-band OFDM symbols, a typical ZF equalizer will be of the form.

$$G_{n_f}^{ZF} = \frac{1}{H_{n_f}}, \tag{4.5}$$

where the frequency response of PLC channel H_{n_f} as a denominator cannot be zero. The received signal after the ZF equalizer can be given as

$$R_{n_f}^{ZF} = Y_{n_f} G_{n_f}^{ZF} = (X_{n_f} H_{n_f} + W_{Sn_f}) G_{n_f}^{ZF}. \tag{4.6}$$

However, in the PLC system, we required a real-valued OFDM symbol, thus, Hermitian symmetry has been introduced at the transmitter. This in turn implies that there is frequency diversity that can be exploited at the receiver to improve performance by combining received symbols at the corresponding frequency bins, i.e. as reflected in (4.1). In this thesis, two equalizer approaches, namely, ZF and MMSE have been considered to give a contrast with the novel proposed MRC. For both ZF and MMSE equalizer, the received signal vector can be defined as

$$\mathbf{R} = [R_0 + jR_{N_k}, \frac{1}{2}(R_{n_k} + R_{N_f - n_k}^{\dagger})], \text{ except } n_k = 0, \tag{4.7}$$

where $\mathbf{R} \in \mathbb{C}^{N_k \times 1}$ is the received signal after combining the received symbols. n_k is the index of length of the QAM signal. The received signal sample at the 0-th subcarrier of ZF equalizer is processed as follows

$$\begin{aligned} R_0^{ZF} &= \frac{X_0 H_0}{H_0} + j\frac{X_{N_k} H_{N_k}}{H_{N_k}} \\ &+ \frac{W_{S0}}{H_0} + j\frac{W_{SN_k}}{H_{N_k}} \\ &= X_0 + jX_{N_k} + \frac{W_{S0}}{H_0} + j\frac{W_{SN_k}}{H_{N_k}}. \end{aligned} \tag{4.8}$$

The remaining subcarriers, n_k, are re-constructed by averaging the output of ZF equalizer at the corresponding frequency bins as dictated by the Hermitian symmetry property, i.e.

$$\begin{aligned} R_{n_k}^{ZF} &= \frac{1}{2}\left(Y_{n_k} G_{n_k}^{ZF} + Y_{N_f - n_k}^{\dagger} G_{N_f - n_k}^{ZF\dagger}\right) \\ &= \frac{1}{2}\left(\frac{X_{n_k} H_{n_k} + W_{Sn_k}}{H_{n_k}} + \frac{X_{N_f - n_k}^{\dagger} H_{N_f - n_k}^{\dagger} + W_{S N_f - n_k}^{\dagger}}{H_{N_f - n_k}^{\dagger}}\right) \\ &= \frac{1}{2}\left(X_{n_k} + X_{N_f - n_k}^{\dagger} + \frac{W_{Sn_k}}{H_{n_k}} + \frac{W_{S N_f - n_k}^{\dagger}}{H_{N_f - n_k}^{\dagger}}\right) \\ &= X_{n_k} + \frac{1}{2}\left(\frac{W_{Sn_k}}{H_{n_k}} + \frac{W_{S N_f - n_k}^{\dagger}}{H_{N_f - n_k}^{\dagger}}\right), \ except \ n_k = 0. \end{aligned} \tag{4.9}$$

4.4.2 Minimum Mean Square Equalizer

As the term suggests, MMSE is to get the minimized mean square deviation between the actual transmitted signal and the detected signal. The received signal using MMSE equalizer can be defined as

$$R_{n_f}^{MMSE} = G_{n_f}^{MMSE} Y_{n_f} = X_{n_f} H_{n_f} G_{n_f}^{MMSE} + W_{Sn_f} G_{n_f}^{MMSE}, \tag{4.10}$$

where G^{MMSE} denotes the MMSE coeffcient which can be demonstrated as

$$G_{n_f}^{MMSE} = \frac{H_{n_f}^{\dagger}}{H_{n_f} H_{n_f}^{\dagger} + \frac{1}{\gamma_s}}, \tag{4.11}$$

where γ_s represents the signal-noise-ratio in linear. In QAM system, γ_s represents the $SNR \times \log_2(M)$ in linear, where M is the order of QAM modulator. Combining Eq.(4.7), (4.10) and (4.11), the received signal sample of MMSE at the 0-th subcarrier, is processed as follows

$$\begin{aligned} R_0^{MMSE} &= \frac{X_0 H_0^2 \gamma_s}{H_0^2 \gamma_s + 1} + j \frac{X_{N_k} H_{N_k}^2 \gamma_s}{H_{N_k}^2 \gamma_s + 1} \\ &+ \frac{W_{S0} H_0^{\dagger} \gamma_s}{H_0^2 \gamma_s + 1} + j \frac{W_{SN_k} H_{N_k}^{\dagger} \gamma_s}{H_{N_k}^2 \gamma_s + 1} \\ &= X_0 + j X_{N_k} + \frac{W_{S0} H_0^{\dagger} \gamma_s - X_0}{H_0^2 \gamma_s + 1} + j \frac{W_{SN_k} H_{N_k}^{\dagger} \gamma_s - X_{N_k}}{H_{N_k}^2 \gamma_s + 1}, \end{aligned} \tag{4.12}$$

The remaining subcarriers, n_k, are re-constructed by averaging the output of MMSE equalizer at the corresponding frequency bins is demonstrated as

$$
\begin{aligned}
&R_{n_k}^{MMSE} = \\
&= \frac{1}{2}\left(\frac{X_{n_k}|H_{n_k}|^2\gamma_s}{|H_{n_k}|^2\gamma_s+1} + \frac{W_{Sn_k}H_{n_k}^{\dagger}\gamma_s}{|H_{n_k}|^2\gamma_s+1} + \frac{X_{N_f-n_k}^{\dagger}|H_{N_f-n_k}|^2\gamma_s}{|H_{N_f-n_k}|^2\gamma_s+1} + \frac{W_{S_{N_f-n_k}}^{\dagger}H_{N_f-n_k}\gamma_s}{|H_{N_f-n_k}|^2\gamma_s+1}\right), \\
&= \frac{1}{2}\left(X_{n_k} + X_{N_f-n_k} + \frac{W_{Sn_k}H_{n_k}^{\dagger}\gamma_s - X_{n_k}}{|H_{n_k}|^2\gamma_s+1} + \frac{W_{S_{N_f-n_k}}^{\dagger}H_{N_f-n_k}\gamma_s - X_{N_f-n_k}^{\dagger}}{|H_{N_f-n_k}|^2\gamma_s+1}\right), \\
&= X_{N_k} + \frac{1}{2}\left(\frac{W_{Sn_k}H_{n_k}^{\dagger}\gamma_s - X_{n_k}}{|H_{n_k}|^2\gamma_s+1} + \frac{W_{S_{N_f-n_k}}^{\dagger}H_{N_f-n_k}\gamma_s - X_{N_f-n_k}^{\dagger}}{|H_{N_f-n_k}|^2\gamma_s+1}\right), \qquad (4.13)
\end{aligned}
$$

(except $n_k = 0$).

where $|H|^2 = HH^{\dagger}$.

4.4.3 Maximum Ratio Combining

The MRC principle is that each uncorrelated diversity branch at the receiver is phase-corrected, weighted and added according to the appropriate variable gain and then sent to the detector for coherent detection. Normally, this approach is utilized in MIMO system [98, 99] or other fading channels [100, 101]. In this thesis, Because the real-valued input OFDM signal is a conjugate matrix, the received signal can be regarded as two parts. The SISO-PLC system can be regarded as a SIMO system. The MRC detector can be utilized at the receiving end to adjust the influence of the fading channel.

The MRC receiver works in a similar manner for the 0-th subcarrier, that is

$$R_0^{MRC} = R_0^{ZF} \approx R_0^{MMSE}. \qquad (4.14)$$

However, for the remaining subcarriers, it combines the corresponding samples as

$$R_{n_k}^{MRC} = \frac{Y_{n_k}H_{n_k}^{\dagger} + Y_{N_f-n_k}^{\dagger}H_{N_f-n_k}}{|H_{n_k}|^2 + |H_{N_f-n_k}|^2}. \qquad (4.15)$$

After substituting (4.4) and some straight-forward mathematical manipulations, we

obtain

$$\begin{aligned} R_{n_k}^{MRC} =& \frac{X_{n_k} H_{n_k} H_{n_k}^{\dagger} + X_{N_f-n_k}^{\dagger} H_{N_f-n_k}^{\dagger} H_{N_f-n_k}}{|H_{n_k}|^2 + |H_{N_f-n_k}|^2} \\ &+ \frac{W_{Sn_k} H_{n_k}^{\dagger} + W_{S_{N_f-n_k}}^{\dagger} H_{N_f-n_k}}{|H_{n_k}|^2 + |H_{N_f-n_k}|^2} \\ =& X_{n_k} + \frac{W_{Sn_k} H_{n_k}^{\dagger} + W_{S_{N_f-n_k}}^{\dagger} H_{N_f-n_k}}{|H_{n_k}|^2 + |H_{N_f-n_k}|^2}, \\ & (\text{ except } n_k = 0). \end{aligned} \tag{4.16}$$

A closer look at (4.9) and (4.16) reveals that the only difference is in the manner that the noise part of the received signal is processed.

4.4.4 Analysis of LLR in QAM system

At decoded part, the LLR calculation will be based on the PDFs value of SαS impulsive noise. According to (3.42), the elements of the PDF matrix, $\mathbf{P} \in \mathbb{C}^{M \times N_k}$, of the M-ary QAM output symbols can be calculated as

$$P_{mn_k} = \frac{1}{2\pi} \int_{-\infty}^{\infty} \exp(-\gamma^{\alpha} |t|^{\alpha}) e^{-jt|C_m - R_{n_k}|} dt, \tag{4.17}$$

where R_{n_k} is the received signal independent of the equalizer in use at the receiver, $m = 0, 1, \ldots, M-1$, M is the number of order of QAM, $|C_m - R_{n_k}|$ is the Euclidean distance which can be defined as

$$|C_m - R_{n_k}| = \sqrt{[\mathbf{Re}(C_m) - \mathbf{Re}(R_{n_k})]^2 + [\mathbf{Im}(C_m) - \mathbf{Im}(R_{n_k})]^2}. \tag{4.18}$$

When α is 2, the SαS distribution noise is regarded as AWGN. The variance in Gaussian distribution σ^2 is $2\gamma^2$ in SαS. Hence, the standard SαS distribution noise PDF with the M-ary symbols can be derived as

$$p(|C_m - R_{n_k}|,\ \gamma) = \frac{1}{2\gamma\sqrt{\pi}} \exp \frac{(-|C_m - R_{n_k}|^2)}{(2\gamma)^2}. \tag{4.19}$$

Assume that the system gives 16-QAM modulation input signal with $\alpha = 2$ of the impulsive noise, the bit $b_0,\ b_1,\ b_2,\ b_3$ was given by the received symbols R_k. For the

Gray constellation of 16-QAM, the bit can be defined as

$$b_0 = \begin{cases} 0, \ C^{\mathrm{I}} = -3, -1 \\ 1, \ C^{\mathrm{I}} = +1, +3, \end{cases} b_1 = \begin{cases} 0, \ C^{\mathrm{I}} = -3, +3 \\ 1, \ C^{\mathrm{I}} = -1, +1, \end{cases} \tag{4.20}$$

$$b_2 = \begin{cases} 0, \ C^{\mathrm{Q}} = -3, -1 \\ 1, \ C^{\mathrm{Q}} = +1, +3, \end{cases} b_3 = \begin{cases} 0, \ C^{\mathrm{Q}} = -3, +3 \\ 1, \ C^{\mathrm{Q}} = -1, +1, \end{cases} \tag{4.21}$$

where C^{I} is the real part of the constellation and C^{Q} is the imaginary part of the constellation. According to the equation (4.19), the $LLR_{R_{n_k}}(b_0)$ of the received symbol at the n_k-th subcarrier, R_{n_k}, can be computed as

$$\begin{aligned} LLR_{R_{n_k}}(b_0) &= \ln \frac{p(R_{n_k}|b_0 = 1)}{p(R_{n_k}|b_0 = 0)} \\ &= \ln \frac{e^{\frac{(-|R^{\mathrm{I}}_{n_k} - 1|^2)}{(2\gamma)^2}} + e^{\frac{(-|R^{\mathrm{I}}_{n_k} - 3|^2)}{(2\gamma)^2}}}{e^{\frac{(-|R^{\mathrm{I}}_{n_k} + 1|^2)}{(2\gamma)^2}} + e^{\frac{(-|R^{\mathrm{I}}_{n_k} + 3|^2)}{(2\gamma)^2}}}. \end{aligned} \tag{4.22}$$

The value of the $LLR_{R_{n_k}}(b_0)$ can be easy to calculate as

$$LLR_{R_{n_k}}(b_0) = \begin{cases} \frac{2}{\gamma^2}(R^{\mathrm{I}}_{n_k} + 1), & R^{\mathrm{I}}_{n_k} < -2 \\ \frac{1}{\gamma^2} R^{\mathrm{I}}_{n_k}, & -2 \leqslant R^{\mathrm{I}}_{n_k} < 2 \\ \frac{2}{\gamma^2}(R^{\mathrm{I}}_{n_k} - 1), & R^{\mathrm{I}}_{n_k} > 2. \end{cases} \tag{4.23}$$

The relationship between received bits and the Gray constellation has been defined in equations (4.20)-(4.21), hence, the LLR of b_1, b_2, b_3 can be calculated as

$$LLR_{R_{n_k}}(b_1) = -\frac{1}{\gamma^2}(|R^{\mathrm{I}}_{n_k}| + 2), \ \forall \ R^{\mathrm{I}}_{n_k}, \tag{4.24}$$

$$LLR_{R_{n_k}}(b_2) = \begin{cases} \frac{2}{\gamma^2}(R^{\mathrm{Q}}_{n_k} + 1), & R^{\mathrm{Q}}_{n_k} < -2 \\ \frac{1}{\gamma^2} R^{\mathrm{Q}}_{n_k}, & -2 \leqslant R^{\mathrm{Q}}_{n_k} < 2 \\ \frac{2}{\gamma^2}(R^{\mathrm{Q}}_{n_k} - 1), & R^{\mathrm{Q}}_{n_k} > 2, \end{cases} \tag{4.25}$$

$$LLR_{R_{n_k}}(b_3) = -\frac{1}{\gamma^2}(|R^{\mathrm{Q}}_{n_k}| + 2), \ \forall \ R^{\mathrm{Q}}_{n_k}. \tag{4.26}$$

Based on the calculation, the $LLR_{R_{n_k}}(b_{\log_2(M)-1})$, of all received symbols R_{n_k} in M-ary QAM system can be calculated. The SC decoder of the polar codes system and the LDPC decoder [78] can give the soft decision to get the output information

bit $\hat{u} = \left\{\hat{u}_0, \hat{u}_1, \ldots, \hat{u}_{K-1}\right\}$ by using the $LLR_{R_k}(b_{\log_2(M)-1})$.

4.5 Results

In our investigation, the BER vs. E_b/N_0 diagram has been utilized to measure the performance of the PLC channel system by using different equalizers over either uncoded or coded system. With the different multipaths of the PLC channel, the performance shows in the BER diagram has a considerable difference as well. To make a fair comparison in the simulation, the length of the information data has been set to 1024 with 1/2 code rate in all coded systems. Thus, the size of the input codeword is 2048 and the length of the input 16-QAM signal is 512. The length of the OFDM subcarrier after Hermitian symmetry is the double length of the 16-QAM signal, which is 1024. The PLC channel bandwidth of 20 MHz is considered and the sample frequency is 50 MHz, which is larger than twice of the bandwidth. The length of the impulse response of the PLC system is 200, because the value of CIR is almost 0 after the 200^{th} subcarrier. Meanwhile, the length of the CP is the 1/4 of the length of the subcarrie which is larger than the CIR.

4.5.1 Multipath PLC channel results

Fig. 4.2 presented the BER vs. E_b/N_0 performance by using 4-path, 5-path and 15-path PLC over uncoded AWGN noise channel system. Meanwhile, three types of equalizers have been used to avoid channel fading. The performance of ZF and MMSE over the same circumstance have a more negligible difference. The E_b/N_0 gap between MRC and MMSE over the 4-path PLC channel is about 22 dB when the BER of 10^{-4}. Also, in 5-path and 15-path PLC channel model, the gap between two equalizers is about 15.5 dB and 14 dB when the BER of 10^{-4}. In other words, the MRC approach can give better BER performance than ZF and MMSE over uncoded multipath PLC channels. Compared to different multipath path PLC channel models over MRC equalizer, the E_b/N_0 of 4-path, 5-path and 15-path is about 15, 20.5 and 32 dB when the BER of 10^{-4}, respectively.

Fig. 4.3 attains the performance of the 4-path, 5-path and 15-path PLC channel over the LDPC coded system. The LDPC codes can significantly improve the performance of each different multipath PLC channel with different equalizers compared

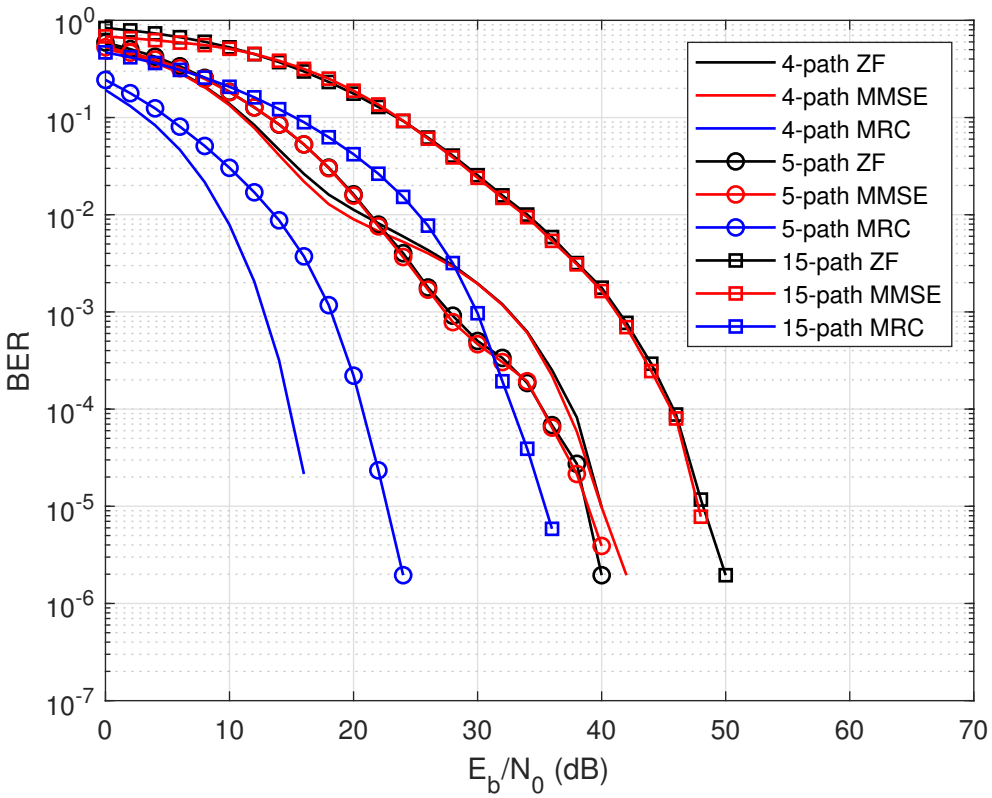

Figure 4.2: 4-path, 5-path and 15-path PLC channel with ZF, MMSE and MRC equalizers over uncoded system.

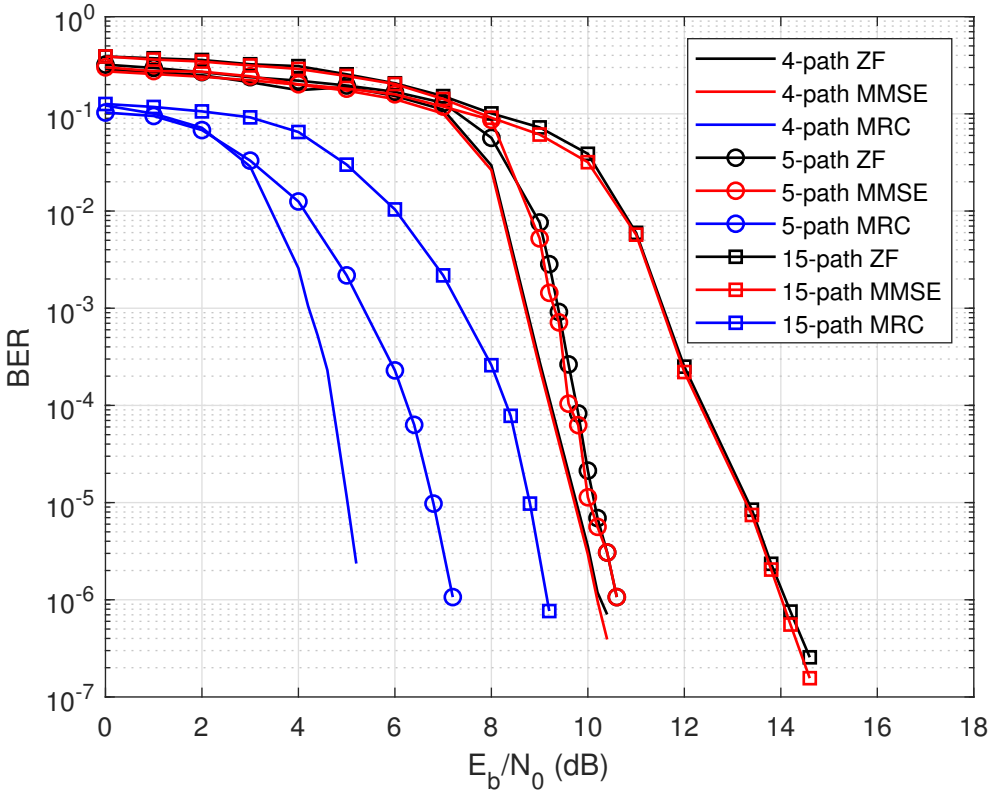

Figure 4.3: Different multipath PLC over LDPC coded system.

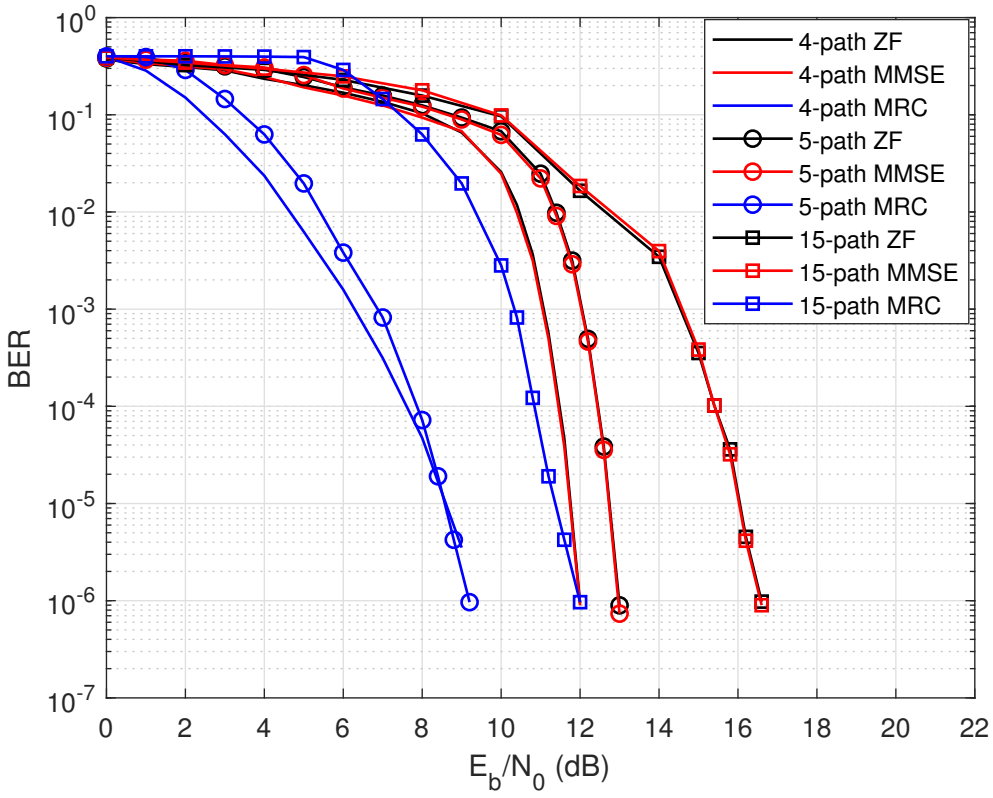

Figure 4.4: Different multipath PLC over polar coded system.

to the uncoded system. In the 4-path PLC channel, at a BER of 10^{-5}, the E_b/N_0 value of ZF is almost the same as the MMSE and worse about 5 dB than the MRC. The same situation can be demonstrated over 5-path and 15-path PLC cahnnel, for instance at a BER of 10^{-5}, there is approximately 3.2 and 4.3 dB improvement in E_b/N_0 between proposed MRC and ZF/MMSE over two different multipath PLC channel systems.

Fig. 4.4 presents the BER performance of polar codes with the design-SNR of the main channel being 0 dB over the PLC channel system with different equalizers. Even the BER performance is better than uncoded system, compared to the LDPC coded system, it still worse about 3.5 dB E_b/N_0 than the system over the 4-path PLC channel with MRC equalizer by using LDPC coded system at a BER of 10^{-5}.

4.5.2 Uncoded SαS noise channel results

Fig. 4.5 investigates the impact of the uncoded PLC system over SαS distribution noise channel with the value of α is $2, 1.8$ and 1.5 including ZF, MMSE and MRC equalizers in contrast on the BER performance. As the value of α is getting smaller, the noise impulse is becoming more and more significant. And the impact is more

substantial. It is evident that the PLC system with MRC equalizer can attain the best BER performance when $\alpha = 2$. The E_b/N_0 with $\alpha = 1.8$ system is about 4.5 dB worse than that of the $\alpha = 2$ at a BER level of 10^{-5}. Moverover, The E_b/N_0 of the system over $\alpha = 1.5$ SαS noise is about 8.5 dB worse than the $\alpha = 1.8$ noise system at the same BER level. Furthermore, the performance of both MMSE and ZF equalizers is worse than the proposed MRC detector over the SαS noise channel. Compared to Fig. 4.2, the impact of SαS impulsive noise significantly against the impact of AWGN noise channel. At a BER of 10^{-4}, the E_b/N_0 of AWGN noise in the PLC channel is about 15 dB. In contrast, the best BER performance of SαS noise is about 22 dB E_b/N_0 at the BER of 10^{-4}, which is much worse than the AWGN niose channel system.

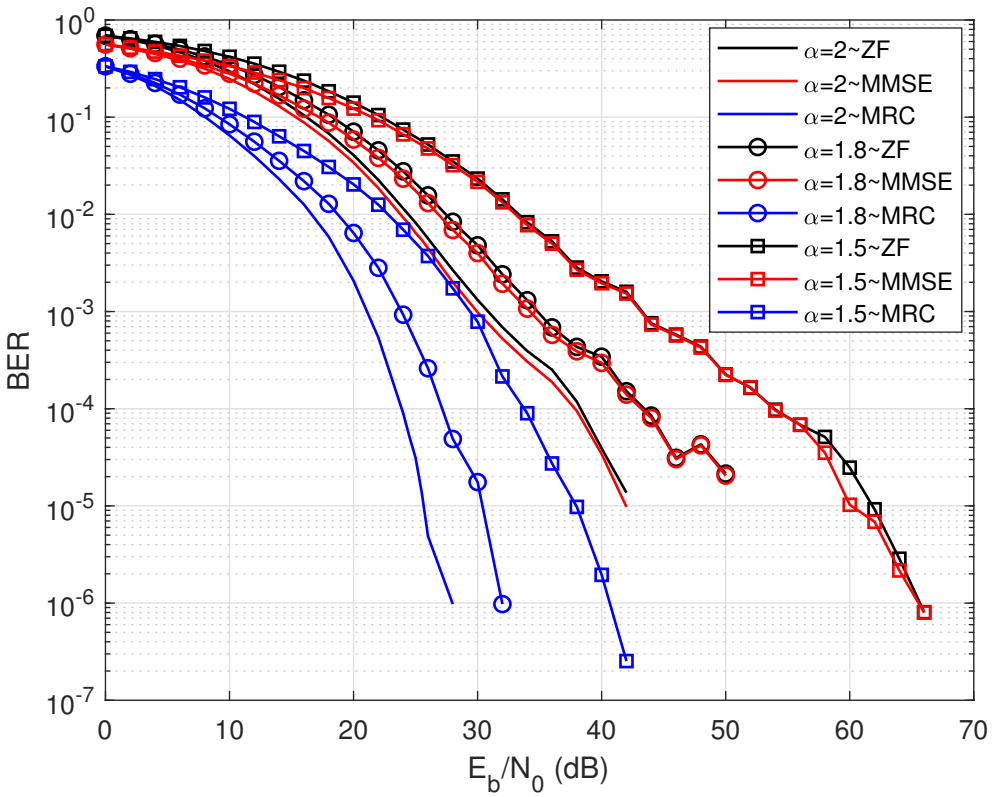

Figure 4.5: 16-QAM PLC over uncoded SαS noise channel with different value of α.

Fig. 4.6 displays the BER peformance by using the SαS distribution noise over the uncoded PLC system with 256-QAM input signal. As expected, the overall value of the E_b/N_0 is totally worse than the 16-QAM system. For instance the E_b/N_0 is about 37 dB over the 256-QAM input signal system with the proposed MRC equalizer and the SαS ($\alpha = 2$) noise at a BER level of 10^{-5}. In contrast, at the same BER level, the E_b/N_0 of the 16-QAM input signal system is just about

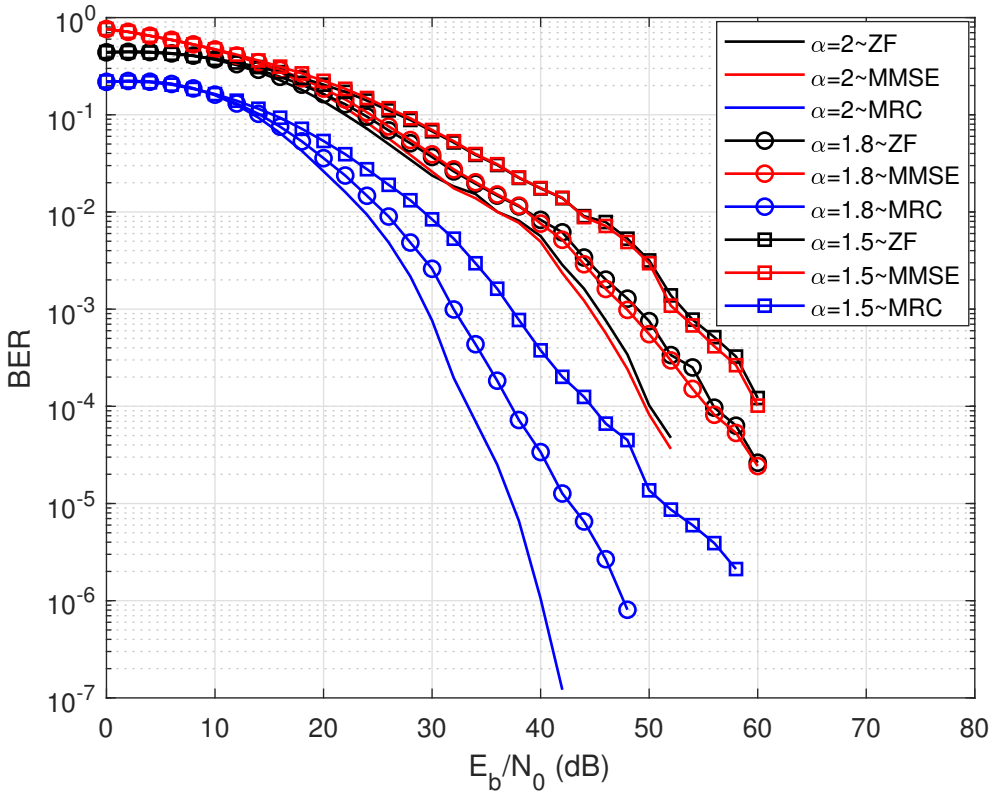

Figure 4.6: 256-QAM PLC over uncoded SαS noise channel with different value of α.

25 dB.

4.5.3 Coded-PLC system over AWGN/SαS noise channel with 16/256-QAM input signal

Fig. 4.7 plots the contrast of BER performance between both LDPC and polar code system over AWGN noise channel. With the same code rate, the LDPC codes can improve significantly against the BER performance of the SISO-PLC channel with AWGN noise compare to the polar codes. The performance of polar code is about 1.5 dB E_b/N_0 worse than the LDPC code with proposed MRC equalizer and 2.5 dB E_b/N_0 worse than LDPC with both ZF and MMSE equalizer at a BER of 10^{-5}.

The contrast between LDPC and polar codes by using in SαS noise channel can be shown in Fig. 4.8, Fig. 4.9 and Fig. 4.10. The different values of the α will affect the LDPC and polar code PLC channel system to varying degrees. It is evident that the proposed MRC equalizer can demonstrate the best BER performance over the 16-QAM coded system by using SαS noise in any value of α. Furthermore, The slightly impulsive channel ($\alpha = 2$) can give a good performance. On the other

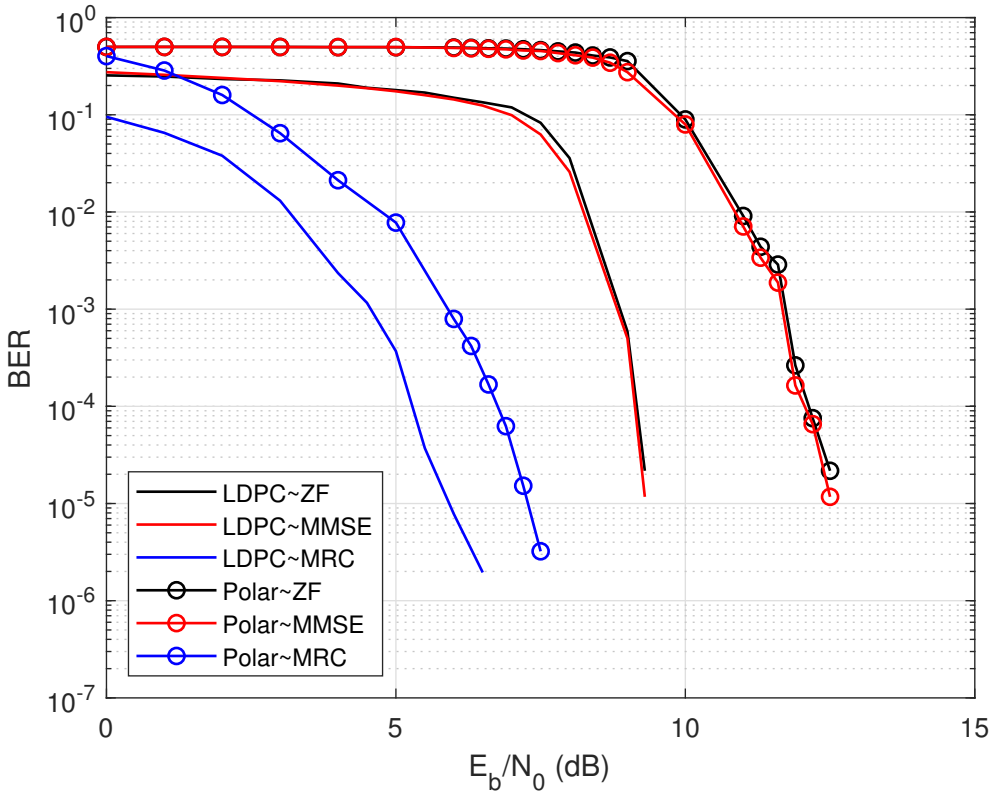

Figure 4.7: 16-QAM PLC over LDPC/Polar code system with AWGN noise.

hand, the extremely impulsive channel ($\alpha = 1.5$) reduces the system's performance. Meanwhile, it can conclude that the LDPC codes can improve the performance of the system better than the polar codes.

The higher order QAM (256-QAM) input signal has been utilized with the SαS noise over coded-PLC channel system. Fig. 4.11, Fig. 4.12 and Fig. 4.13 demonstrated the BER performance by using the different α over 256-QAM coded PLC channel model. As excepted, at a BER of 10^{-5}, the proposed MRC outperforms the alternative equalizers and attains a lowest value of E_b/N_0 is about 14.5 dB when the $\alpha = 2$ by using LDPC codes. With the same situation, the E_b/N_0 is about 17.2 dB by using polar codes which is much worse than the LDPC codes.

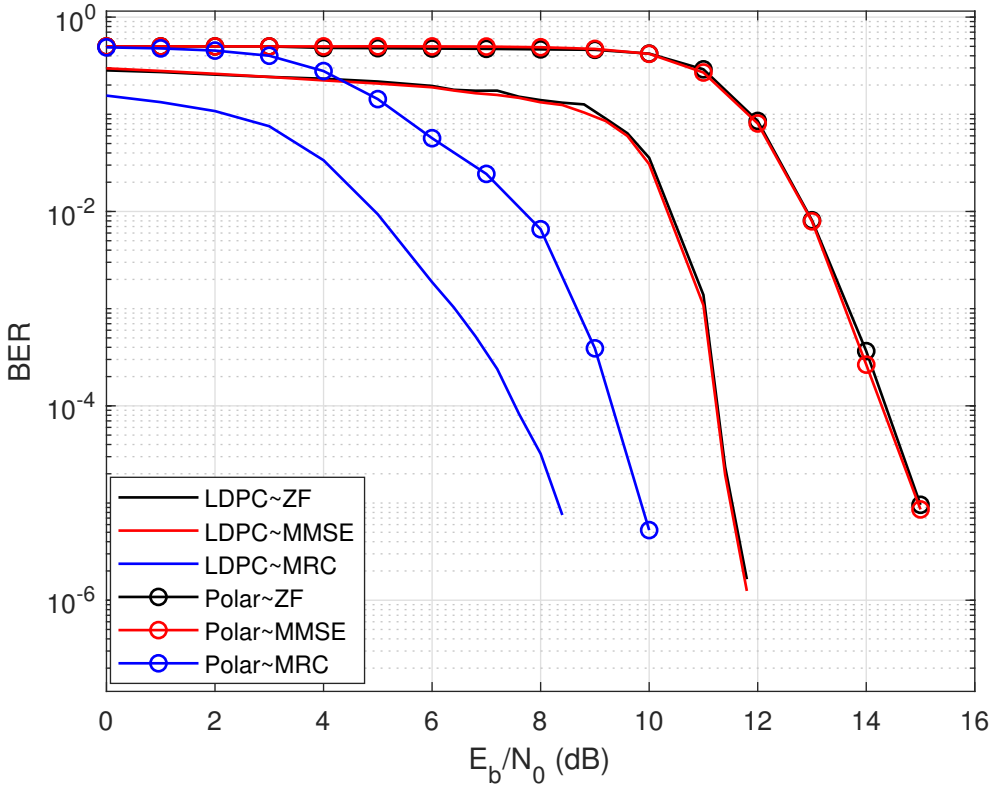

Figure 4.8: 16-QAM PLC over LDPC/Polar code system with SαS noise ($\alpha = 2$).

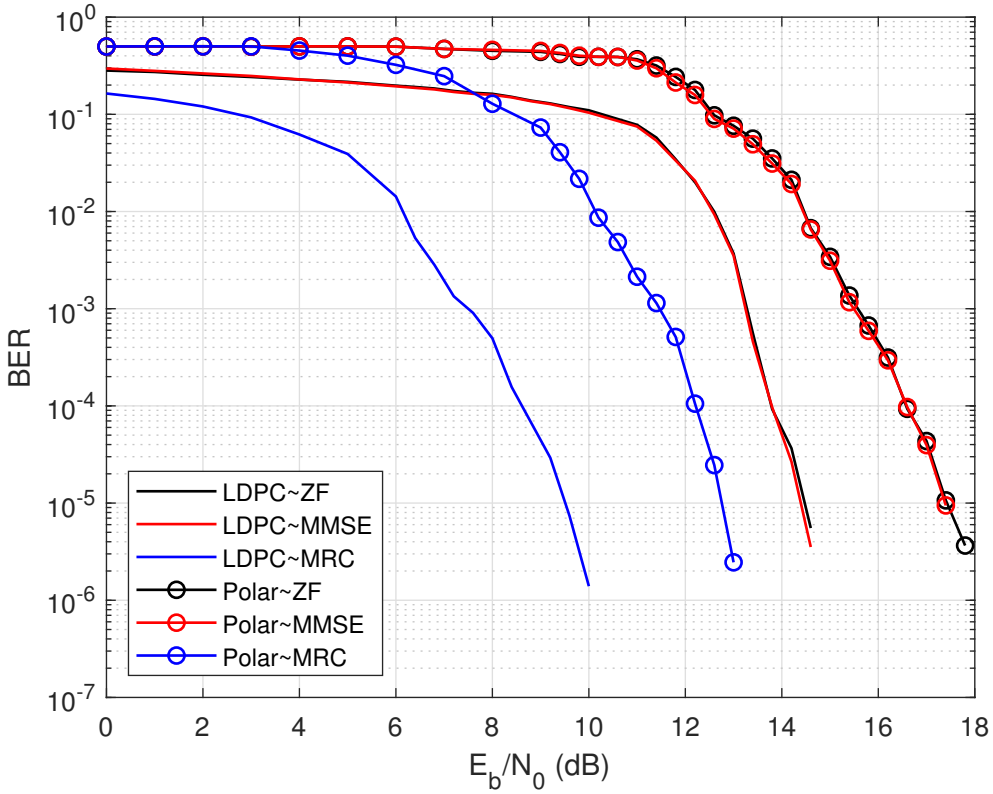

Figure 4.9: 16-QAM PLC over LDPC/Polar code system with SαS noise ($\alpha = 1.8$).

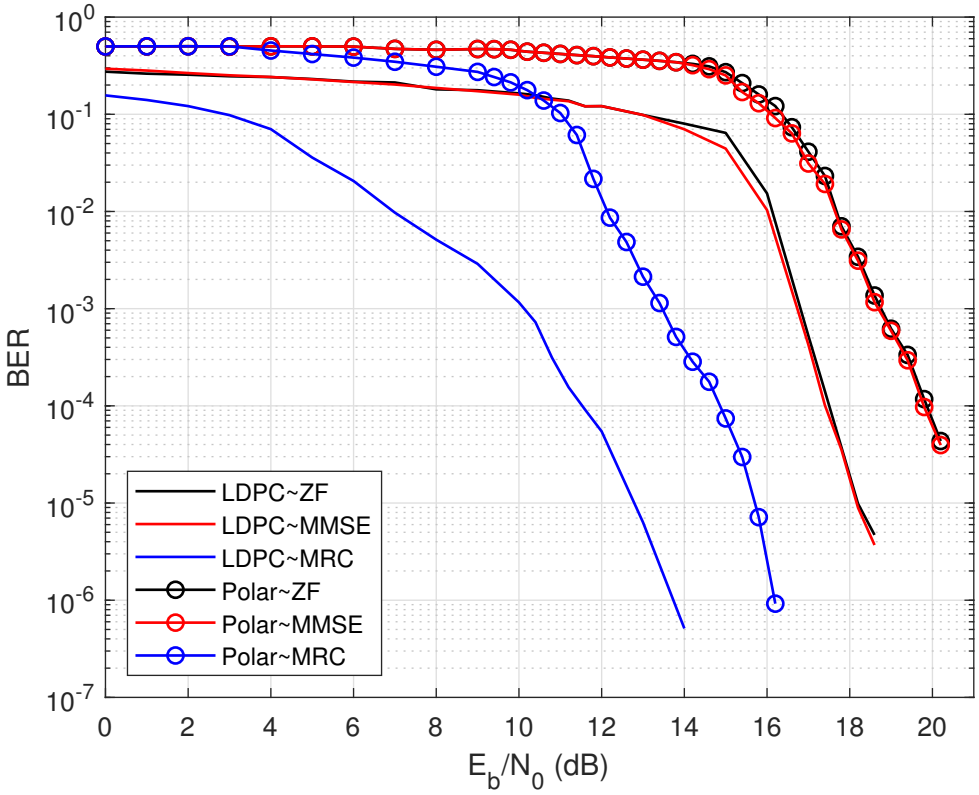

Figure 4.10: 16-QAM PLC over LDPC/Polar code system with SαS noise ($\alpha = 1.5$).

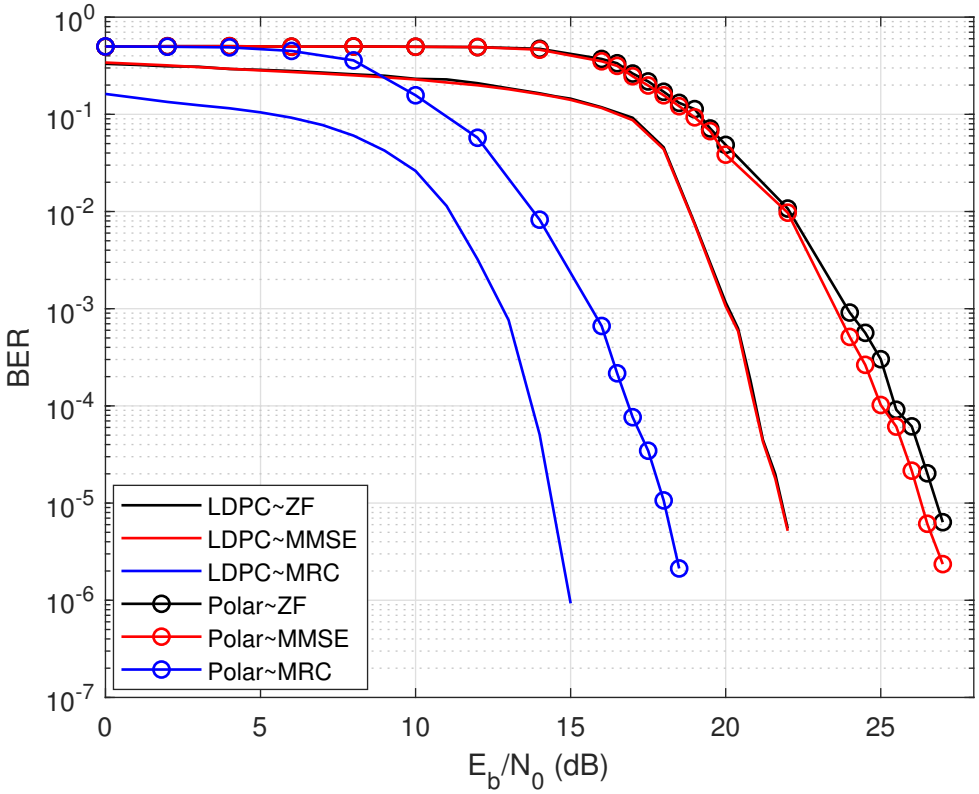

Figure 4.11: 256-QAM PLC over LDPC/Polar code system with SαS noise ($\alpha = 2$).

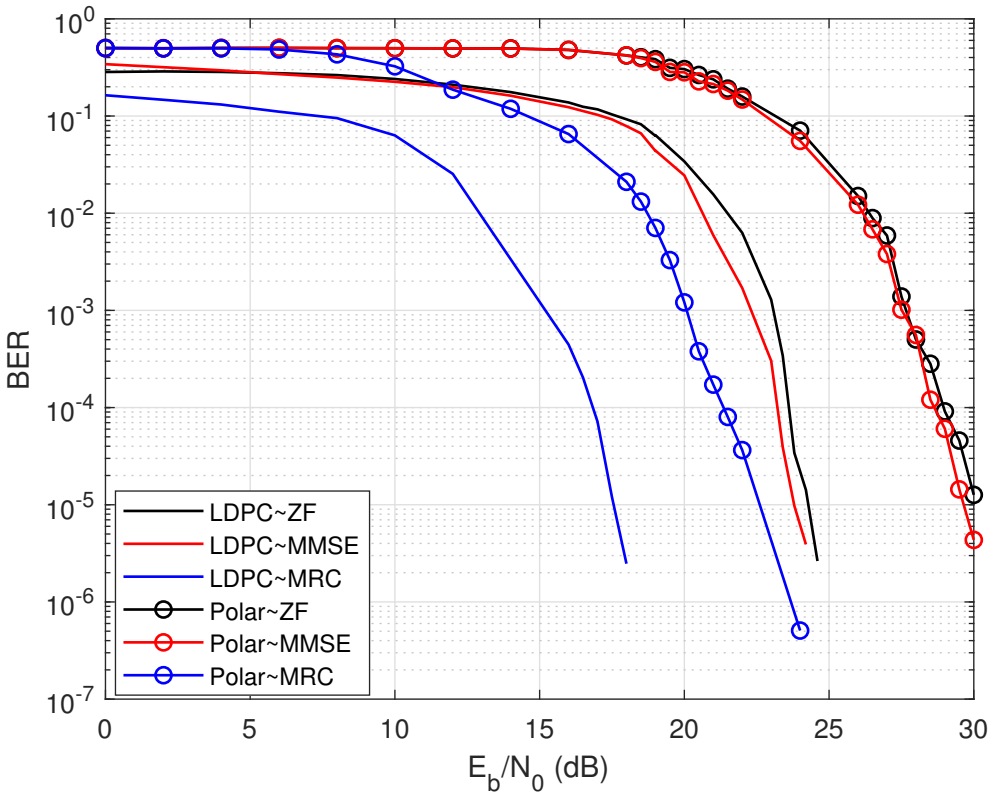

Figure 4.12: 256-QAM PLC over LDPC/Polar code system with SαS noise (α = 1.8).

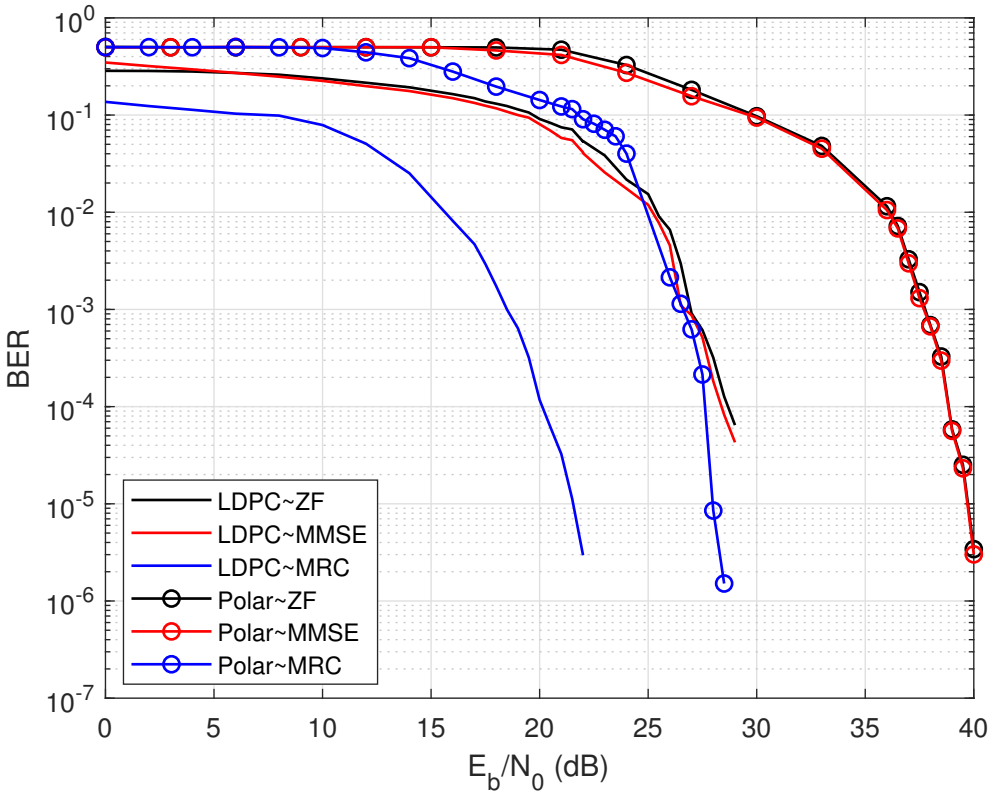

Figure 4.13: 256-QAM PLC over LDPC/Polar code system with SαS noise (α = 1.5).

4.6 Summary of the Chapter

This Chapter investigated the BER performance over 4-path, 5-path and 15-path uncoded/coded PLC channels. Numerical results were provided to demonstrate that the performance of the proposed MRC receiver is much better than the ZF equalizer and MMSE equalizer in either uncoded or coded system with the real-valued OFDM input signal. Moreover, the performance of both LDPC coded and polar coded PLC channel systems with the SαS distribution impulsive noise was analyzed. Compared to the polar codes, the results of the LDPC coded system can demonstrate an improvement in BER performance over both 16-QAM and 256-QAM systems with both AWGN and SαS noise. Furthermore, as expected, the impact of SαS noise on the PLC channel system is much worse than the AWGN and the more severe the impulsive noise parameters, the greater the impact on the system performance, and the worse BER performance is achieved over PLC channel system. In 16-QAM LDPC coded PLC system, the SNR gap between AWGN and SαS noise when $\alpha = 2, 1.8, 1.5$ are 2.4 dB, 3.4 dB and 6.8 dB, respectively, at the BER of 10^{-5}.

Chapter 5

Proposed Averaging - Block/Comb pilot of Channel Estimation over MIMO-PLC system

5.1 Introduction

Nowadays, the MIMO-PLC technology is widely mentioned over the SG and Smart Homes. Thus, more and more researches have been focused on the MIMO-PLC in recent years. This thesis utilizes four different multipath of PLC channels with various parameters to construct a MIMO-PLC model. The block pilot and comb pilot are produced over the MIMO-PLC system to estimate the channel frequency response. The proposed averaging approach is presented to optimize the traditional pilot design method. In this Chapter, the LDPC coded MIMO-PLC channel model with the standard channel estimation method is utilized as a system model. The block pilot and zero-comb pilot, which are the most commonly used in MIMO systems, is presented and utilized using the multipath MIMO-PLC model presented in this chapter.

Furthermore, the proposed averaging approach is shown to operate using both block and the zero-comb (ZCP) pilot approaches. The main elements - weight factors and averaging times of the system that affect the performance of the averaging method are investigated in this chapter. Moreover, the Mean Square Error

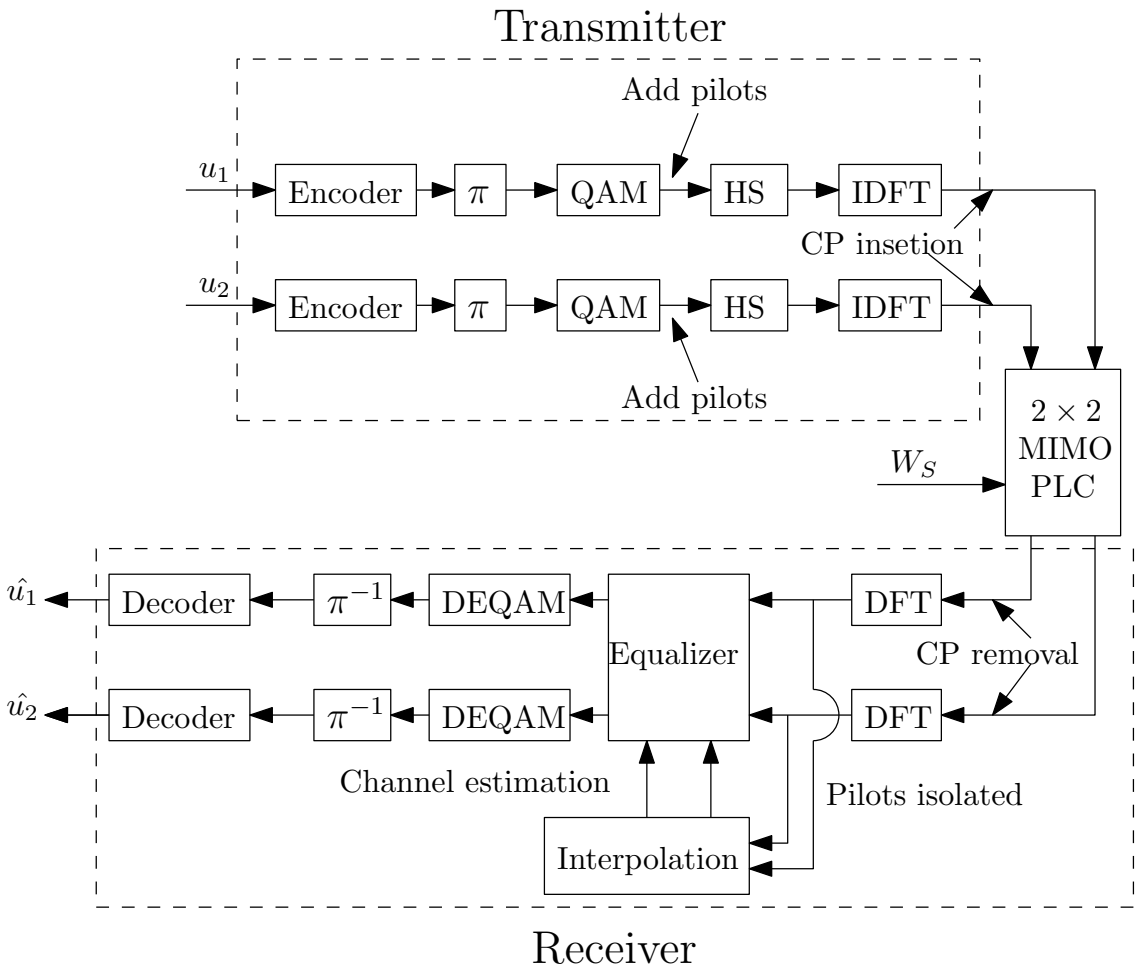

Figure 5.1: Channel Estimation system model.

(MSE) that differentiates between estimated CFR and original CFR is utilized and the performance by using different pilot design methods over distinct conditions of MIMO-PLC channel systems is investigated and analyzed. Finally, the derivation process of the linear and cubic spline interpolation has been demonstrated.

5.2 System model

In Fig. 5.1, a diagram of the channel estimation system structure is illustrated where π denotes the interleaver in the system and π^{-1} represents the deinterleaver. The OFDM modulator/demodulator can be easily achieved by using IFFT/FFT. Before the Hermitian symmetry, the pilot signal is inserted in the constant position of the QAM input signal and isolated before going through the detector. The received pilot can be defined as

$$R_p = P_p H_p + W_{Sp}, \tag{5.1}$$

where p is the index of the pilot position, which is explained in the following section, P denote the input pilot, W_S represents the noise channel, H indicates the original CFR of MIMO-PLC and R_p is the received signal in pilot position.

5.3 Channel Estimation in MIMO system

5.3.1 Block pilot

In the block pilot approach illustrated in Fig. 3.12 (a), the 2×2 MIMO-PLC can be treated as four independent SISO-PLC channels. They can be estimated by transmitting two consecutive pilot blocks, that is, one per transmitter in frequency domain. When the 1st transmitter is activated, $H_{n_f}^{11}$ and $H_{n_f}^{21}$ can be estimated, while $H_{n_f}^{12}$ and $H_{n_f}^{22}$ are obtained when the 2nd transmitter is operated. In this way, cross-channel interference is avoided. The received signal at the n_f-th subcarrier and ρ-th receiver can be given as

$$R_{n_f}^{1,\rho} = X_{n_f}^{1,\rho} H_{n_f}^{1,\rho} + {W_S}_{n_f}^{1,\rho}, \tag{5.2}$$

$$R_{n_f}^{2,\rho} = X_{n_f}^{2,\rho} H_{n_f}^{2,\rho} + {W_S}_{n_f}^{2,\rho}, \tag{5.3}$$

where $R_{n_f}^{1,\rho}$ and $R_{n_f}^{2,\rho}$ are the received samples of the block pilot system. $\rho = 1, 2$ represents the index of the receiver. ${W_S}_{n_f}^{\tau,\rho}$ denotes either AWGN noise or SαS noise, $H_{n_f}^{\tau,\rho}$ is the CFR coefficient of the n_f-th subcarrier of the 2×2 MIMO-PLC channel matrix and $X_{n_f}^{\tau,\rho}$ is the input block pilot OFDM symbol in the frequency domain. For the n_f-th subcarrier, the estimated CFR matrix elements of the block pilot MIMO-PLC system can be estimated as

$$\begin{aligned} \hat{H}_{n_f}^{\tau,\rho} &= \frac{R_{n_f}^{\tau,\rho}}{X_{n_f}^{\tau,\rho}} \\ &= \frac{X_{n_f}^{\tau,\rho} H_{n_f}^{\tau,\rho} + {W_S}_{n_f}^{\tau,\rho}}{X_{n_f}^{\tau,\rho}}. \\ &= H_{n_f}^{\tau,\rho} + \frac{{W_S}_{n_f}^{\tau,\rho}}{X_{n_f}^{\tau,\rho}}. \end{aligned} \tag{5.4}$$

5.3.2 Comb pilot

In the comb pilot system, compared with the traditional SISO system, the Channel State Information (CSI) estimation in the MIMO system is more difficult because the

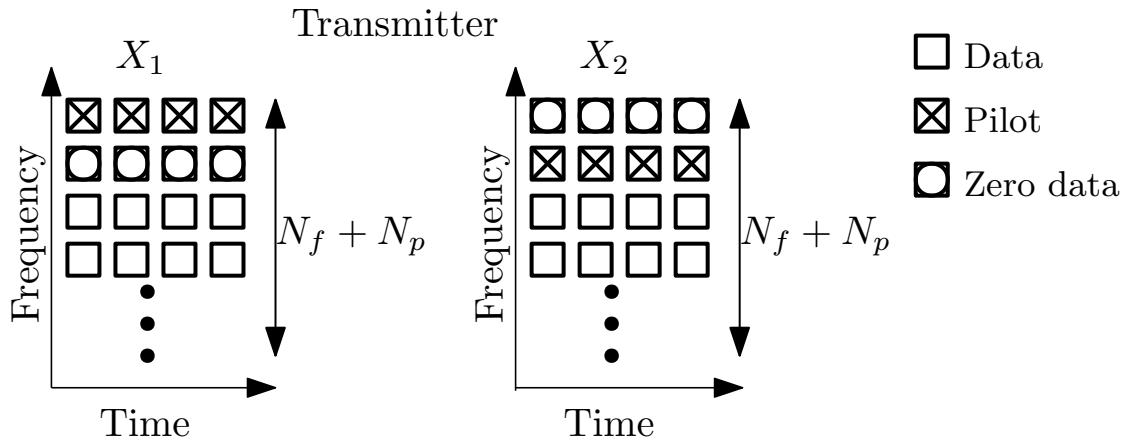

Figure 5.2: Zero-comb pilot model.

signal received on any subcarriers is the superposition of multiple distorted signals due to various devices. The pilot sequences transmitted by different devices need to be orthogonal to each other in the MIMO system. Otherwise, the receiver cannot distinguish each pilot, resulting in channel interference. The time gap, which can be staggered in time, allowing only one device to transmit data at a specific time, has been demonstrated [102].

In block pilot, the number of each OFDM symbol subcarrier is the same as the original OFDM symbol, the system is inserted a new known OFDM symbol in each OFDM block as the pilot. In the comb pilot system, the transmitted OFDM input symbols are the same as the perfectly known channel OFDM input symbols. On the other hand, the length of the subcarrier in each OFDM symbol became large because of the pilot insertion.

5.3.3 Zero-comb pilot

In [103], Lavafi presented a ZCP method to estimate channel frequency domain, which is illustrated in Fig. 5.2. In this paper, the ZCP method is used as a reference method compared to our proposed channel estimation method. In this method, to avoid channel interference, whenever a comb-pilot symbol is added at a subcarrier of a transmitter, a zero subcarrier is added to the subcarrier of adjacent MIMO transmitters. Because the zero subcarrier does not transmit any information data, it can also be regarded as a pilot subcarrier. This approach can only be efficient with small-sized MIMO systems and becomes impractical with dimensions larger than 3×3.

5.3.3.1 Real-valued OFDM creation

At the subcarrier level, the P-I Ratio should be the same as the SISO-PLC system, which is 1:8. Assume that the number of the pilots is the same as the number of zeros data. The length of the QAM symbol subcarrier with pilot should be $N_k+\frac{1}{2}N_p$. The pilot symbols are interleaved with QAM symbols to produce $\mathbf{D}^\tau \in \mathbb{C}^{1\times(N_k+\frac{1}{2}N_p)}$ as

$$\mathbf{D}^1 = [P_0, 0, D_0, ..., D_{15}, P_1, 0, ..., P_{N_p-1}, 0, D_{N_k-16}, ..., D_{N_k-1}], \tag{5.5}$$

$$\mathbf{D}^2 = [0, P_0, D_0, ..., D_{15}, 0, P_1, ..., 0, P_{N_p-1}, D_{N_k-16}, ..., D_{N_k-1}], \tag{5.6}$$

We have assumed here arbitrarily that the same value $P_* = P$ is used for all comb pilots. The zero-data have been set after the pilots in $\mathbf{D}^1$. In $\mathbf{D}^2$, the positions of pilots and zeros data are interchanged. To make the P-I Ratio is 1:8, the nonzero pilot spacing should be 16. The OFDM symbol, which the length of subcarriers is doubled because of applying Hermitian symmetry in (4.1), in the frequency domain with pilots included, $\mathbf{X}^\tau \in \mathbb{C}^{1\times(N_f+N_p)}$ can be given as

$$\mathbf{X}^1 = [\mathrm{Re}\{P\}, 0, D_0, ..., D_{15}, P, 0, ..., D_{N_k-1}, \mathrm{Im}\{P\}, D_{N_k-1}, ..., 0, P, D_{15}, ..., D_0, 0] \tag{5.7}$$

$$\mathbf{X}^2 = [0, P, D_0, ..., D_{15}, 0, P, ..., D_{N_k-1}, 0, D_{N_k-1}, ..., P, 0, D_{15}, ..., D_0, P]. \tag{5.8}$$

5.3.3.2 Received signal over zero-comb pilot method

At the receiver after the FFT operation, the received signal in the frequency domain for the zero-comb pilot system can be given as

$$\begin{aligned} R_p^\rho &= Y_p^{1,\rho} + Y_p^{2,\rho} + W_S p^\rho \\ &= H_p^{1,\rho} X_p^1 + H_p^{2,\rho} X_p^2 + W_S p^\rho \end{aligned} \tag{5.9}$$

where R_p^ρ are the received signals of comb pilot system, $p = (0, 1, ..., \frac{1}{2}N_p - 1) \times (\frac{2(N_f+N_p)}{N_p})$ denotes the index of position of pilot in the first transmitter.

To avoid interference from the MIMO-PLC channel, only one pilot can go through

the channel simultaneously. The other adjacent transmitter must send zero data. The CFR matrix for the zero-comb pilot system can be written as
when $X_p^1 = P$,

$$\begin{aligned} \tilde{H}_p^{1,\rho} &= \frac{R_p^\rho}{X_p^1} \\ &= \frac{H_p^{1,\rho} X_p^1 + 0 + W_{S_p}^\rho}{X_p^1} \\ &= H_p^{1,\rho} + \frac{W_{S_p}^\rho}{X_p^1}; \end{aligned} \tag{5.10}$$

when $X_z^2 = P$,

$$\tilde{H}_z^{2,\rho} = H_z^{2,\rho} + \frac{W_{S_z}^\rho}{X_z^2}; \tag{5.11}$$

where z is the index of position of pilot in the second transmitter data. To eliminate the influence of pilot interference on the system, when subcarrier z transmits the pilots data X_z^2, X_z^1, the transmitted X_p^1, X_p^2 should be zeros in the subcarrier p .

5.4 Averaging approach

The CFR estimation, and thus the BER, can be greatly improved by averaging the effect of the AWGN. In this section, we introduce the proposed averaging approach shown in Fig. 5.3. For the first OFDM symbol, $n_{fr} = 0$, and for each non-pilot subcarrier, n_f, we initialize the CFR averaging as

$$\hat{H}_{n_f}(n_{fr}) = \tilde{H}_{n_f}(n_{fr}). \tag{5.12}$$

For subsequent iterations, when $n_{fr} = 2, ..., N_{fr} - 1$,

$$\hat{H}_{n_f}(n_{fr}) = a\tilde{H}_{n_f}(n_{fr}) + (1-a)\hat{H}_{n_f}(n_{fr} - 1), \tag{5.13}$$

where $\hat{H}_{n_f}$ is the estimated CFR using the averaging method, $\tilde{H}_{n_f}$ is the estimated CFR at each OFDM symbol. $a \in (0, 1)$ is a weight factor, N_{fr} is the frame size and n_{fr} denotes the index of N_{fr}, which is the times of the averaging procession.

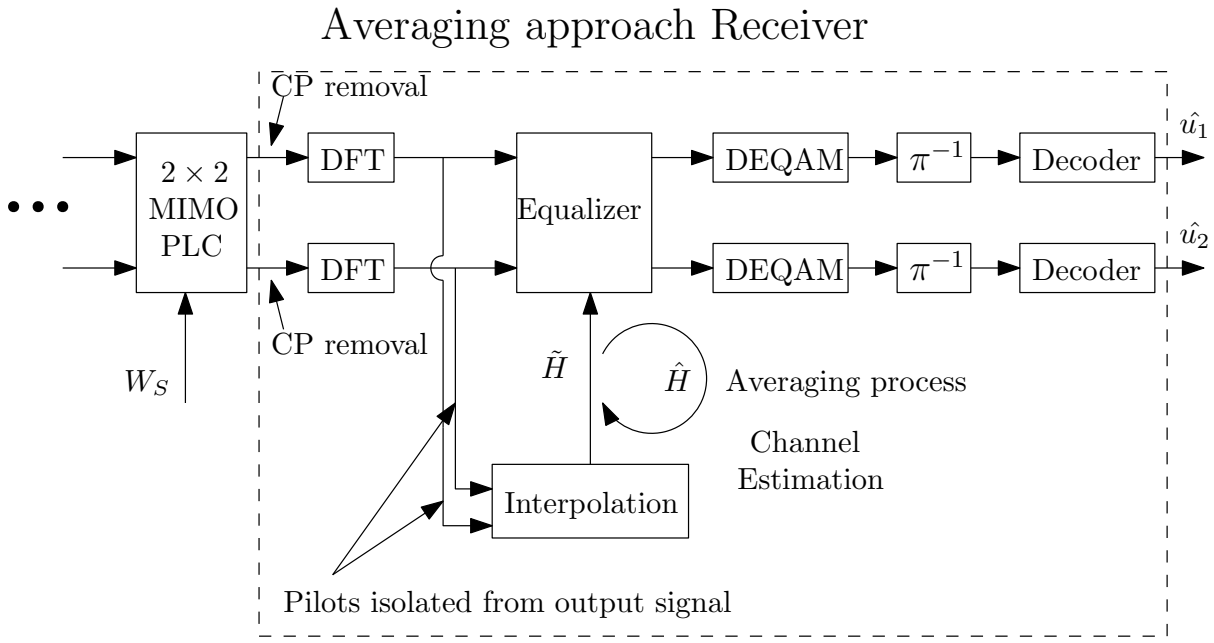

Figure 5.3: Averaging-Comb/Block pilot system model.

5.5 Mean Square Error

The MSE denotes the difference between the original CFR, H_{n_f}, and the estimated CFR, $\hat{H}_{n_f}$. It can be given as

$$MSE = 10\log_{10}\left(\frac{1}{N_f}\sum_{n_f=0}^{N_f-1}\left|H_{n_f}-\tilde{H}_{n_f}\right|^2\right)\ \text{dB}, \tag{5.14}$$

where MSE is given in dB, is the prefect CFR. According to (5.4), (5.10), (6.9) and (5.14), the MSE of each different channel estimation method can be calculated as follows:

- The Block pilot MSE:

$$MSE_{\text{block}} = 10\log_{10}\left(\frac{1}{N_f}\sum_{n_f=0}^{N_f-1}\left|\frac{W_{S_{n_f}}^{\tau,\rho}}{X_{n_f}^{\tau,\rho}}\right|^2\right)\ \text{dB}, \tag{5.15}$$

- The Comb pilot MSE:

$$MSE_{\text{comb}} = 10\log_{10}\left(\frac{1}{N_f}\sum_{n_f=0}^{N_f-1}\left|\frac{W_{S_{n_f}}^{\rho}}{P}\right|^2\right)\ \text{dB}, \tag{5.16}$$

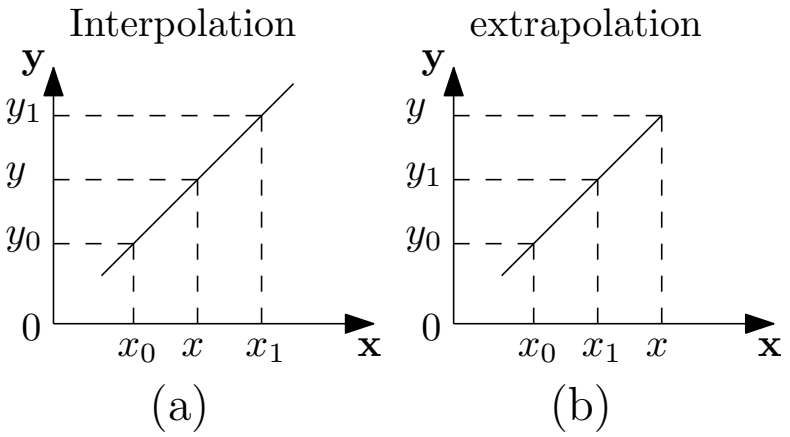

Figure 5.4: Types of linear interpolation: (a)interpolation, (b)extrapolation.

5.6 Interpolation

Interpolation, an essential method for approximation of discrete functions, can be utilized to estimate the approximate other points' value through the value of limited points. In other words, the interpolation can make reasonable compensation for the missing data. In a channel estimation system, the primary function of the interpolation approach is to calculate the rest positions of the estimated CFR value except the pilot positions. In this chapter, two types of interpolation techniques - linear and spline are introduced, including the derivation process.

5.6.1 Linear interpolation

According to the distance between two adjacent data points in a one-dimensional data sequence, linear interpolation allocates their proportion. It estimates their value as can be seen in Fig. 5.4 (a) and (5.18).

$$\frac{y - y_0}{x - x_0} = \frac{y_1 - y_0}{x_1 - x_0}. \tag{5.17}$$

Reshape the (5.17), the value of y can be demonstrated as

$$y = \frac{y_1 - y_0}{x_1 - x_0} x - x_0 + y_0. \tag{5.18}$$

Suppose two adjacent data are on one side of the interpolation point shown in Fig. 5.4 (b), which is called extrapolation. The same function can be used to calculate the value of the evaluation point as the interpolation method. However, the linear interpolation method only uses the corresponding values of two points to calculate

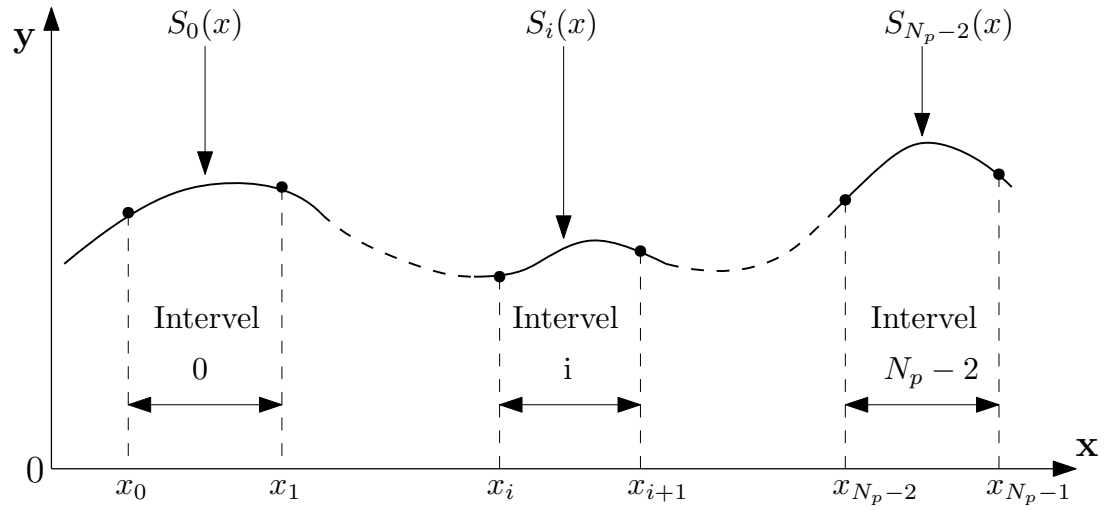

Figure 5.5: Types of cubic spline function interpolation.

the corresponding values between two points. The corresponding values of the two points are often affected by various accidental factors. The linear interpolation results may have significant errors.

5.6.2 Cubic spline function interpolation

The Runge phenomenon, which is also called the violent oscillation phenomenon, can have a significant impact on the channel estimation system. Under this circumstance, the system divides all data into several parts. Each small piece uses different functions by interpolation. Furthermore, each piecewise function is constructed in the form of a higher-order function [104]. Finally, all these different functions are used to express the original sequence. This method not only avoids the Runge phenomenon but also ensures the smooth connection between the processes is called cubic spline function interpolation Fig. 5.5.

The basic principles of the cubic spline function interpolation can be defined as

$$S_i(x) = a_i + b_i(x - x_p) + c_i(x - x_p)^2 + d_i(x - x_p)^3, \tag{5.19}$$

where $S(*)$ is the piecewise functions which has $N_p - 1$ equations, $i = 0, 1, ..., N_p - 2$ denotes the index of the piecewise functions and $p = 0, 1, ..., N_p - 1$ denotes the index of the pilots in channel estimation system. a, b, c, d are the coefficients of different order in the function. With the four unknown coefficients in each piecewise function, the system needs $4 \times (N_p - 1)$ equations to obtain the full (a, b, c, d)s. The system should satisfy four following conditions to achieve the approach and calculate all the

coefficients [105–108]:

Condition 1. The function S should pass through all known nodes.

$$S_i(x_i) = y_i, \quad i = 0, 1, ..., N_p - 2, \tag{5.20}$$

where y is the output of the system. At the final node:

$$S_{N_p-2}(x_{N_p-1}) = y_{N_p-1}. \tag{5.21}$$

This condition can obtain N_p equations.

Condition 2. The values of adjacent functions at nodes are the same.

$$S_i(x_{i+1}) = S_{i+1}(x_{i+1}). \tag{5.22}$$

These equations denote that the system is 0-order continuous at all nodes except the first and the final node. The condition obtains $N_p - 2$ equations.

Condition 3. To ensure that both sides of the node have the same slope, there is no sharp jump on the original function curve. The system should be 1-order continuous at all nodes except the first and the final node.

$$S_i^{'}(x_{i+1}) = S_{i+1}^{'}(x_{i+1}). \tag{5.23}$$

This condition abtains $N_p - 2$ equations as well.

Condition 4. To ensure that both sides of the node have the same curvature, the system should be 2-order continuous at all nodes except the first and the final node.

$$S_i^{''}(x_{i+1}) = S_{i+1}^{''}(x_{i+1}). \tag{5.24}$$

This condition abtains $N_p - 2$ equations. The number of equations of all conditions add up to $4N_p - 6$.

The 1-order and 2-order of $S(*)$ functions (except the final node) can be defined

as

$$S_i^{'}(x) = b_i + 2c_i(x - x_i) + 3d_i(x - x_i)^2, \tag{5.25}$$

$$S_i^{''}(x) = 2c_i + 6d_i(x - x_i). \tag{5.26}$$

Combining (5.19) and (5.20),

$$\begin{aligned} S_i(x_i) &= a_i + b_i(x_i - x_i) + c_i(x_i - x_i)^2 + d_i(x_i - x_i)^3 \\ &= a_i = y_i. \end{aligned} \tag{5.27}$$

Combining (5.19) and (5.22),

$$S_i(x_{i+1}) = a_i + b_i(x_{i+1} - x_i) + c_i(x_{i+1} - x_i)^2 + d_i(x_{i+1} - x_i)^3. \tag{5.28}$$

Assume that $\Delta_i = x_{i+1} - x_i$,

$$\begin{aligned} S_i(x_{i+1}) &= a_i + \Delta_i b_i + \Delta_i^2 c_i + \Delta_i^3 d_i \\ &= S_{i+1}(x_{i+1}) = y_{i+1}. \end{aligned} \tag{5.29}$$

According to (5.23), the function can be derived as

$$S_i^{'}(x_{i+1}) = b_i + 2c_i\Delta_i + 3d_i\Delta_i^2; \tag{5.30}$$

$$\begin{aligned} S_{i+1}^{'}(x_{i+1}) &= b_{i+1} + 2c_{i+1}(x_{i+1} - x_{i+1}) + 3d_{i+1}(x_{i+1} - x_{i+1})^2, \\ &= b_{i+1}, \\ &= S_i^{'}(x_{i+1}) = b_i + 2c_i\Delta_i + 3d_i\Delta_i^2. \end{aligned} \tag{5.31}$$

Reshaped the (5.35), the equation is derived as

$$b_i + 2c_i\Delta_i + 3d_i\Delta_i^2 - b_{i+1} = 0. \tag{5.32}$$

The 2-order equations of two adjacent $S(*)$ functions can be demonstrated as

$$S_i^{''}(x_{i+1}) = 2c_i + 6d_i(x_{i+1} - x_i) = 2c_i + 6d_i\Delta_i, \tag{5.33}$$

$$S_{i+1}^{''}(x_{i+1}) = 2c_{i+1} + 6d_{i+1}(x_{i+1} - x_{i+1}) = 2c_{i+1}, \tag{5.34}$$

$$2c_i + 6d_i\Delta_i - 2c_{i+1} = 0. \tag{5.35}$$

Assume that $\Lambda_i = S_i^{''}(x_i) = 2c_i$,

$$d_i = \frac{\Lambda_{i+1} - \Lambda_i}{6\Delta_i}. \tag{5.36}$$

Combining (5.27), (5.32), (5.35) and (5.36), the equation about unknown element Λ can be defined as

$$\Delta_i\Lambda_i + 2(\Delta_i + \Delta_{i+1})\Lambda_{i+1} + \Delta_{i+1}\Lambda_{i+2} = 6(\frac{y_{i+2} - y_{i+1}}{\Delta_{i+1}} - \frac{y_{i+1} - y_i}{\Delta_i}). \tag{5.37}$$

The final step of the cubic spline interpolation method is to create boundary condition equations, which can be separated into three types - free boundary condition, fixed boundary condition and non-nodal boundary condition. Each situation obtains two equations combining with the equations before, the total $4 \times (N_p - 1)$ equations have been constructed to calculate the four groups of coefficients (a, b, c, d)s.

Type 1. Natural spline allows the slope of the endpoint to maintain balance at a certain position freely, which means that the swing of the curve is the smallest. The Free boundary condition, which produced the natural spline, is defined as $S_0^{''}(x_0) = 0$ and $S_{N_p-2}^{''}(x_{N_p-1}) = 0$. According to (5.26), the derivation process is derived as

$$2c_0 + 6d_0(x_0 - x_0) = 2c_0, \tag{5.38}$$

thus,

$$\Lambda_0 = 0. \tag{5.39}$$

And

$$2c_{N_p-2} + 6d_{N_p-2}(x_{N_p-1} - x_{N_p-2}) = 2(\frac{\Lambda_{N_p-2}}{2}) + 6(\frac{\Lambda_{N_p-1} - \Lambda_{N_p-2}}{6\Delta_{N_p-2}})(\Delta_{N_p-2}), \tag{5.40}$$

$$\Lambda_{N_p-2} + \Lambda_{N_p-1} - \Lambda_{N_p-2} = \Lambda_{N_p-1} = 0. \tag{5.41}$$

Combining (5.37) and the free boundary condition, the cubic spline function can be

demonstrated as

$$\begin{bmatrix} 1 & 0 & 0 & & \dots & 0 \\ \Delta_0 & 2(\Delta_0+\Delta_1) & \Delta_1 & 0 & \dots & \\ 0 & \Delta_1 & 2(\Delta_1+\Delta_2) & \Delta_2 & 0 & \vdots \\ 0 & 0 & \Delta_2 & 2(\Delta_2+\Delta_3) & \Delta_3 & \\ \vdots & & \ddots & \ddots & \ddots & \\ 0 & \dots & & 0 & 0 & 1 \end{bmatrix} \begin{bmatrix} \Lambda_0 \\ \Lambda_1 \\ \Lambda_2 \\ \Lambda_3 \\ \vdots \\ \Lambda_{N_p-1} \end{bmatrix}$$

$$= 6 \begin{bmatrix} 0 \\ \frac{y_2-y_1}{\Delta_1} - \frac{y_1-y_0}{\Delta_0} \\ \frac{y_3-y_2}{\Delta_2} - \frac{y_2-y_1}{\Delta_1} \\ \vdots \\ \frac{y_{N_p-1}-y_{N_p-2}}{\Delta_{N_p-2}} - \frac{y_{N_p-2}-y_{N_p-3}}{\Delta_{N_p-3}} \\ 0 \end{bmatrix} \tag{5.42}$$

Type 2. The clamped spline, which has a fixed slope at the beginning point and the final point, gives a fixed boundary condition which can be defined as $S_0^{'}(x_0) = A$ and $S_{N_p-2}^{'}(x_{N_p-1}) = B$, where A and B are the two constant elements. Combining with (5.25), the first condition can be reshaped as

$$b_0 + 2c_0(x_0 - x_0) + 3d_0(x_0 - x_0)^2 = b_0, \tag{5.43}$$

$$b_0 = \frac{y_1 - y_0}{\Delta_0} - \frac{\Delta_0\Lambda_0}{2} - \frac{\Delta_0(\Lambda_1 - \Lambda_0)}{6} = A. \tag{5.44}$$

After simplifying the equation is written as

$$2\Delta_0\Lambda_0 + \Delta_0\Lambda_1 = 6(\frac{y_1 - y_0}{\Delta_0} - A). \tag{5.45}$$

The second condition can be demonstrated as

$$\begin{aligned} B &= b_{N_p-2} + 2c_{N_p-2}(x_{N_p-1} - x_{N_p-2}) + 3d_{N_p-2}(x_{N_p-1} - x_{N_p-2})^2 \\ &= \frac{y_{N_p-1} - y_{N_p-2}}{\Delta_{N_p-2}} + \frac{\Delta_{N_p-2}\Lambda_{N_p-2}}{2} + \frac{\Delta_{N_p-2}(\Lambda_{N_p-1} - \Lambda_{N_p-2})}{3} \end{aligned} \tag{5.46}$$

$$6(B - \frac{y_{N_p-1} - y_{N_p-2}}{\Delta_{N_p-2}}) = \Delta_{N_p-2}\Lambda_{N_p-2} + 2\Delta_{N_p-2}\Lambda_{N_p-1}. \tag{5.47}$$

The cubic spline function can be demonstrated as

$$\begin{bmatrix} 2\Delta_0 & \Delta_0 & 0 & 0 & 0 & \dots & 0 \\ \Delta_0 & 2(\Delta_0+\Delta_1) & \Delta_1 & 0 & 0 & \dots & 0 \\ 0 & \Delta_1 & 2(\Delta_1+\Delta_2) & \Delta_2 & 0 & \dots & \vdots \\ \vdots & & & & \ddots & \ddots & \vdots \\ \vdots & \dots & 0 & 0 & \Delta_{N_p-3} & 2(\Delta_{N_p-3}-\Delta_{N_p-2}) & \Delta_{N_p-2} \\ 0 & \dots & 0 & 0 & 0 & \Delta N_p - 2 & 2(\Delta_{N_p-2}) \end{bmatrix}$$
$$\begin{bmatrix} \Lambda_0 \\ \Lambda_1 \\ \Lambda_2 \\ \Lambda_3 \\ \vdots \\ \Lambda_{N_p-1} \end{bmatrix} = 6 \begin{bmatrix} \frac{y_1-y_0}{\Delta_0} - A \\ \frac{y_2-y_1}{\Delta_1} - \frac{y_1-y_0}{\Delta_0} \\ \frac{y_3-y_2}{\Delta_2} - \frac{y_2-y_1}{\Delta_1} \\ \vdots \\ \frac{y_{N_p-1}-y_{N_p-2}}{\Delta_{N_p-2}} - \frac{y_{N_p-2}-y_{N_p-3}}{\Delta_{N_p-3}} \\ B - \frac{y_{N_p-1}-y_{N_p-2}}{\Delta_{N_p-2}} \end{bmatrix} \tag{5.48}$$

Type 3. The non-nodal boundary requires that the third derivative of the cubic function of the first segment S_0 and the second segment S_1 is continuous at the second data point x_1, and the third derivative of the penultimate segment S_{N_p-3} and the last segment S_{N_p-2} is continuous at the penultimate data point x_{N_p-2}, thus,

$$S_0'''(x_1) = S_1'''(x_1), \tag{5.49}$$

$$S_{N_p-3}'''(x_{N_p-2}) = S_{N_p-2}'''(x_{N_p-2}). \tag{5.50}$$

As $S_i(x) = 6d_i$, the derivation process of the first condition is derived as

$$d_0 = d_1 \rightarrow \Delta_1(\Lambda_1 - \Lambda_0) = \Delta_0(\Lambda_2 - \Lambda_1), \tag{5.51}$$

$$-\Delta_1\Lambda_0 + (\Delta_0 + \Delta_1)\Lambda_1 - \Delta_0\Lambda_2 = 0. \tag{5.52}$$

Meanwhile, the second condition is demonstrated as

$$d_{N_p-3} = d_{N_p-2} \rightarrow \Delta_{N_p-2}(\Lambda_{N_p-2} - \Lambda_{N_p-3}) = \Delta_{N_p-3}(\Lambda_{N_p-1} - \Lambda_{N_p-2}), \tag{5.53}$$

$$-\Delta_{N_p-2}\Lambda_{N_p-3}+(\Delta_{N_p-2}+\Delta_{N_p-3})\Lambda_{N_p-2}-\Delta_{N_p-3}\Lambda_{N_p-1}=0. \tag{5.54}$$

The cubic spline function in non nodal boundary can be demonstrated as

$$\begin{bmatrix} -\Delta_1 & \Delta_0+\Delta_1 & -\Delta_0 & 0 & 0 & \dots & 0 \\ \Delta_0 & 2(\Delta_0+\Delta_1) & \Delta_1 & 0 & 0 & \dots & 0 \\ 0 & \Delta_1 & 2(\Delta_1+\Delta_2) & \Delta_2 & 0 & \dots & \vdots \\ \vdots & & & & \ddots & \ddots & \vdots \\ \vdots & \dots & 0 & 0 & \Delta_{N_p-3} & 2(\Delta_{N_p-3}-\Delta_{N_p-2}) & \Delta_{N_p-2} \\ 0 & \dots & 0 & 0 & -\Delta_{N_p-3} & \Delta_{N_p-2}+\Delta_{N_p-3} & -\Delta_{N_p-3} \end{bmatrix}$$

$$\begin{bmatrix} \Lambda_0 \\ \Lambda_1 \\ \Lambda_2 \\ \Lambda_3 \\ \vdots \\ \Lambda_{N_p-1} \end{bmatrix} = 6 \begin{bmatrix} 0 \\ \frac{y_2-y_1}{\Delta_1}-\frac{y_1-y_0}{\Delta_0} \\ \frac{y_3-y_2}{\Delta_2}-\frac{y_2-y_1}{\Delta_1} \\ \vdots \\ \frac{y_{N_p-1}-y_{N_p-2}}{\Delta_{N_p-2}}-\frac{y_{N_p-2}-y_{N_p-3}}{\Delta_{N_p-3}} \\ 0 \end{bmatrix} \tag{5.55}$$

The cubic spline interpolation can give a smoother line of the estimated CFR than the linear interpolation. In the results part, the BER performance and MSE performance of both two types of interpolation methods has been given. The cubic spline can improve the system performance rapidly than the linear interpolation.

5.7 Results

In this section, we numerically evaluate the performance of the channel estimation with two pilot design approaches, i.e. block pilot and comb pilot. The simulations utilized a 2×2 MIMO-PLC channel model, with four different multipaths per link which is shown in Fig. 3.5. The CIR and CFR for this channel are shown in Figs. (3.3) and (3.2). Furthermore, the performance of proposed averaging approach has been in the block/comb pilot methods to give a better BER results than the traditional block/comb pilot approaches. Finally, the MSE results of various channel estimation methods have been computed as a function of SNR. At the receiver,

we consider MMSE detection. The MMSE Equalizer coefficient is computed as

$$\mathbf{C}_{n_f}^{\mathrm{MMSE}} = \frac{\mathbf{H}_{n_f}^{\dagger}}{\mathbf{H}_{n_f}\mathbf{H}_{n_f}^{\dagger} + \frac{1}{\gamma_s}\mathbf{I}^{2\times 2}}, \tag{5.56}$$

where $\mathbf{H}_{n_f}$ is the channel frequency response matrix of 2×2 MIMO-PLC system, $\dagger$ denotes the Moore-Penrose inverse of the matrix, $\mathbf{I}$ indicates the 2×2 unit matrix and γ_s represents the linear signal-noise-ratio.

In this part of simulation results, the length of information data is set to $K = 1024$ in binary with 1/2 code rate of the LDPC code system. After the 16-QAM modulation, the length of the QAM input signal is $N_k = 512$ and the size of the OFDM subcarrier is $N_f = 2 \times N_k + N_p$ because of the Hermitian symmetry and the pilot data adding.

5.7.1 The effect of the Pilot-Information Ratio (P-I Ratio)

According to the block/comb pilot model (Fig. 3.12) and zero-comb pilot (Fig. 5.2), as the number of pilots increased, the information data is reduced and the P-I Ratio is increased. As the P-I Ratio changed, the performance of the channel estimation approaches are changed. Fig. 5.6 plots the BER performance by using the block pilot method with the P-I Ratio is 1:2, 1:4, 1:8, 1:16, 1:32 and 1:64. The BER results had a slight difference between different P-I Ratios. On the contrary, the simulation result can be seen in Fig. 5.8 which displays the BER performance by using the comb pilot method with the P-I Ratio is also 1:2, 1:4, 1:8, 1:16, 1:32 and 1:64. Before the data rate decreased to 1:16, the BER performance had a slight difference with different P-I Ratios. When the data rate continues to decline, the BER performance is reduced over high SNR. As the P-I Ratio is down to 1:32 and 1:64, the estimated system can hardly restore an approximate value of the original CFR. However, the effective information transmission rate increased as the number of pilots decreased. So that the number of the pilot should be as low as the system can give the good BER performance.

Fig. 5.7 and Fig. 5.9 demonstrate the MSE vs. E_b/N_0 performance by using both block pilot and comb pilot with different P-I Ratios. For the block pilot approach, the subcarrier of the first OFDM symbol in each block is entirely pilot data. No matter how many OFDM symbols are in one block, the estimated CFR

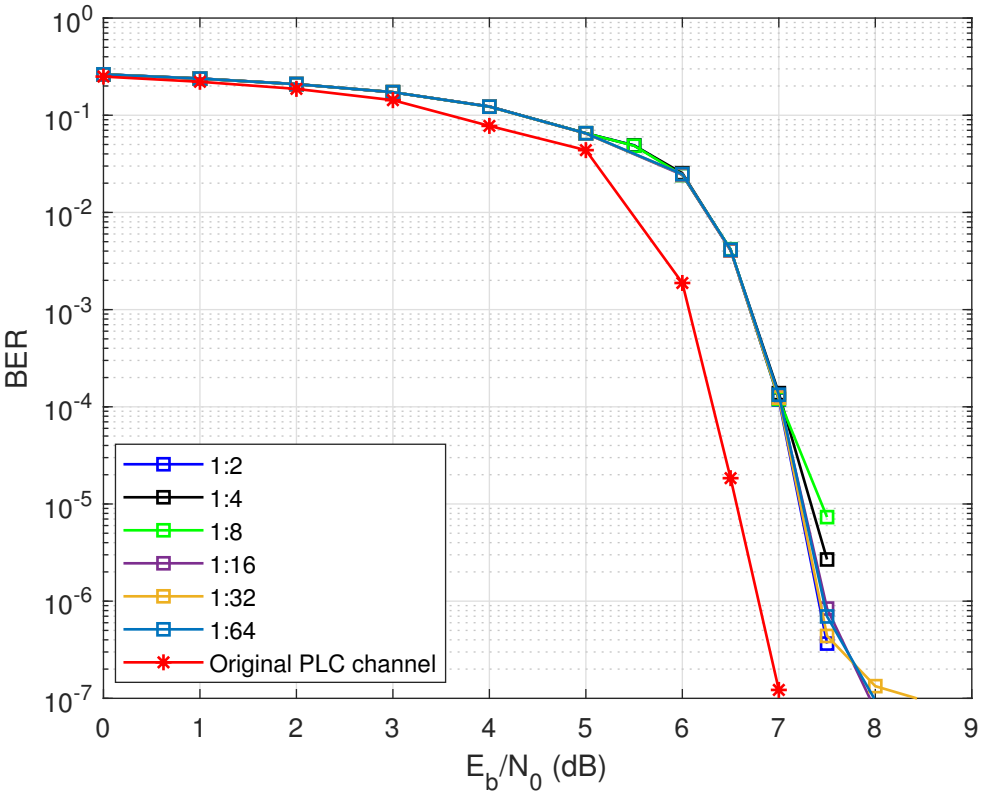

Figure 5.6: BER performance using the block pilot method with the different P-I Ratios for LDPC coded systems.

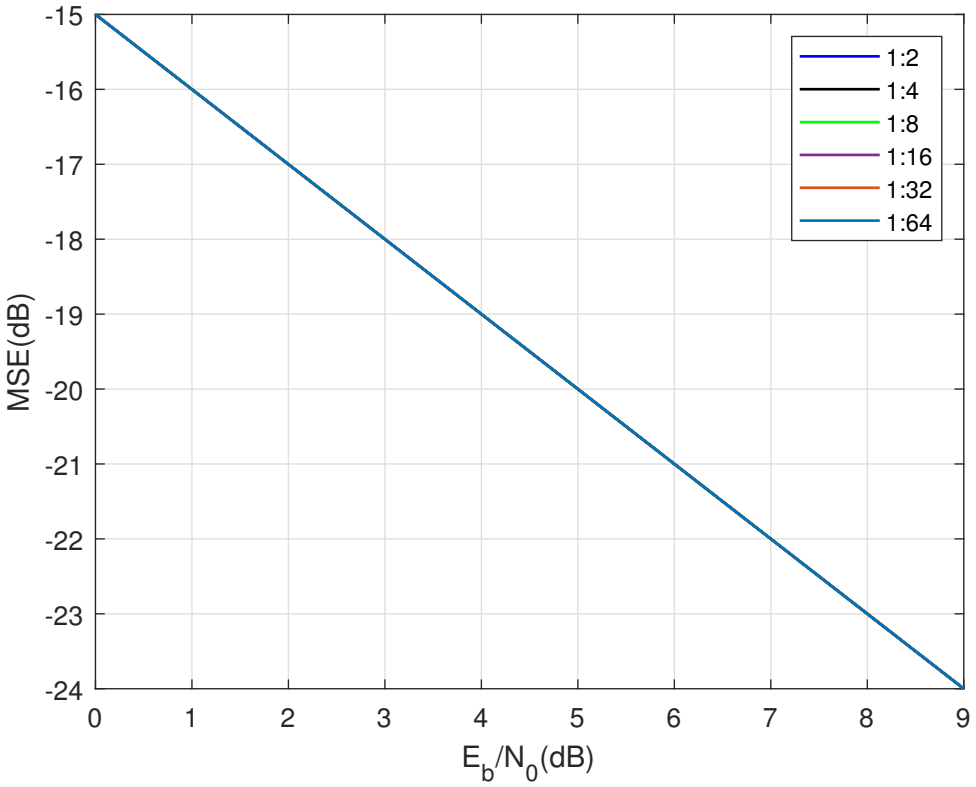

Figure 5.7: MSE vs. E_b/N_0 using Block pilot method with the different P-I Ratios for LDPC coded systems.

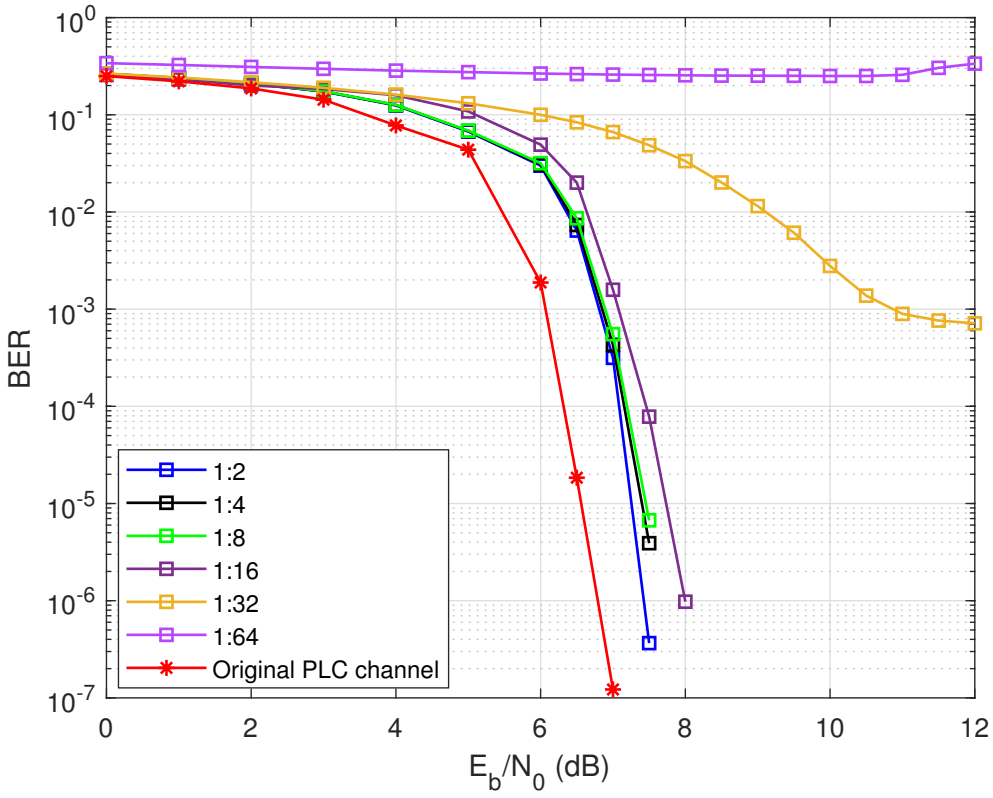

Figure 5.8: BER performance using the comb pilot method with the different P-I Ratios for LDPC coded systems.

does not change. For this reason, the MSE values in the different P-I Ratios of the block pilot system are all the same. Moreover, as the value of the original CFR of MIMO-PLC is constant in this thesis, the BER performance in different P-I Ratios estimated channel system are all the same. For the comb pilot, the pilot componets are set to some of the subcarriers of each OFDM symbol. Thus, at the pilot subcarrier positions, the estimated CFR can be calculated by using the pilot signal. Other subcarriers' estimated CFR are derived by using the interpolation method. In Fig. 5.9, at a E_b/N_0 of 8 dB, with the P-I Ratio is 1:8, 1:16, 1:32 and 1:64, the value of MSE is 22.5, 18, 12.5 and 6 dB. As the MSE grows to 1:4 and 1:2, the MSE is down to the 23 dB ata the E_b/N_0 of 8 dB and no more goes down.

Even the small pilot gap can slightly improve the BER performance of the system, it still wastes too much capacity to transmit the valid information. To simulated an accuracy system, meanwhile, save the capacity of the PLC channel, all the following simulation systems are utilized a 1:8 P-I Ratio.

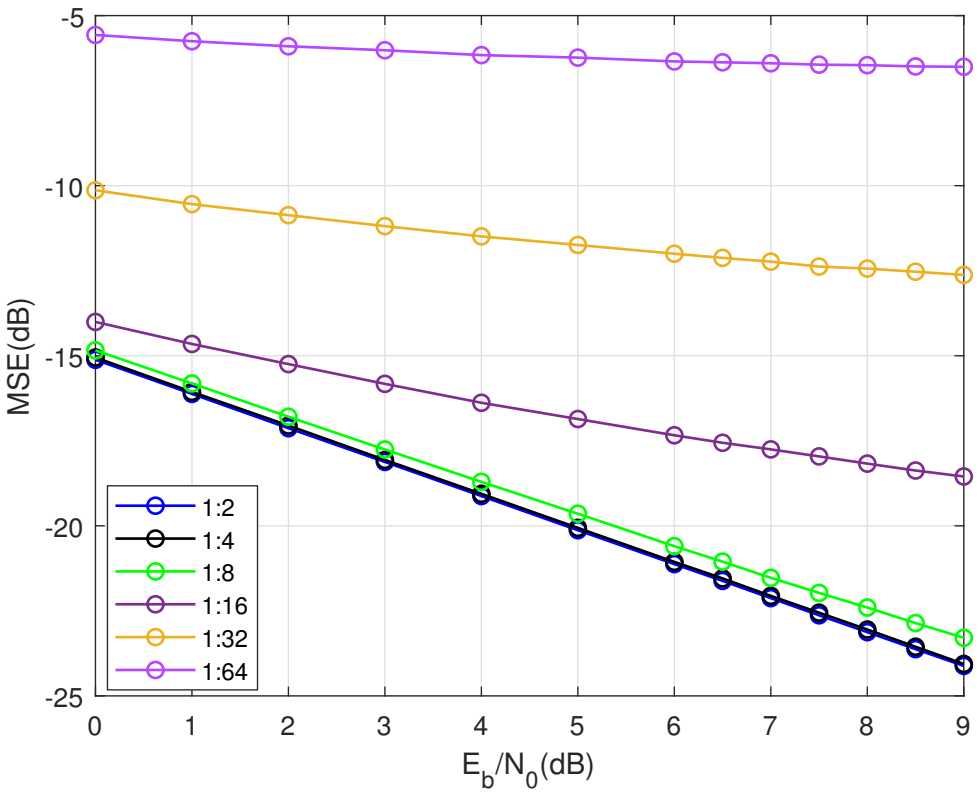

Figure 5.9: MSE vs. E_b/N_0 using comb pilot method with the different P-I Ratios for LDPC coded systems.

5.7.2 The effect of different interpolation methods

There is a contrast between linear and spline interpolation methods using in the comb pilot method over the MIMO-PLC channel system in Fig. 5.10. The BER vs. E_b/N_0 performance by using the spline approach is about 0.3 dB better than the linear at a BER of 10^{-5}. In Fig. 3.2, the CFR magnitude of each multipath channel of the MIMO-PLC system is derived. Under the amplitude frequently fluctuates, compared to the linear interpolation, the spline, which needs to use four known points to determine the trend of the estimated CFR, can give a more accurate result. Thus, the estimated CFR is closer to the original CFR and optimized the performance of the comb pilot channel estimation design.

The result of MSE over comb pilot system with both linear and spline interpolation methods is derived in Fig. 5.11. At a E_b/N_0 of 8 dB, the MSE is -22.4 dB in the spline interpolation comb pilot system. For the linear interpolation system, the MSE is down to -21.1 dB at a E_b/N_0 of 8 dB. It computes against that the spline interpolation method can improve the performance of the comb pilot channel estimation system by using linear interpolation.

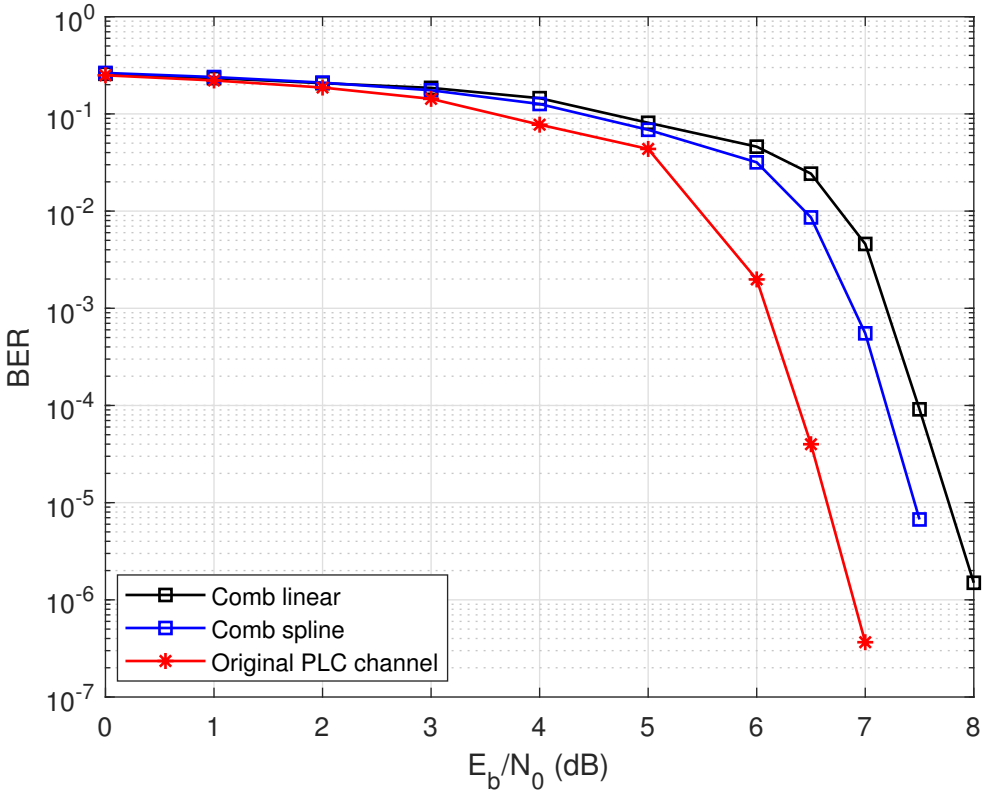

Figure 5.10: The contrast of BER performance over both Linear and Spline interpolation methods using the comb pilot channel estimation over LDPC coded system.

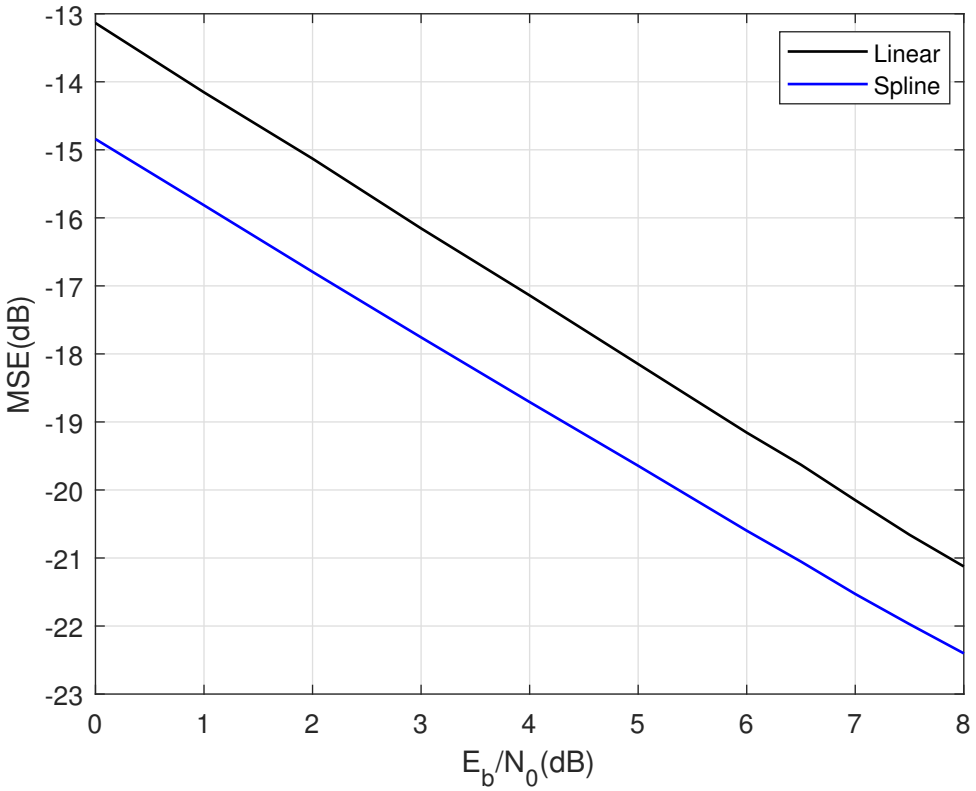

Figure 5.11: The contrast of MSE vs. E_b/N_0 over Linear and Spline interpolation methods using the comb pilot channel estimation over LDPC coded system.

5.7.3 The averaging approach

This section derived the results of the BER performance by using the channel estimation methods with the averaging process over MIMO-PLC.

Fig. 5.12 displays the BER vs. E_b/N_0 performance by using different n_{fr} and a values for the averaging block pilot system. The weight factor of the averaging processing has been set to $a = 0.1$ in the following simulation, thus, the BER performance is getting better as the number of averaging frame increased from 10 to 500. At a BER of 10^{-5}, the E_B/N_0 is about 7.4, 7.05 and 6.6 dB for 10, 100, 500 averaging frames. It is worth noting that when the system change to be 2000 frames, the BER performance has no difference compare with that of 500 frames. In other words, the averaging method in 500 times averaging is enough to adjust the impact of the AWGN in the MIMO-PLC channel estimation system. Fig. 5.13 shows the MSE of each different weight factor and averaging frames in block pilot model, giving a more intuitive comparison of the difference between the original CFR and estimated CFR. The smaller the values of the MSE is, the smaller the difference between original CFR and estimated CFR becomes. In other words, the pilot method that achieves the lowest MSE exhibits the best BER performance. This figure demonstrated that when the averaging frames is larger than 500, the system can achieve the best BER performance. The following simulation about other types of the channel estimation methods are all under the 500 averaging frames to investigate the BER performance and the MSE results.

Another main point to affect the performance of the averaging process is the weight factor. According to the (5.12) and (5.13), as the value of weight factor increased, the proportion of the present estimated CFR value became larger. On the contrary, the proportion of the present estimated CFR value became smaller. As can be seen in Fig. 5.14, the frame is set to 500 and the weight factor is set to 0.9, 0.5, 0.1, 0.01 and it demonstrated that as the value of the weight factor increased, the BER performance became better. It is worth noting that when the weight factor is 0.01, the BER performance is worse than the system with 0.1 weight factor. This phenomenon indicates that if the present estimation CFR value continues to decrease after reaching a limit point, the system performance will deteriorate. Thus, this limit point is set to 0.1 in the thesis by many experiments. Fig. 5.15 plots the MSE vs. E_b/N_0 of all systems with different values of the weight factor. The MSE of the

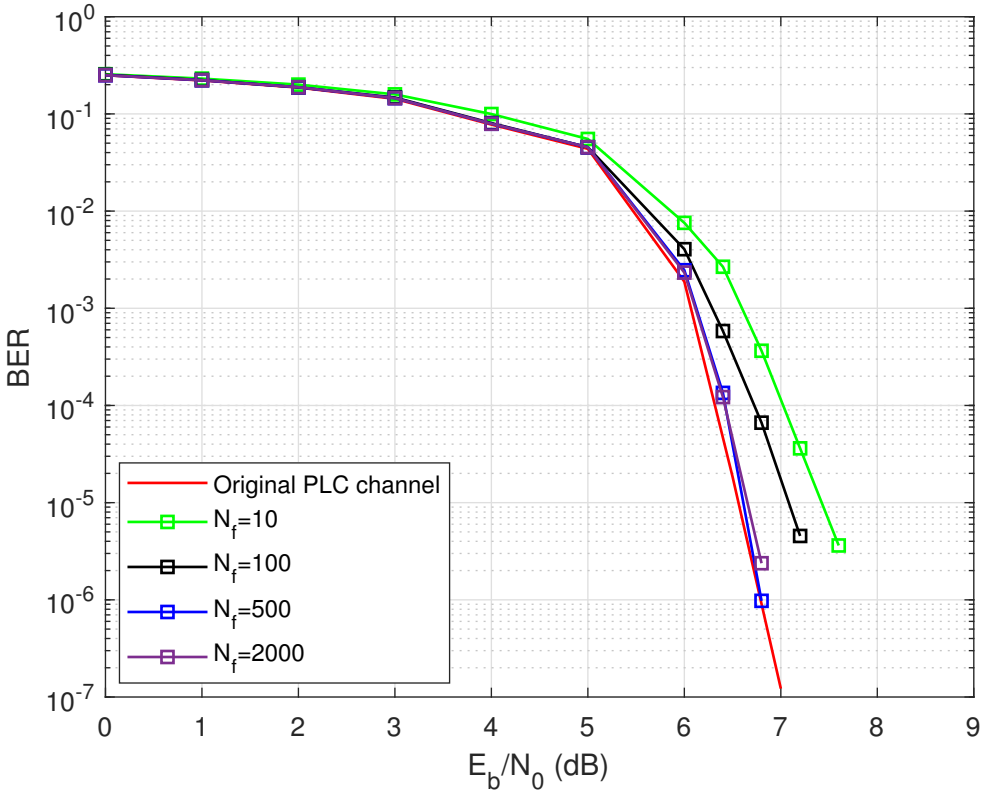

Figure 5.12: BER performance of the averaging block pilot using the same weight factor a=0.1 and different frame - 10, 100, 500 and 2000 over LDPC coded system.

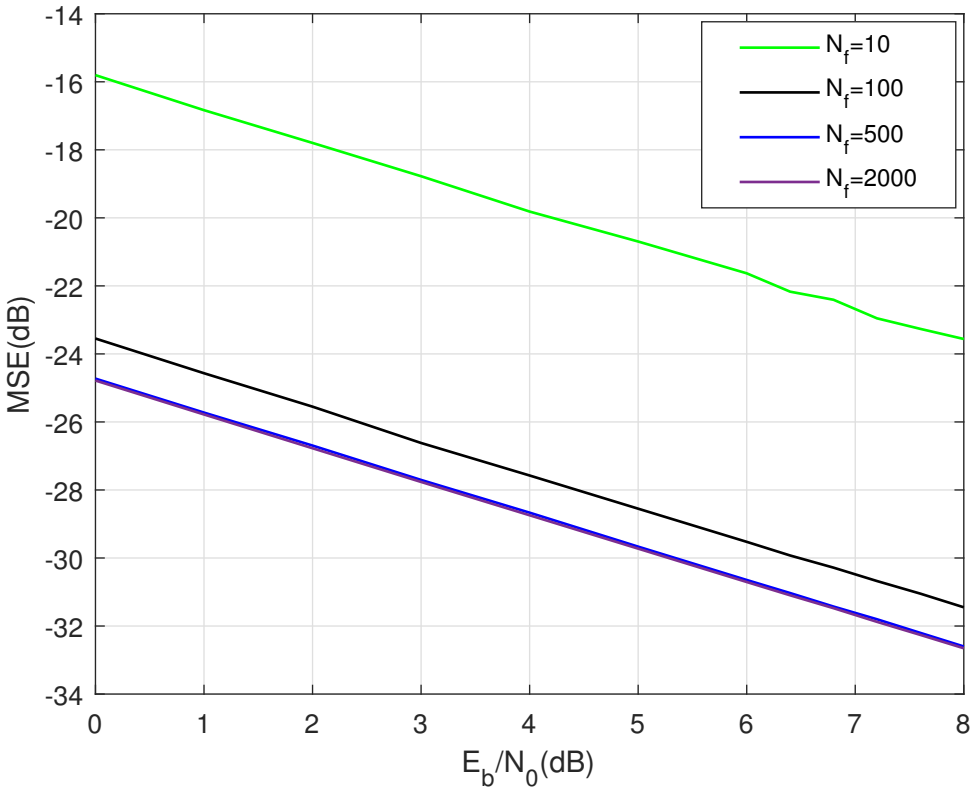

Figure 5.13: MSE vs. E_b/N_0 of the averaging block pilot using the same weight factor a=0.1 and different frame - 10, 100, 500 and 2000 over LDPC coded system.

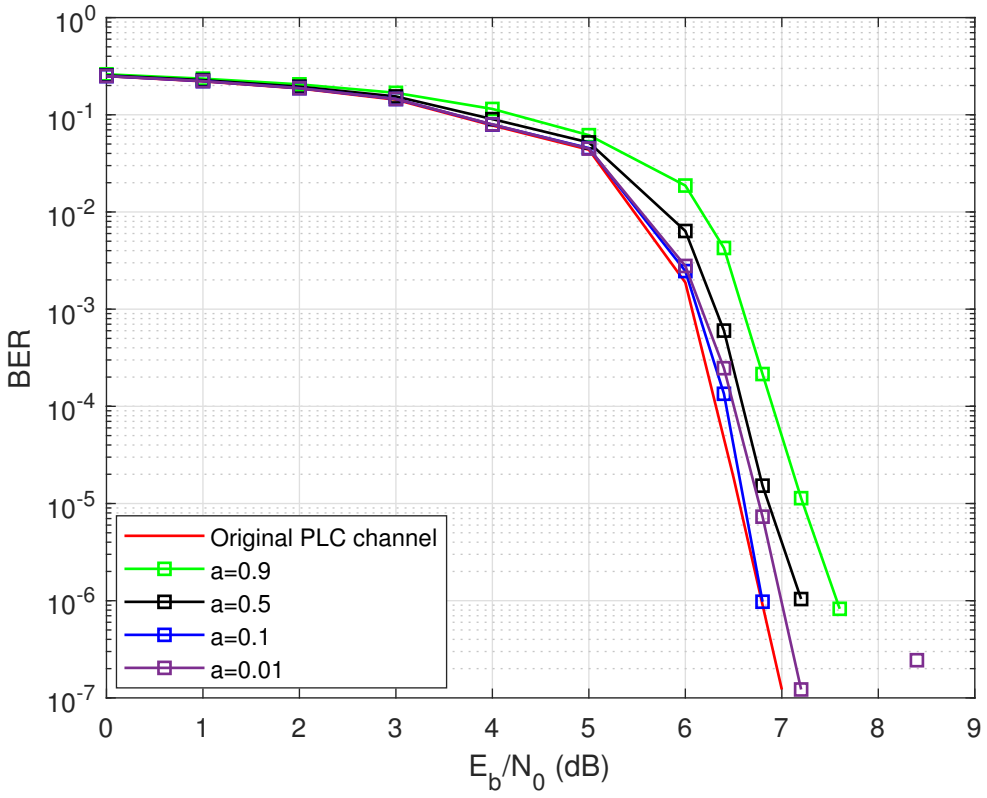

Figure 5.14: The BER performance by using averaging block pilot with the frame=500 and different weight factor - 0.9, 0.5, 0.1 and 0.01 over LDPC coded system.

system with the 0.01 weight factor is larger than the 0.1 weight factor system. In conclusion, the block pilot system with the 0.1 weight factor averaging approach can give the best BER performance and lowest MSE. The following simulation about other types of the channel estimation methods are all under the 0.1 weight factor to investigate the BER performance and the MSE results.

As it can be seen in Fig. 5.16, the BER performances over both block pilot and comb pilot systems demonstrate a significant improvement by using the averaging method. At the BER of 10^{-5}, the SNR gap between averaging process and non-averaging process over block pilot and comb pilot methods are 0.6 dB and 0.9 dB, respectively. The value of MSE of both channel estimation approaches are reduced rapidly, which is displayed in Fig. 5.17. Meanwhile, the performance of the block pilot is better than the comb pilot because only noise can affect the performance of channel estimation in the block pilot with the constant mimo-PLC CFR. However, the comb pilot system can be affected by not only the noise but also the error of interpolation method. With the same value of the P-I Ratio and the constant CFR of the MIMO-PLC, the performance of the block pilot is always better than the

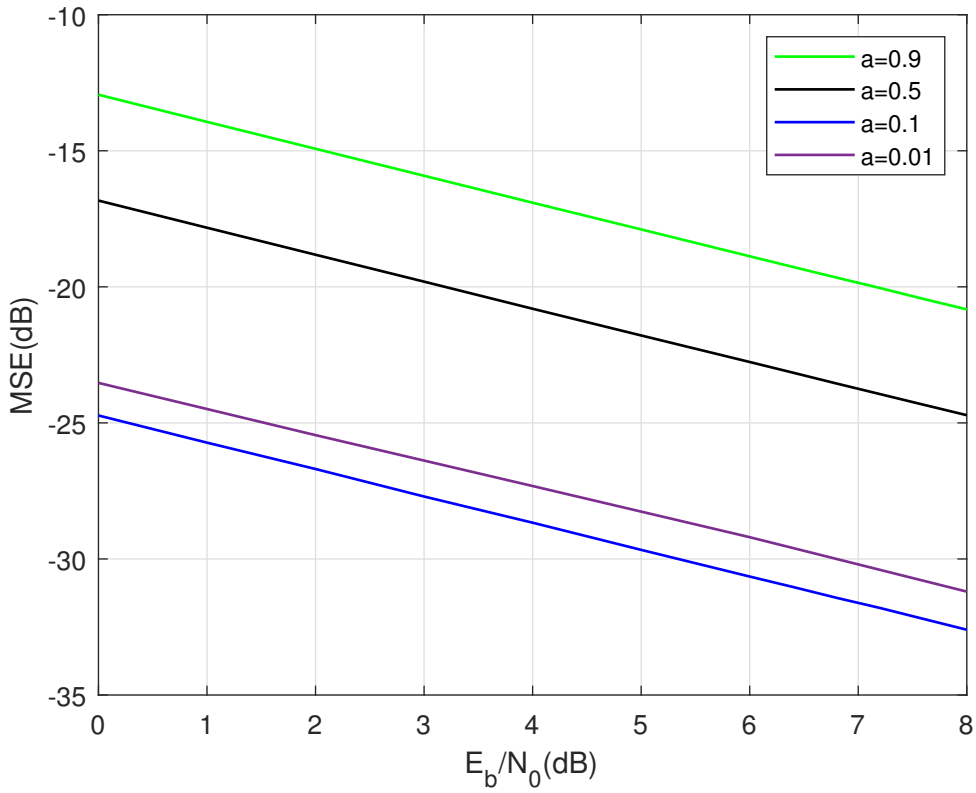

Figure 5.15: The MSE vs. E_b/N_0 by using averaging block pilot with the frame=500 and different weight factor - 0.9, 0.5, 0.1 and 0.01 over LDPC coded system.

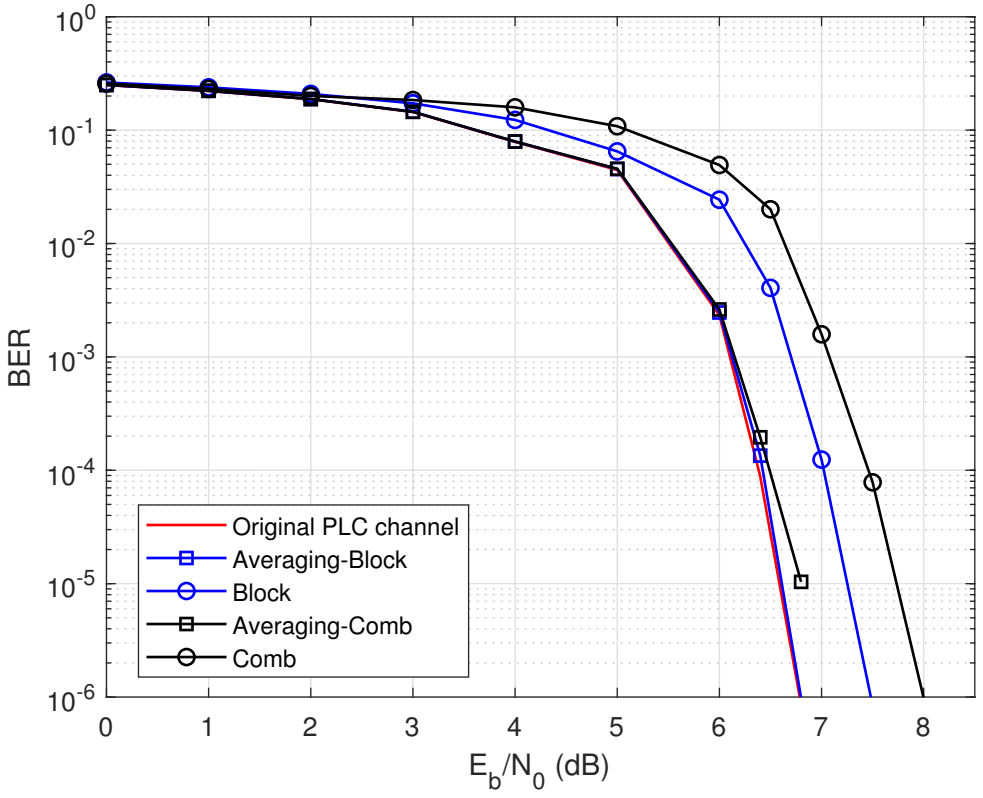

Figure 5.16: The BER performance over the averaging block pilot and the comb pilot method over LDPC coded system.

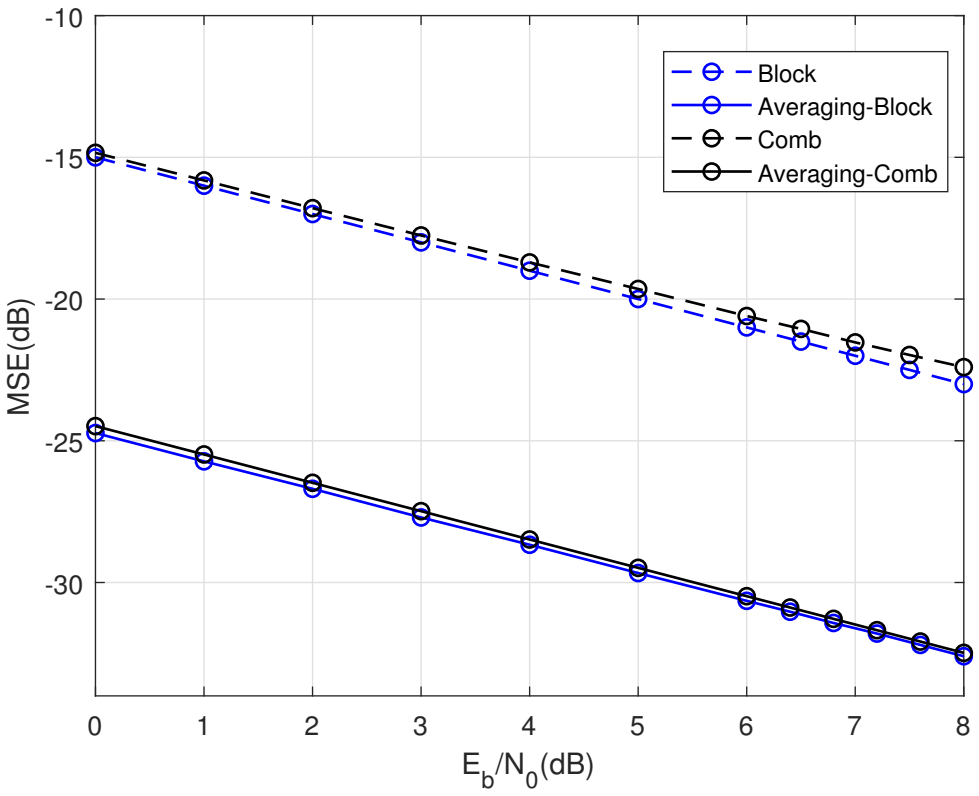

Figure 5.17: The MSE vs. E_b/N_0 over the averaging block pilot and the comb pilot method over LDPC coded system.

comb pilot.

5.7.4 M-ary QAM input signal in channel estimation system

Nowadays, many kinds of researches are focus on the higher-order QAM modulation to increase the transmission speed in the transmitter part. As the order of QAM increased, the BER performance became worse even the speed of transmission was faster. In [109], the calculation of QAM bit error probability has been presented. The research plotted the BER performance of the system is reduced with the higher-order QAM modulation. In this thesis, the proposed averaging approach has been investigated in higher-order QAM systems as well. As it can be seen in Fig. 5.18, the BER performance by using the averaging block and the comb pilot over 64-QAM, 256-QAM and 1024-QAM input signal are attained and give a contrast between the original PLC system performance and estimated channel performance. As excepted, the averaging approach using in any pilot design can give a massive improvement in BER performance. the BER performance over estimated CFR is very close to that of the original CFR.

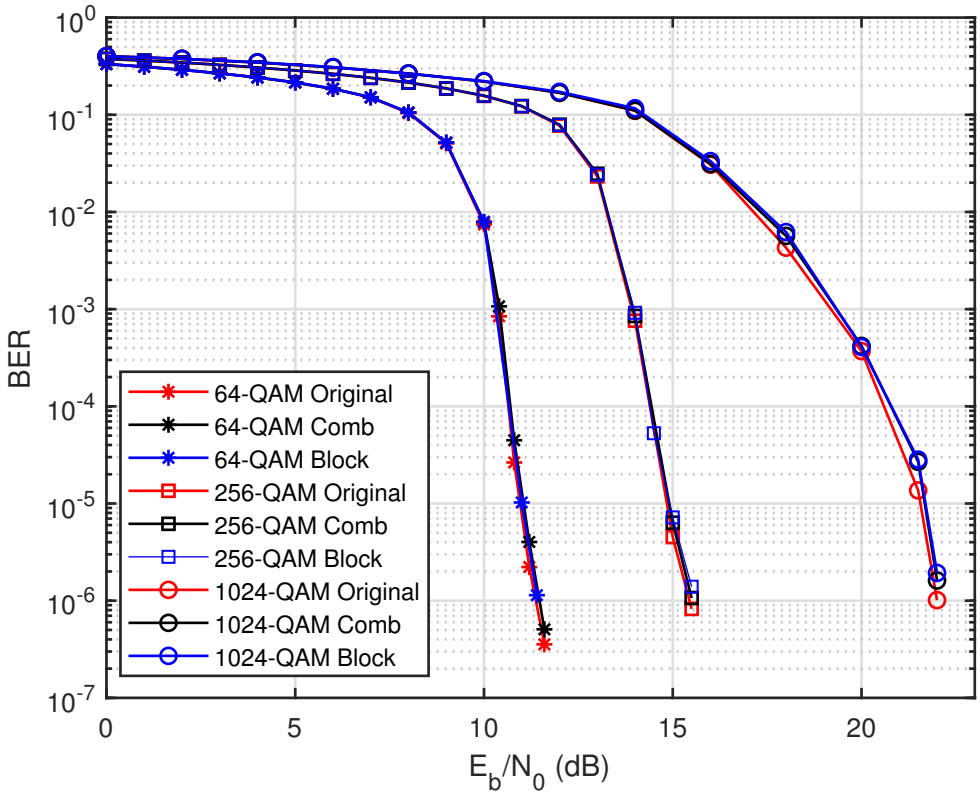

Figure 5.18: BER performance over the averaging block and comb pilot system with 64, 256 and 1024-QAM input signal over LDPC coded system.

Fig. 5.19 shows the MSE vs. E_b/N_0 over the averaging block and the comb pilot system with 64-QAM, 256-QAM and 1024-QAM input signal. All the values of MSE are no larger than -26 even the E_b/N_0 is 0 dB, in other words, the estimated CFR produced by either Av-comb pilot or Av-block pilot is very close to the original CFR. Moreover, the averaging block method has slightly better performance than the averaging comb pilot method. Even more interesting is that the MSE of the higher-order QAM system (1024-QAM) is lower than the MSE of lower-order QAM (64-QAM). In the simulations, the value of pilot is defined as

$$P = (\sqrt{M} - 1) + (\sqrt{M} - 1)j. \tag{5.57}$$

As the value of M increased, the magnitude of pilot value increased, and the power of the pilot data became more extensive, the impact of the noise reduced. Thus, the MSE of the higher-order QAM system is reduced and the estimated CFR is closer to the original CFR.

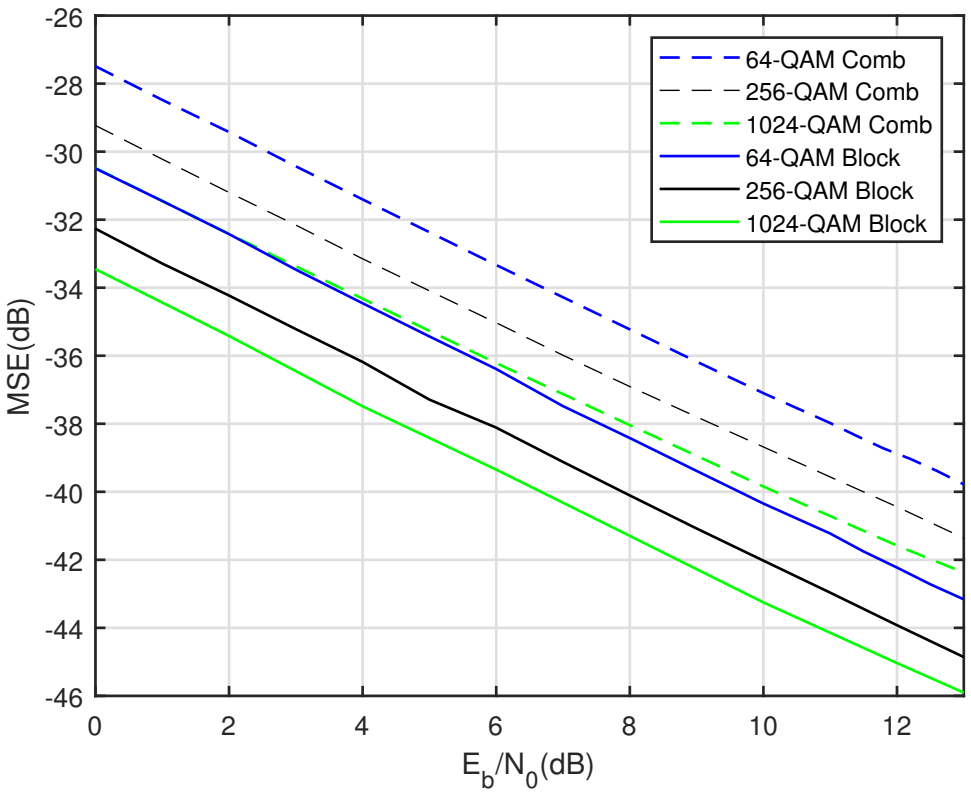

Figure 5.19: The MSE vs. E_b/N_0 over the averaging block and the comb pilot system with 64, 256 and 1024-QAM input signal over LDPC coded system.

5.7.5 The averaging channel estimation method over SαS noise channel

In Chapter 4, the SαS distribution noise channel has been investigated in the SISO-PLC system. In this section, the investigation is focused on the channel estimation MIMO-PLC system. Fig. 5.20 demonstrated a comparison of the BER vs. E_b/N_0 for both the averaging block pilot and the averaging comb pilot MIMO-PLC channel estimation system over either SαS noise or AWGN. At a BER of 10^{-5}, the E_b/N_0 of the averaging block pilot over the AWGN noise channel is about 6.6 dB, and the averaging comb pilot is about 6.8 dB. Both methods have better BER performance of the system over SαS noise channel, which is about 7.8 dB E_b/N_0. Fig. 5.21 derived the MSE of two types channel estimation methods using in MIMO-PLC system over SαS noise and AWGN. Even the SαS distribution noise ($\alpha = 2$) conforms to Gaussian distribution and the averaging approach can improve the system's performance, the impulsive noise still have a more significant impact on the MIMO-PLC system than the AWGN. Thus, the value of MSE by using both pilot methods is increased over SαS noise.

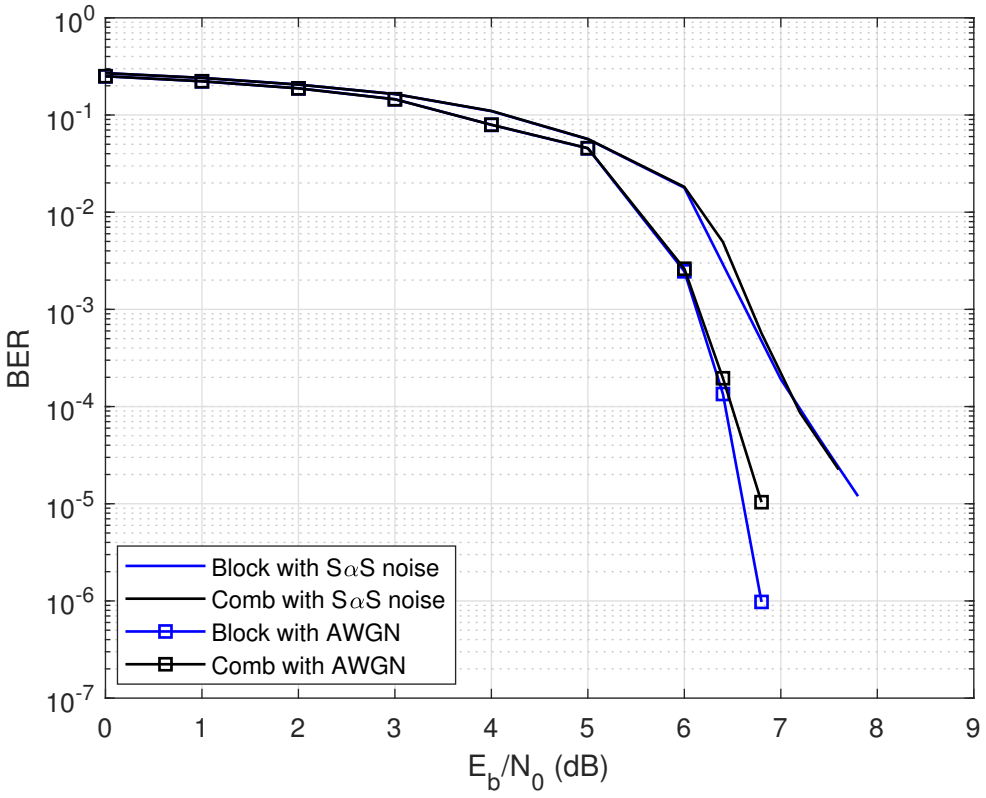

Figure 5.20: The BER performance in channel estimation LDPC coded system over SαS noise and AWGN.

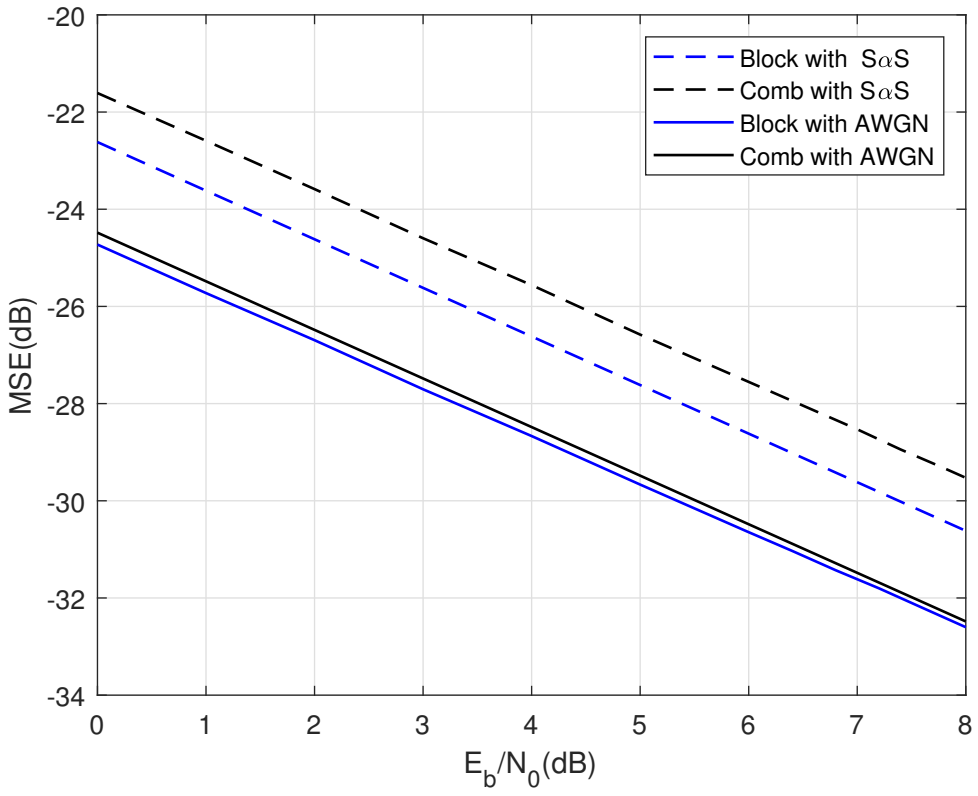

Figure 5.21: The MSE vs. E_b/N_0 in channel estimation LDPC coded system over SαS noise and AWGN.

5.7.6 The averaging channel estimation method using the MRC equalizer

In Chapter 4, the MRC equalizer at the receiver part can optimize the SISO-PLC performance. In this section, the MRC technology is utilized in the MIMO-PLC system as well. Moreover, the estimated CFR has been investigated to produce the MRC equalizer and demonstrated a the BER performance contrast between both two types of pilot design methods. Fig. 5.22 derives the BER performance over the original PLC system and both averaging block and comb pilot systems with MRC equalizer. Compared to Fig. 5.16, the performance of the MIMO-PLC system has considerable optimization. For the MRC equalizer, the E_b/N_0 is lower than 7 dB when the BER of 10^{-7}. On the other hand, the E_b/N_0 is about 7 dB when the BER is more significant than 10^{-7} with the MMSE equalizer. Fig. 5.23 plots the MSE of both two pilot methods over the MRC equalizer. Compared to Fig. 5.17, the value of both MSE are totally same. In other words, the different type of the equalizer cannot affect the performance of the channel estimation method. Back to Fig. 5.22, There are noticeable differences in the BER performance between the two-channel estimated systems and the original system. Thus, based on these results it can be concludes that using the MRC equalizer, the slight difference of CFR is amplified and this leads to the BER performance to become more prominent.

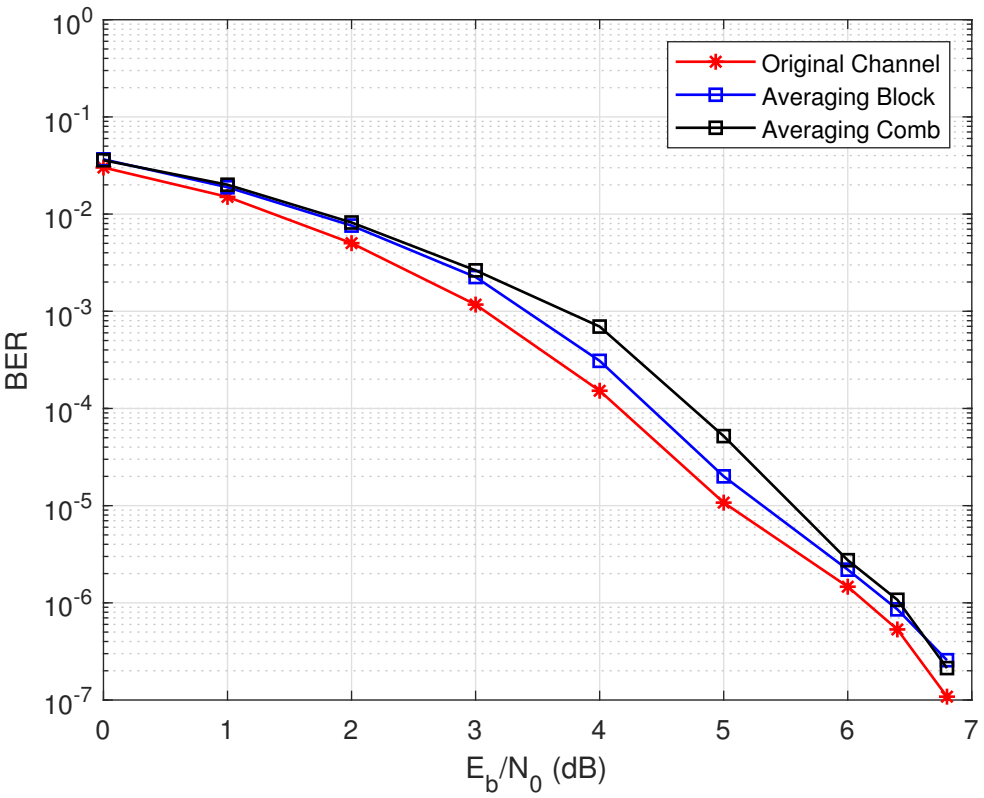

Figure 5.22: The BER performance in both the averaging block pilot and the comb pilot over LDPC coded system by using MRC equalizer.

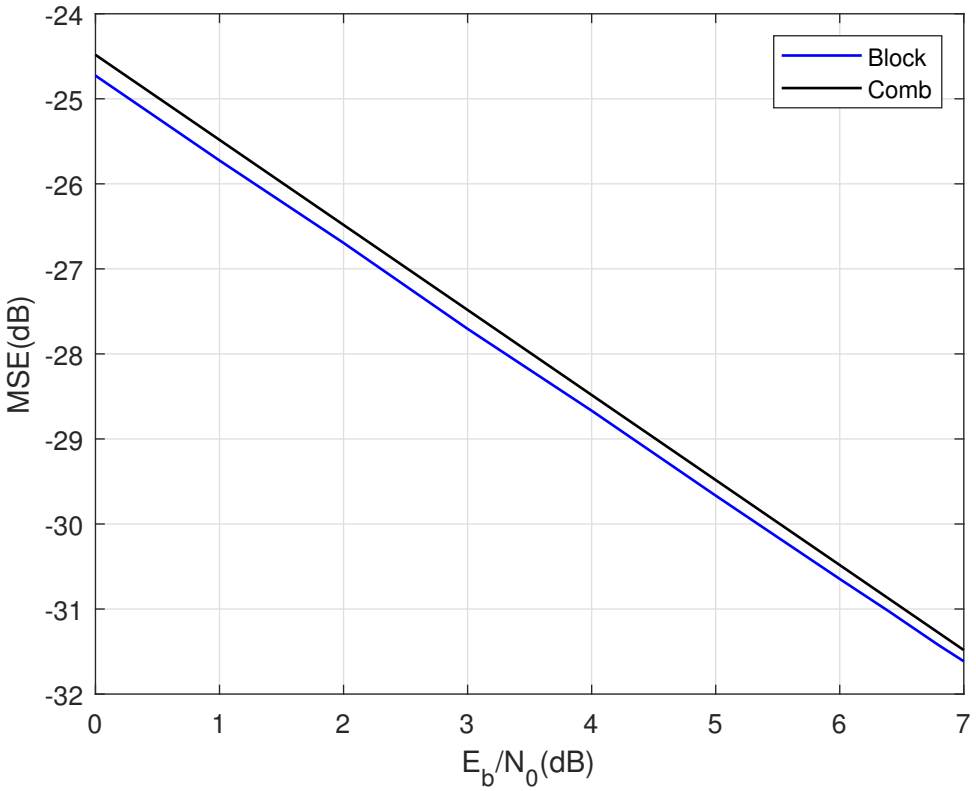

Figure 5.23: The MSE vs. E_b/N_0 in both the averaging block pilot and the comb pilot over LDPC coded system by using MRC equalizer.

5.8 Summary of the Chapter

In this Chapter, it can be focused on the investigation of the performance of different channel estimation methods. Two types of pilot design, i.e. block pilot and comb pilot have been introduced and their BER performance has been investigated for different P-I Ratios. The numerical results ontained show that for a P-I Ratio of 1:8 is optimal in terms of BER performance at minimal signal overhead. Furthermore, two interpolation methods were investigated for the comb pilot based channel estimation. The BER performance for these two systems has been plotted in Fig. 5.10 and Fig. 5.11. The comb pilot systems utilized spline interpolation method to obtain improved BER performance and lower MSE. Finally, the proposed averaging approach has been presented in this Chapter to further improve the performance of traditional channel estimation methods. Fig. 5.16 to Fig. 5.21 plotted the results of both block and comb pilot combined with the averaging process for different conditions of the MIMO-PLC channel system, including the higher-order QAM and SαS based impulsive noise. According Fig. 5.16 and Fig. 5.17, At the BER of 10^{-5}, the SNR gap between averaging process and non-averaging process over block pilot and comb pilot methods are 0.6 dB and 0.9 dB, respectively. According to other results, using the averaging approach, the estimated CFR produced by both block and comb pilot methods closely matches the original MIMO-PLC CFR over MIMO-PLC. The BER performance over other conditions of the MIMO-PLC systems can also have a greater improvement.

Chapter 6

Nonzero-Comb Pilot

6.1 Introducion

In the 2×2 MIMO systems, the pilot space of zero-comb pilot approach is 16 to get a P-I Ratio of 1:8 over each frame. Thus, the interpolation method cannot accurately estimate CFR by such a large gap between each pilot. Thus, there is no significant improvement in the BER performance over MIMO-PLC system by using zero-comb pilot design. In this Chapter, a novel pilot design method is proposed referred to as NZCP in order to fix the problem introduced by the zero-comb pilot insertion required to avoid pilot contamination in MIMO systems. The NZCP removes the zero data and maintains the P-I Ratio of 1:8. Meanwhile, the impact of channel interference brought by the MIMO system can be eliminated as well. The novel idea of the NZCP design is elaborated at the beginning. Furthermore, the derivation process of the proposed pilot design method is described. Moreover, the caculation of NZCP MSE is computed. In addition, the averaging approach is utilized in the NZCP design and gives a vast improvement in terms of BER and MSE performance. Finally, the numerical results sectopm provides the a performance comparison between NZCP and alternative types of pilot estimation methods.

6.2 Novelty of the proposed NZCP approach

The received signal on pilot position at the first receiver of the 2×2 MIMO-PLC channel can be defined as

$$R_p^1 = H_p^{1,1} X_p^1 + H_p^{2,1} X_p^2 + W_{S_p}^1, \tag{6.1}$$

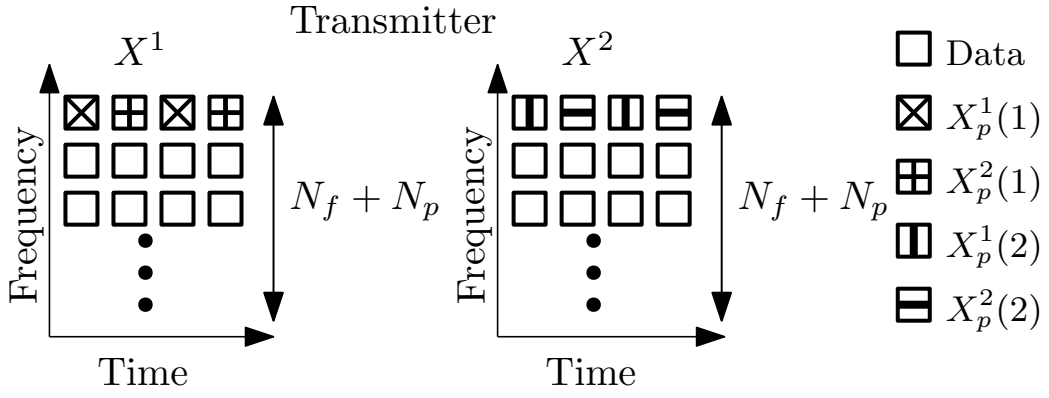

Figure 6.1: Nonzero comb pilot model.

where R^1 is received signal at the first receiver, $H^{1,1}$ and $H^{2,1}$, are the original CFR from two transmitters, X^1 and X^2 are the two transmitted signals for two transmitters, ${W_S}^1$ is the noise part of the first receiver and p is the index of pilot position. Even the input and the output signal are all known with the ignoring noise part, the function cannot get the solution of two values of CFR. To solve for the two unknown channel gains - $H^{1,1}$ and $H^{2,1}$, we need two functions. The zero-comb pilot method is achieved by inserting zeros in pilot subcarriers of adjacent MIMO channels. There is only one unknown variable in the zero-comb pilot function. Pilot contamination will result in an underdetermined system of equations with two unknown variables and only two equations to solve the problem. The proposed NZCP method to estimate the channel interference is presented next.

6.3 Analysis of the NZCP

To solve the 2×2 system of equations in (5.9) for the four unknown channel gains, $H_p^{1,\rho}$ and $H_p^{2,\rho}$, $\rho = \{1, 2\}$, with one received OFDM symbol is impossible, since the system is underdetermined. To overcome this problem, we assume the PLC channel is static over two received OFDM symbols and use two subsequent received symbol vectors to solve (6.1), that is

$$R_p^{\rho}(\zeta) = H_p^{1,\rho} X_p^1(\zeta) + H_p^{2,\rho} X_p^2(\zeta) + {W_S}_p^{\rho}(\zeta), \tag{6.2}$$

where R_p^{ρ} is the received OFDM signals, $\zeta = \{1, 2\}$ denotes the OFDM symbol index. The proposed nonzero comb pilot system model with a the pilot spacing of 8 can be seen in Fig. 6.1, where the number of pilot subcarriers is $N_p = 512$, and

total number of subcarriers is $N_{fft} + N_p = 4608$. According to (6.2), the original channel frequency response can be derived as

$$H_p^{1,\rho} = \frac{R_p^{\rho}(1) - H_p^{2,\rho} X_p^2(1) - W_{S_p}^{\rho}(1)}{X_p^1(1)}, \tag{6.3}$$

$$H_p^{2,\rho} = \frac{R_p^{\rho}(2) - H_p^{1,\rho} X_p^1(2) - W_{S_p}^{\rho}(2)}{X_p^2(2)}. \tag{6.4}$$

Combining (6.3) and (6.4), we can only solve for one of the unknown elements, i.e. the value of $H_p^{1,\rho}$, that is

$$\begin{aligned} H_p^{1,\rho} &= \frac{R_p^{\rho}(1) - \frac{R_p^{\rho}(2) - H_p^{1,\rho} X_p^1(2) - W_{S_p}^{\rho}(2)}{X_p^2(2)} X_p^2(1)}{X_p^1(1)} \\ &\quad - \frac{W_{S_p}^{\rho}(1)}{X_p^1(1)} \end{aligned} \tag{6.5}$$

After straight forward mathematical manipulations, $H_p^{1,\rho}$ can be re-written as

$$H_p^{1,\rho} = \frac{R_p^{\rho}(1) X_p^2(2) - R_p^{\rho}(2) X_p^2(1)}{X_p^1(1) X_p^2(2) - X_p^2(1) X_p^1(2)} + V_p^{1,\rho}, \tag{6.6}$$

where $V_p^{1,\rho}$ represents the value of the noise part of the signal given as

$$V_p^{1,\rho} = \left| \frac{W_{S_p}^{\rho}(2) X_p^2(1) + W_{S_p}^{\rho}(1) X_p^1(1)}{X_p^1(1) X_p^2(2) - X_p^2(1) X_p^1(2)} \right|. \tag{6.7}$$

To estimate the CFR, the noise part in is ignored in (6.6), i.e.

$$\tilde{H}_p^{1,\rho} = H_p^{1,\rho} - V_p^{1,\rho} \tag{6.8}$$

$H_p^{2,\rho}$ is computed using a similar approach.

It can be shown that the estimated CFR matrix of MIMO-PLC in nonzero-comb pilot system can be computed as

$$\begin{aligned} \tilde{H}_p^{1,\rho} &= H_p^{1,\rho} - V^{1,\rho} \\ &= \frac{R_p^{\rho} 1 X_p^2(2) - R_p^{\rho}(2) X_p^2(1)}{X_p^1(1) X_p^2(2) - X_p^2(1) X_p^1(2)}, \end{aligned} \tag{6.9}$$

$$\tilde{H}_p^{2,\rho} = \frac{R_p^{\rho}(1)X_p^1(2) - R_p^{\rho}(2)X_p^1(1)}{X_p^2(1)X_p^1(2) - X_p^1(1)X_p^2(2)}. \tag{6.10}$$

The NZCP approach requires the following condition, which is necessary to avoid a zero in the denominator of (6.6), i.e.

$$X_p^2(1)X_p^1(2) \neq X_p^1(1)X_p^2(2). \tag{6.11}$$

As the OFDM symbol in the frequency domain is complex-valued, we need to consider both the real and imaginary parts of the pilot symbols. Thus, we can rewrite (6.11), the condition of the pilot design as

$$\mathrm{Re}\{X_p^2(1)X_p^1(2)\} \neq \mathrm{Re}\{X_p^1(1)X_p^2(2)\}, \tag{6.12}$$

$$\mathrm{Im}\{X_p^2(1)X_p^1(2)\} \neq \mathrm{Im}\{X_p^1(1)X_p^2(2)\}. \tag{6.13}$$

To improve the SNR and thus the channel estimation and BER performance, it is advantageous to use for pilots QAM constellation symbols that are the farthest away from the origin (0,0), as they have the highest energy. To achieve this, the value of all the pilots in the NZCP are selected as

$$X_p^1(1) = X_p^2(1) = X_p^1(2) = -X_p^2(2) = (\sqrt{M} - 1)(1 + j), \tag{6.14}$$

where M denotes the order of QAM and $j^2 = -1$. It is worth noting that $X_p^2(2) = -(\sqrt{M} - 1)(1 + j)$ so that the condition is met (6.11).

The nonzero-comb pilot method does not need zero data to avoid channel interference. In other words, it can save half the number of pilot positions and transmit the information data instead to increase the channel capacity.

6.4 MSE of NZCP

Using (5.14), (6.7) and (6.8), the MSE of the NZCP method can be given as

$$\begin{aligned} V_p^{1,\rho} &= |H_p^{1,\rho} - \tilde{H}_p^{1,\rho}| \\ &= \left| \frac{W_{S_p}^{\rho}(2)X_p^2(1) + W_{S^p}^{\rho}(1)X_p^1(1)}{X_p^1(1)X_p^2(2) - X_p^2(1)X_p^1(2)} \right|. \end{aligned} \tag{6.15}$$

Here, X_p represents the pilot symbols and can be replaced by P. Hence, (6.15) can be re-written as

$$\begin{aligned} \left|H_p^{1,\rho} - \tilde{H}_p^{1,\rho}\right| &= \left|\frac{W_{S_p^\rho}(2)P + W_{S_p^\rho}(1)P}{-PP - PP}\right| \\ &= \left|\frac{W_{S_p^\rho}(1) + W_{S_p^\rho}(2)}{2P}\right|. \end{aligned} \tag{6.16}$$

Combining (5.14) and (6.16), the MSE of NZCP method can be demonstrated as

$$MSE_{\text{nz}} = 10\log_{10}\left(\frac{1}{N_{fft}}\sum_{n_{fft}=1}^{N_{fft}}\left|\frac{W_{S_{n_{fft}}^\rho}(1) + W_{S_{n_{fft}}^\rho}(2)}{2P}\right|^2\right). \tag{6.17}$$

where $X_{n_{fft}}^{\tau,\rho}$ is the value of block pilot and P is the value of comb pilot.

6.5 Results

This section focus on the performance of the proposed NZCP channel estimation method. The research results will be displayed from the following aspects. First of all, the investigation focused on the impact of the P-I Ratio on the performance of the NZCP system. Meanwhile, the result plots the performance contrast between the block/comb pilot and the NZCP system. Secondly, the optimal extent of the averaging approach to the NZCP method has been derived in this section. Furthermore, the proposed averaging NZCP method is utilized over the high order QAM system and optimizes the system's performance. Moreover, the BER performance and MSE value by using the averaging NZCP method over SαS noise channel have been demonstrated. Finally, an MRC equalizer is applied in the estimated channel system to optimize the BER performance of the estimated channel system.

6.5.1 NZCP and averaging NZCP over 16-QAM system

Fig. 6.2 plots the BER performance over the NZCP method system with P-I Ratio is 1:2, 1:4, 1:8, 1:16, 1:32 and 1:64. As it can be seen in this figure, there is no difference between the BER performance with 1:2, 1:4,1:8 and 1:16 P-I Ratios. When the P-I Ratio reduced to 1:32, the E_b/N_0 is about 7.9 dB at a BER of 10^{-6}. For the 1:64 rate system, the BER performance cannot be lower than 10^{-3} even the value of SNR

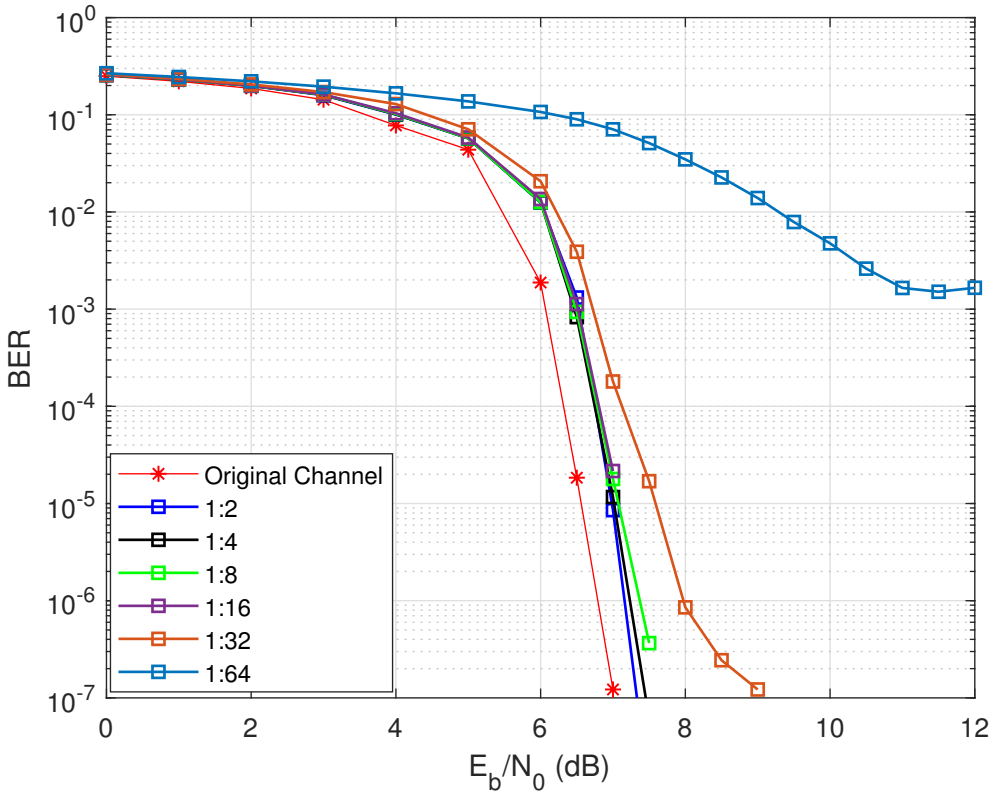

Figure 6.2: BER performance of the NZCP method using the ratio of pilot and information data as 1:2, 1:4, 1:8, 1:16, 1:32 and 1:64 over LDPC coded system.

increases to 12 dB.

Fig. 6.3 derives the MSE vs. E_b/N_0 of the NZCP method with the different P-I Ratio system. Compared to the results of the comb pilot method, which have been shown in Fig. 5.8 and Fig. 5.9, The value of MSE should be lower than -15 dB so that the system can get a more accurate estimated CFR and the BER performance can be close to the original PLC channel. It is worth noting that the BER performance and the value of MSE in the 1:32 P-I ratio comb pilot system are more similar to the 1:64 P-I rate NZCP system. Thus, the important number of elements contrast between comb pilot and NZCP has been demonstrated in the table. 6.1. It is worth noting that the BER results cannot reduce to 10^{-2} over the both 1:64 P-I rate NZCP and zero-comb pilot systems. The table uses $E_b/N_0 = 7$ as a condition to give a contrast of the BER value between different P-I Ratio systems.

The pilot gap denotes the length of data between two pilots' data except for the zero data. The BER performance and the value of MSE in the 1:32 P-I Ratio comb pilot system are more similar to the 1:64 P-I Ratio of NZCP system because they have the same pilot gap. Hence, we can summarize that the pilot gap has

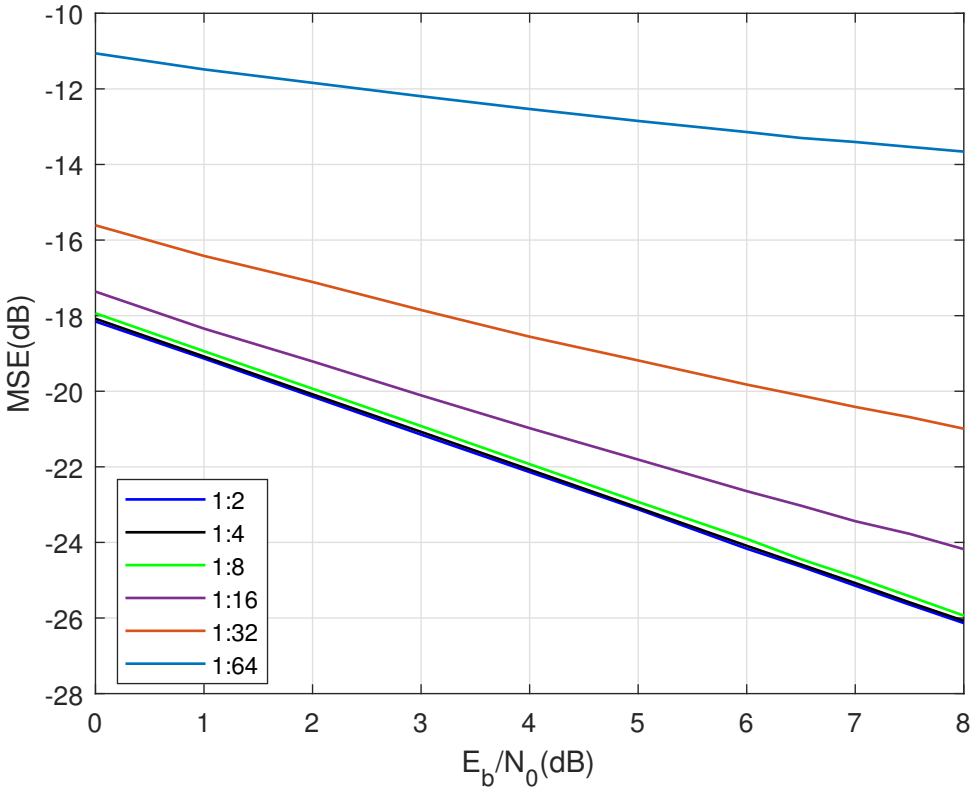

Figure 6.3: MSE vs. SNR of the NZCP method using the ratio of pilot and information data as 1:2, 1:4 and 1:8 over LDPC coded system.

Table 6.1: NZCP vs. traditional comb pilot (E_b/N_0=7).

P-I Rate	Method	Pilot	Zero	Information	Pilot gap	BER
1:8	Comb	256	256	4096	16	5.5×10^{-4}
	NZCP	512	0	4096	8	1.79×10^{-5}
1:16	Comb	128	128	4096	32	1.6×10^{-3}
	NZCP	256	0	4096	16	2.16×10^{-5}
1:32	Comb	64	64	4096	64	6.6×10^{-2}
	NZCP	128	0	4096	32	1×10^{-4}
1:64	Comb	32	32	4096	128	0.259
	NZCP	64	0	4096	64	0.071

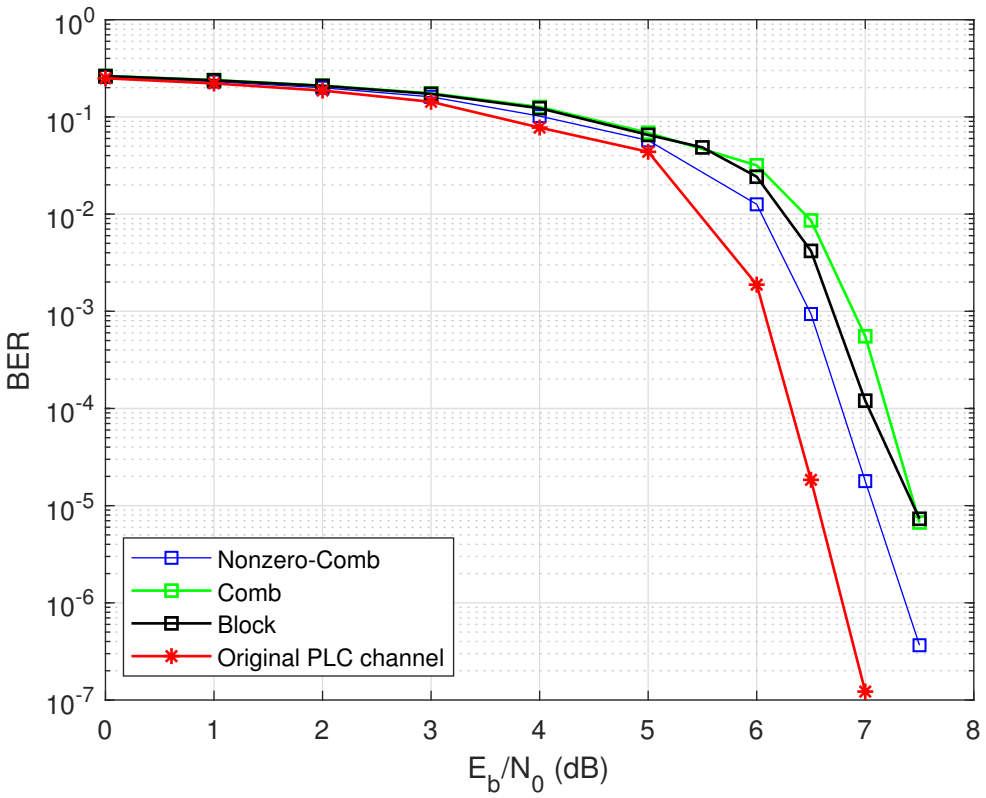

Figure 6.4: The contrast between the BER performance over NZCP, Block and Comb pilot system.

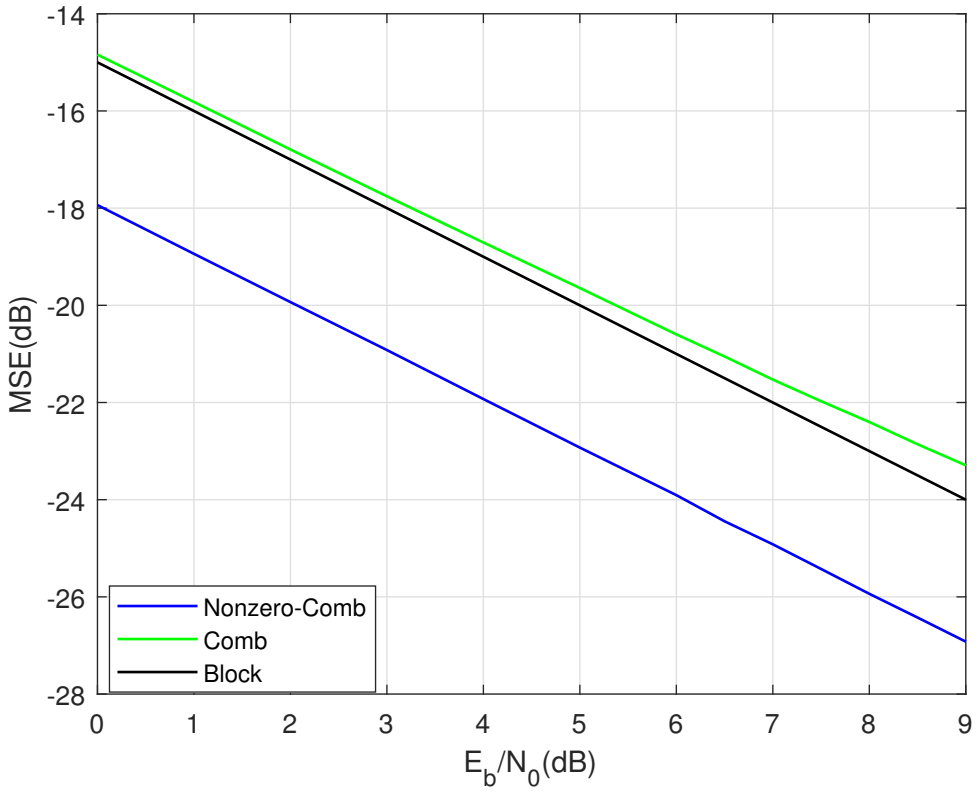

Figure 6.5: The contrast between the MSE vs. SNR over NZCP, Block and Comb pilot system.

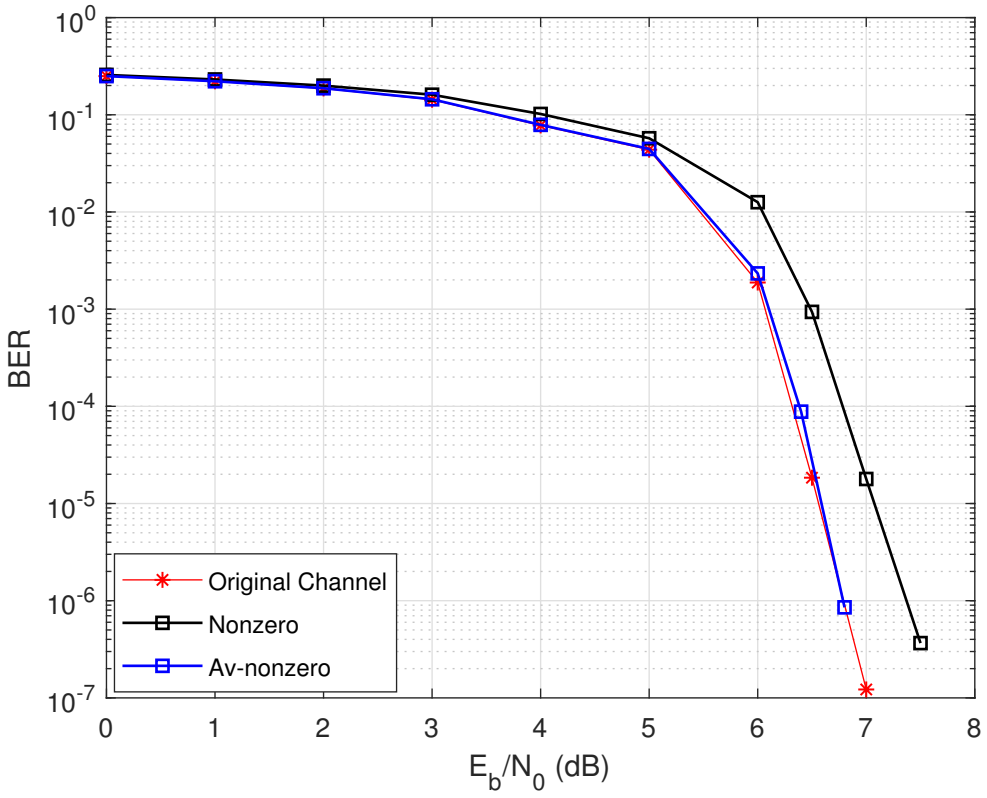

Figure 6.6: The BER performance by using averaging NZCP.

the most significant impact on the performance of the interpolation method. We can conclude that the performance of the channel estimation method. That is because the performance of the interpolation method can be affected by the density of the pilot over the input symbols. As the pilot gap reduces, the number of the pilot increases, the error of the interpolation becomes lower and the performance of interpolation method is improved. Besides, with the same pilot gap, the NZCP method can avoid the interference of the channel without the zero data. So that the zero data positions can be saved to transmit the information data. Thus, the BER performance and MSE contrast between block, comb and NZCP with 1:8 P-I Ratio are plotted in Fig. 6.4 and Fig. 6.5. At a BER of 10^{-5}, there is an improvement in E_b/N_0 of 0.3 dB against the block and the comb approaches by using the NZCP, respectively. Furthermore, the MSE of the NZCP method is lower 2.8 and 3.6 dB against the block pilot and the comb pilot at a E_b/N_0 of 9 dB. It is evident that the NZCP can rapidly optimize the performance of the system than other traditional channel estimation methods.

As it can be seen in Fig. 6.6, the BER performance of the proposed averaging NZCP methods outperforms the proposed NZCP approach. This also the case when

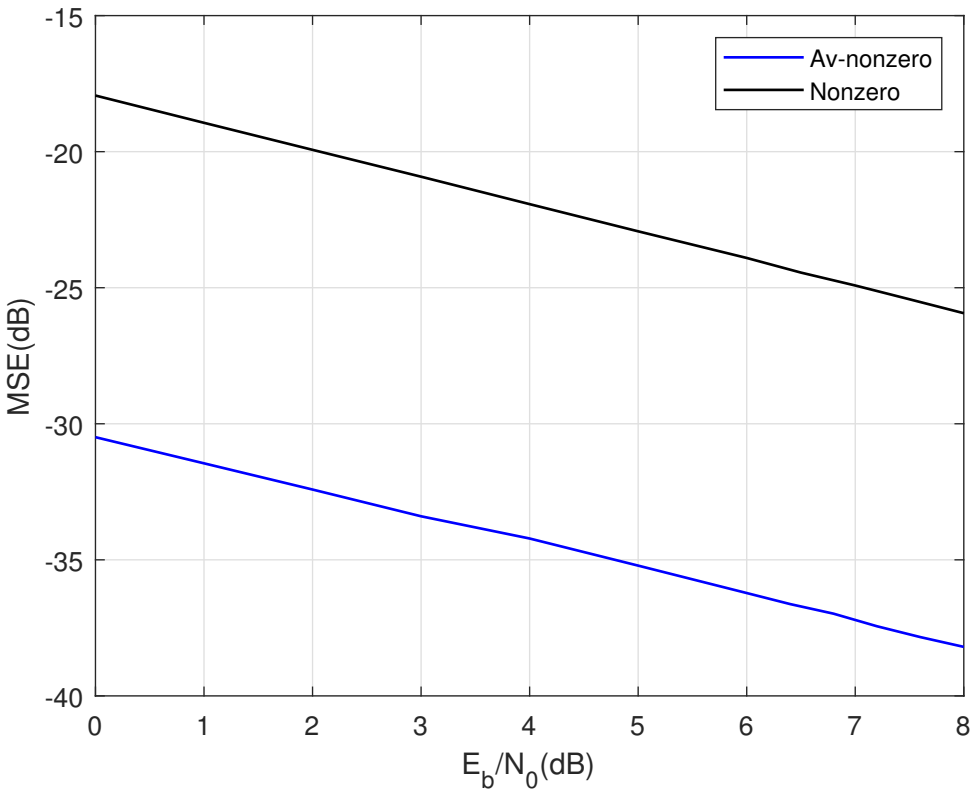

Figure 6.7: The MSE vs. SNR by using averaging NZCP.

averaging is utilized to improve performance against AWGN. There is approximately 0.5 dB improvement in E_b/N_0 between the averaging NZCP and the proposed NZCP without averaging approach, respectively. The improvement of the MSE of the averaging NZCP method can be seen in Fig. 6.7. There is more than 12 dB MSE gap between two methods at a E_b/N_0 of 8 dB.

It is worth noting that when the P-I Ratio reduce to 1:32, the averaging approach cannnot optimize the performance of the channel estimation system anymore. In Fig. 6.8 and Fig. 6.9, there are almost identical between the performance of the averaging NZCP and non-averaging NZCP method under both 1:32 and 1:64 P-I Ratio.

6.5.2 Averaging NZCP for higher-order QAM systems

The results of the averaging NZCP method using in higher order QAM system can be seen in Fig. 6.10 and Fig. 6.11. Compared to the block and comb pilot approaches, the averaging NZCP can give a better BER performance in higher order QAM system. The BER performance of the channel estimation system is extremely close to the original PLC channel system. Meanwhile, the MSE of averaging NZCP

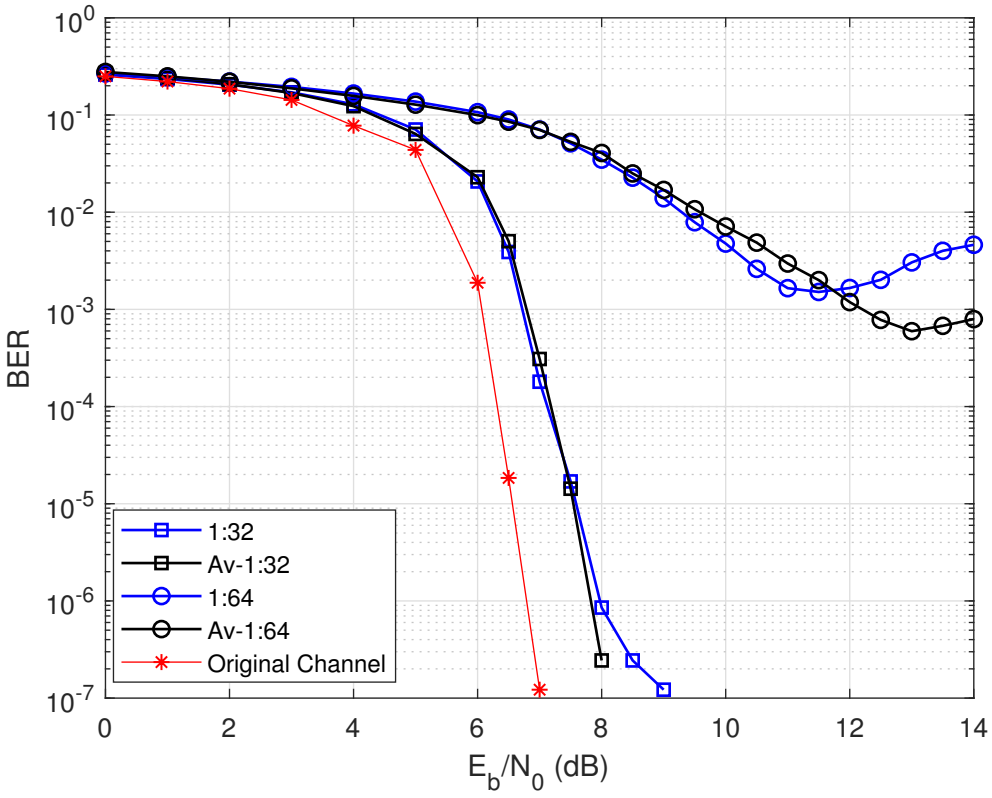

Figure 6.8: The BER performance by using NZCP and averaging NZCP over 1:32 and 1:64 P-I Ratio.

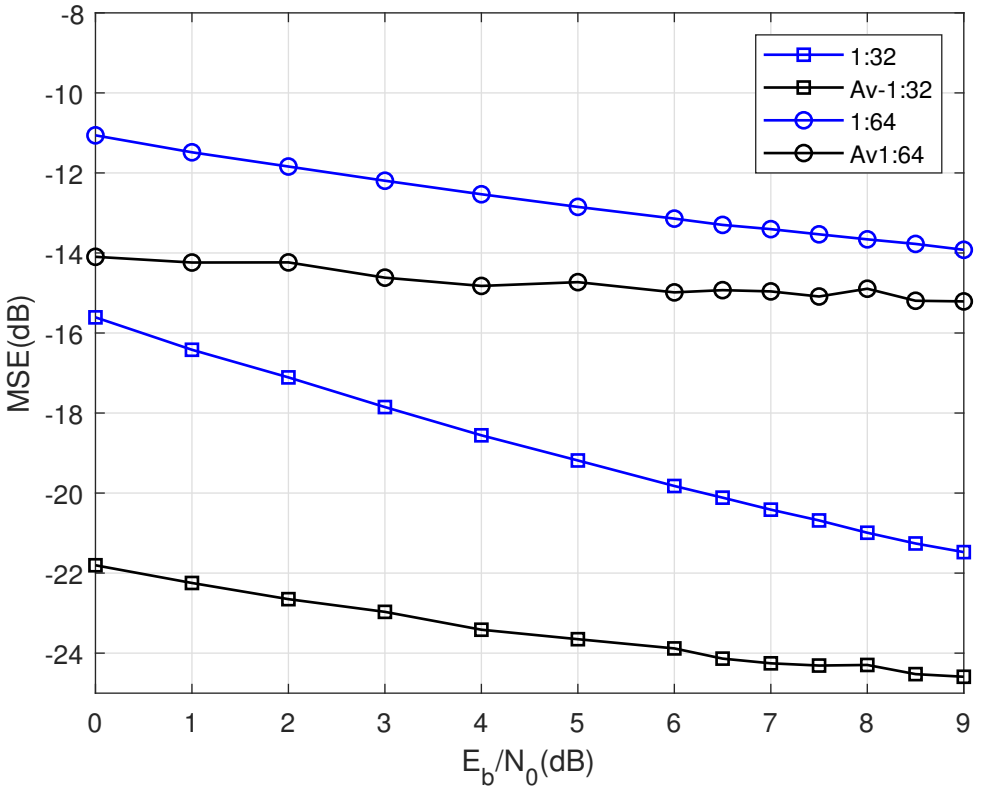

Figure 6.9: The MSE vs. SNR by using NZCP and averaging NZCP over 1:32 and 1:64 P-I Ratio.

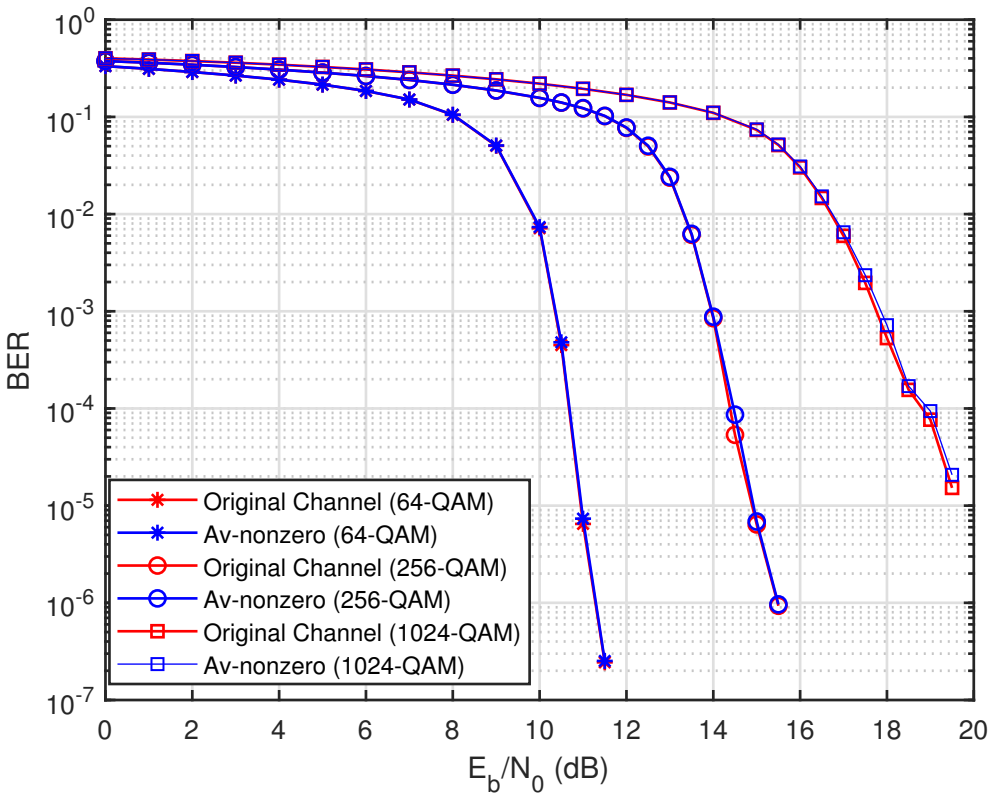

Figure 6.10: The BER performance over averaging NZCP system with 64-QAM, 256-QAM and 1024-QAM input signal.

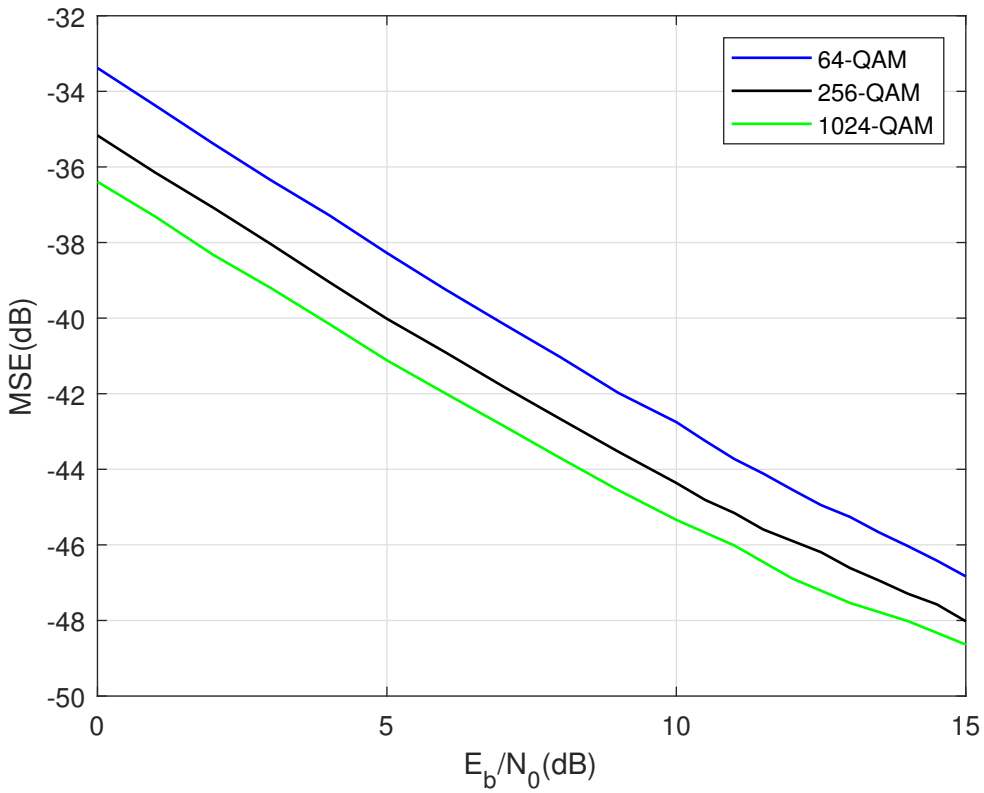

Figure 6.11: The MSE vs SNR over averaging NZCP system with 64-QAM, 256-QAM and 1024-QAM input signal.

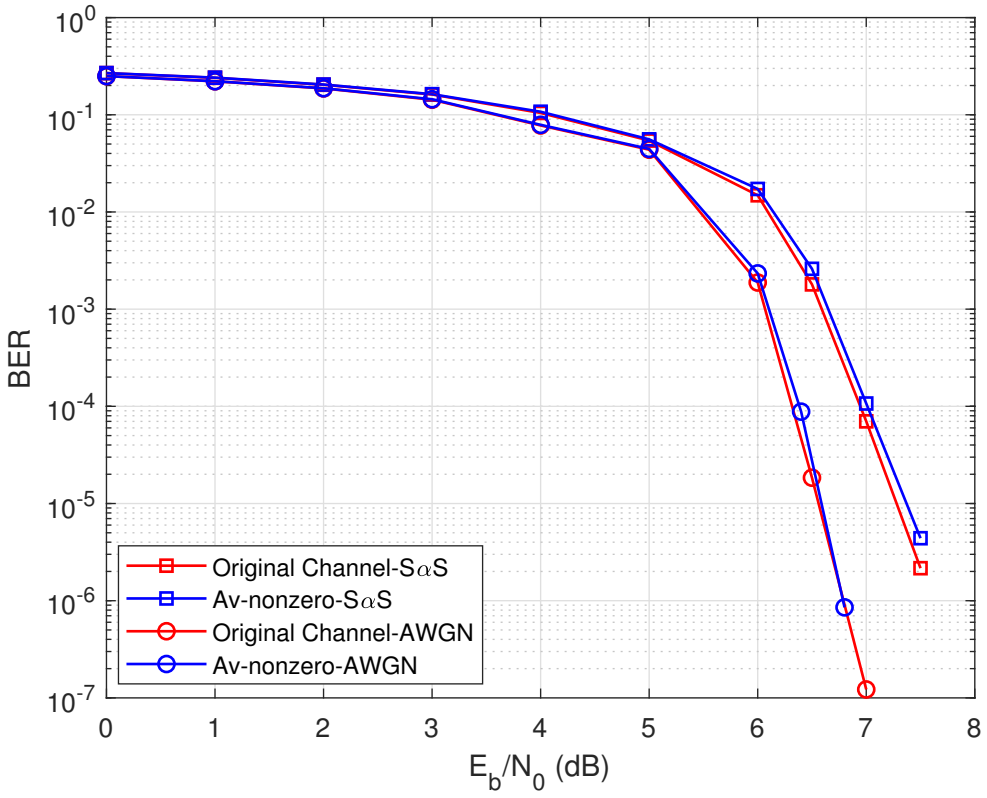

Figure 6.12: The BER performance by using averaging NZCP system over SαS noise and AWGN.

becomes lower against both block and comb pilot methods. There is the same situation compared with the block pilot system that as the order of QAM increased, the MSE of the system became lower.

6.5.3 Averaging NZCP over SαS noise channel

Fig. 6.12 and Fig. 6.13 display the BER performance and MSE results comparison between the SαS noise channel system and AWGN channel system by using the averaging NZCP channel estimation approach. Compared to the AWGN noise channel, the estimated channel by using the averaging NZCP over SαS noise can also give a great BER performance compared to the original channel result. It is evident that the averaging NZCP method can be utilized to improve the performance of channel estimation approach over any Gaussian distribution noise channel.

6.5.4 Averaging NZCP with MRC equalizer

In Fig. 6.14, the BER performance by using the averaging NZCP pilot over MRC equalizer has been derived to make a comparison to the system over MMSE equalizer.

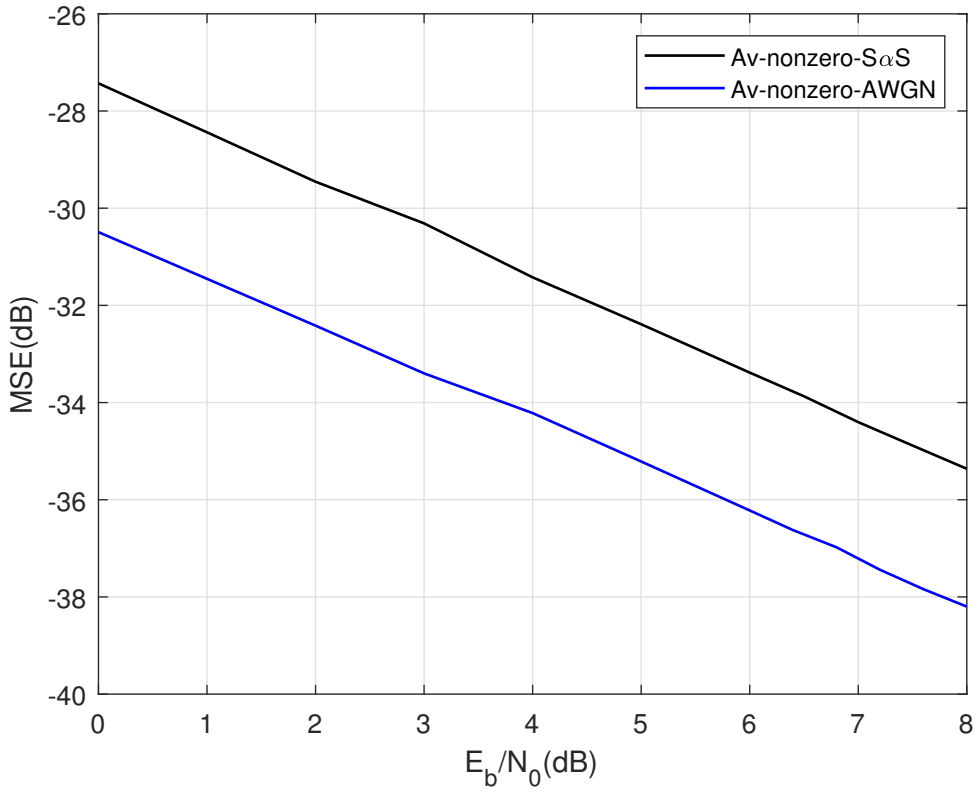

Figure 6.13: The MSE vs. SNR by using averaging NZCP system over SαS noise and AWGN.

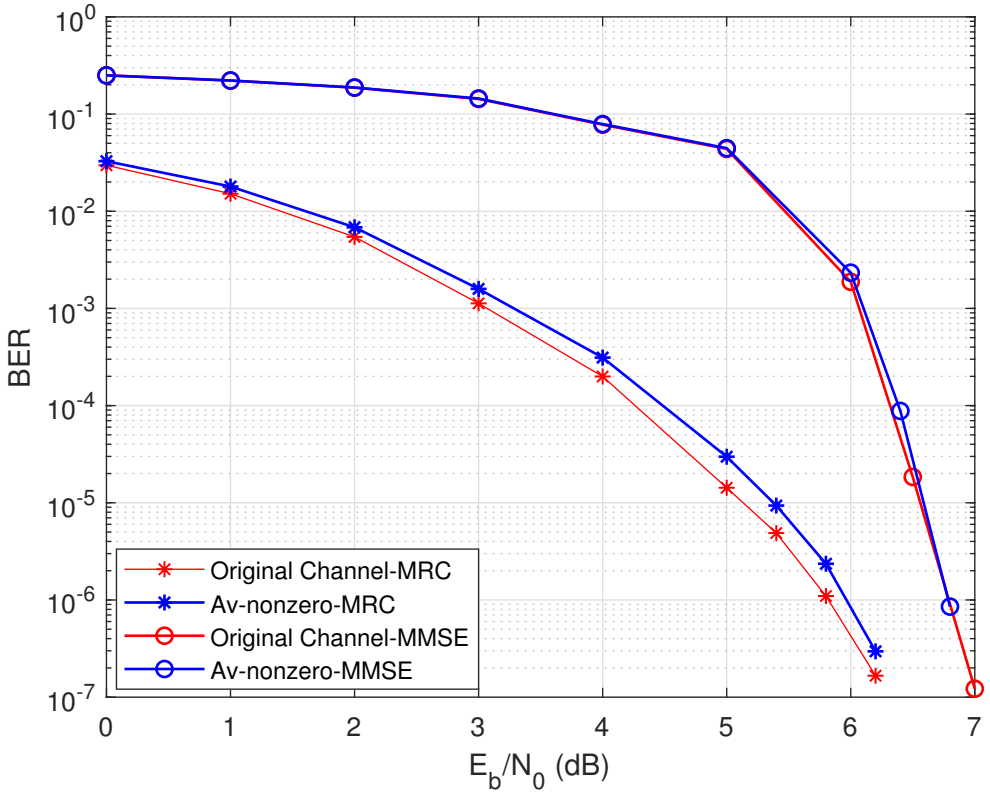

Figure 6.14: The BER performance over averaging NZCP system with MRC equalizer.

As the receiver does not affect the estimated CFR, the MSE of both equalizers should be the same. The BER performance of the averaging NZCP system can also be close to the usual performance trend. That means the averaging NZCP method can be utilized in the system with an MRC equalizer.

6.6 Summary of the Chapter

In this Chapter, the investigation focused on the proposed NZCP method for MIMO-PLC systems. The numerical results presented show that at a P-I Ratio of 1:8, the BER performance is the best and pilot overhead and channel capacity are optimal. Moreover, both comb pilot and NZCP methods depend on the performance of the interpolation method utilized. The NZCP approach allows the density of the pilot to increase, thus making the pilot gap became smaller. This in turn improved the performance of the pilot interpolation method and resulted in improved BER performance for both the comb pilot and NZCP approaches. Furthermore, it was demonstrated that the NZCP can save half of the pilot capacity at the same pilot gap compared to the traditional zero-comb pilot method while maintaining the BER performance. Furthermore, it was shown that the averaging approach can immensely improve the performance of the NZCP method. Finally, the BER performance of the NZCP method using averaging has been demonstrated for different higher-order QAM systems. The MSE results show that there is a slight difference between the estimated CFRs and the perfectly known CFRs by using the averaging-NZCP in the higher-order QAM system. Thus, the BER results over these systems have little difference between the perfectly known channel and estimated channel. Meanwhile, the BER results of the estimated PLC system over the SαS impulsive noise channel has a greater improvement by utilizing the averaging-NZCP method as well.

Chapter 7

Conclusions and Future Work

7.1 Conclusion

The investigation of this thesis is focused on the optimization of the performance of the PLC system. In SISO-PLC, LDPC and polar code are presented to utilize in the multipath PLC channel system. As the effect of SαS distribution impulsive noise on the PLC system had not been considered, this thesis compares the impact of AWGN and SαS noise on the performance of the PLC channel system. Moreover, the proposed MRC equalizer in the receiver part has been presented. Because of the real-valued OFDM input signal produced by the Hermitian symmetry, the MRC can reduce the impact of debilitation to a greater extent than the ZF and MMSE equalizer.

Furthermore, the channel estimation technology has been investigated in the MIMO-PLC channel system. The traditional block and comb pilot design methods have been utilized in the MIMO-PLC to estimate the CFR and give similar performance to the original PLC channel system. According to the results, there are still big gap between the BER performance over the estimated channel system and the original system. Thus, the proposed averaging approach has been presented to optimize the standard pilot design methods. Finally, to eliminate the impact of the channel interference of multiple channel systems and remove the zero data of the comb pilot method to increase the transmitter's capacity, the proposed NZCP has been constructed and utilized in the MIMO-PLC channel system. Meanwhile, combining with the proposed averaging approach, the MIMO-PLC channel system using averaging NZCP approach could demonstrate the best BER performance of

all channel estimation methods in this thesis.

In Chapter 4, the construction of SISO-multipath PLC with coded real-valued OFDM input signal over SαS noise channel was presented. As the symmetric OFDM input signal in frequency domain and asymmetric PLC channel frequency response, the proposed MRC equalizer in receiver part can give better a result than the ZF and MMSE equalizer over either AWGN or SαS noise channel. In addition, the BER performance contrast between LDPC and polar code over PLC channel has been derived. With the different conditions of the system, including different order QAM input signal, the different value of α in SαS noise channel and different multipath PLC channel systems, the BER performance by using LDPC code system is always better than that of the polar code system.

Chapter 5 constructed the MIMO-PLC channel with the LDPC coded system. The channel estimation methods - the block pilot and the comb pilot, have been utilized in MIMO-PLC system in this chapter. With the same P-I Ratio, the same length of the input signal and the OFDM input symbols, the block pilot can estimate a better BER performance over PLC channel rather than the comb piot. Furthermore, the proposed averaging approach had been utilized in both block and comb pilot methods to reduce the impact of the noise. The investigation indicated that both the frame (averaging time) of the system and the weight factor of the averaging approach could affect the performance of the channel estimation method. Meanwhile, with the 500 frames of the system and 0.1 weight factor, the BER performance over the estimated system is better than other values of these two elements. The BER performance by using both block and comb pilot without the averaging approach is much worse than the estimated system with the averaging approach. Moreover, there is almost the same BER performance by using the averaging process as the original PLC channel.

The proposed NZCP design is presented in chapter 6. To avoid interference from Multi-channel, the traditional comb pilot added zero data which is the same size as the pilot data in MIMO-PLC channel system. The proposed NZCP method only allowed the pilot data to insert the information QAM symbol. Thus, the new method can save the transmitter data's position to increase the channel's capacity while optimizing the BER performance. Combining with the proposed averaging approach, the performance of the NZCP system has dramatically improved as well.

In conclusion, the multipath SISO-PLC model over SαS noise channel, includ-

ing the real-valued OFDM input signal, has been constructed. The proposed MRC equalizer has been utilized to reduce the impact of the noise at the receiver end. In the MIMO-PLC system, the primary investigation is focused on the optimization of the channel estimation method. With the proposed averaging process, the performance of the block and comb pilot system can give a dramatically significant improvement. New pilot design method - NZCP can be satisfied to avoid interference and improve the performance of the estimated system. Finally, the proposed NZCP method with the averaging approach had been demonstrated to maximize the system's BER performance than other channel estimation methods.

7.2 Future works

The following suggestions can be considered in future research based on the work reported in this thesis.

- The construction of LDPC code in either SISO-PLC or MIMO-PLC is created by the Gallager random construction method because of low complexity. However, other types of LDPC construction method such as progressive edge growth (PEG) can give a better BER performance over the fading channel. In future work, the LDPC construction can be change to other types of the construction method to enhance the PLC coded system.

- In the MIMO-PLC channel estimation system, as the averaging process can extremely improve the performance of both block and comb pilot methods, there is little difference between the estimated CFR and the original CFR. Both block and comb pilot can be combined as a new pilot design method. Each block contains several OFDM symbols and one pilot symbol. This pilot symbol subcarriers can include not only the pilot data but also the information data and use interpolation method to compute the estimated CFR. Even the BER performance of this method may become worse, the number of the transmitted pilot data can be decreased. In other words, the capacity of the channel can be increased. However, the averaging approach utilized in this pilot method can greatly optimize the performance of the estimated system. This kind of pilot design method will be good research in future work.

- The precoding technology can be inserted in the MIMO-PLC estimated channel system.

- In chapter 5, the weight factor of the averaging approach investigation is a constant value. For the Gaussian distribution noise channel, the best weight factor should suit the number of the frame to give the accurate average value of the estimated CFR to avoid the impact of the Gaussian distribution noise. Furthermore, the non-Gaussian distribution noise channel should match the different weight factors of the averaging approach. Thus, the subsequent investigation will be focused on other kinds of non-Gaussian distribution noise channel by using averaging channel estimation approach.

- Combining the block pilot and the NZCP method, presented in chapter 6, the new pilot design can be produced to optimize the performance of channel estimation technology.

References

[1] M. Zimmermann and K. Dostert, "A multipath model for the powerline channel," *IEEE Transactions on communications*, vol. 50, no. 4, pp. 553–559, 2002.

[2] H. Philipps, "Modeling of powerline communication channels," in *Proc. of 3rd International Symposium on Power-Line Communications and its Applications (ISPLC'99)*, 1999, pp. 14–21.

[3] A. I. Chiuta and N. D. Secareanu, "Theoretical postulation of plc channel model," *Journal of Electrical and Electronics Engineering*, no. 1, p. 129, 2009.

[4] S. Goldfisher and S. Tanabe, "Ieee 1901 access system: An overview of its uniqueness and motivation," *IEEE Communications Magazine*, vol. 48, no. 10, pp. 150–157, 2010.

[5] S. Zhang, C. Tsimenidis, H. Cao, and S. Boussakta, "Coded ofdm in plc channels with sas distribution impulsive noise using mrc detector," in *2019 UK/China Emerging Technologies (UCET)*. IEEE, 2019, pp. 1–4.

[6] G. Prasad, H. A. Latchman, Y. Lee, and W. A. Finamore, "A comparative performance study of ldpc and turbo codes for realistic plc channels," in *18th IEEE International Symposium on Power Line Communications and Its Applications*. IEEE, 2014, pp. 202–207.

[7] M. Sung, S. Kang, J. Shim, J. Lee, and J. Jeong, "Dft-precoded coherent optical ofdm with hermitian symmetry for fiber nonlinearity mitigation," *Journal of lightwave technology*, vol. 30, no. 17, pp. 2757–2763, 2012.

[8] A. A. M. Picorone, T. R. Oliveira, and M. V. Ribeiro, "Plc channel estimation based on pilots signal for ofdm modulation: A review," *IEEE Latin America Transactions*, vol. 12, no. 4, pp. 580–589, 2014.

[9] T.-T. Cao and Z.-W. Zheng, "Research on the non-blind channel estimation technologies for the mimo-ofdm communication systems," in *2011 International Conference on Electronics, Communications and Control (ICECC)*. IEEE, 2011, pp. 424–428.

[10] J.-S. Park, J.-K. Lee, and J.-U. Kim, "Block type pilot protection technique for clipping in ofdm systems," in *The 9th International Conference on Advanced Communication Technology*, vol. 1. IEEE, 2007, pp. 844–847.

[11] Z. Aida and B. Ridha, "Lmmse channel estimation for block-pilot insertion in ofdm systems under time varying conditions," in *2011 11th Mediterranean Microwave Symposium (MMS)*. IEEE, 2011, pp. 223–228.

[12] T. Shongwey, A. H. Vinck, and H. C. Ferreira, "On impulse noise and its models," in *18th IEEE International Symposium on Power Line Communications and Its Applications*. IEEE, 2014, pp. 12–17.

[13] M. Shao and C. L. Nikias, "Signal processing with fractional lower order moments: stable processes and their applications," *Proceedings of the IEEE*, vol. 81, no. 7, pp. 986–1010, 1993.

[14] M. Nassar, K. Gulati, M. R. DeYoung, B. L. Evans, and K. R. Tinsley, "Mitigating near-field interference in laptop embedded wireless transceivers," *Journal of Signal Processing Systems*, vol. 63, no. 1, pp. 1–12, 2011.

[15] G. Laguna-Sanchez and M. Lopez-Guerrero, "On the use of alpha-stable distributions in noise modeling for plc," *IEEE Transactions on Power Delivery*, vol. 30, no. 4, pp. 1863–1870, 2015.

[16] I. R. Casella and A. Anpalagan, *Power Line Communication Systems for Smart Grids*. Institution of Engineering and Technology, 2018.

[17] J. Song, S.-W. Lee, H. Park, and C. Lim, "Developing a plc module of electricity neter for amr," in *2008 IEEE International Symposium on Power Line Communications and Its Applications*. IEEE, 2008, pp. 342–344.

[18] Y. Yao, D. Zhang, C. Wang, Y. Sun, and D. Xu, "Design of remote street lamp monitoring and communicating node controller based on spread spectrum car-

rier," in *2006 IEEE International Symposium on Industrial Electronics*, vol. 3. IEEE, 2006, pp. 1642–1645.

[19] J. G. Proakis and M. Salehi, *Digital communications*. McGraw-Hill., 2008.

[20] A. Wyner, "Recent results in the shannon theory," *IEEE Transactions on information Theory*, vol. 20, no. 1, pp. 2–10, 1974.

[21] R. Gallager, "Low-density parity-check codes," *IRE Transactions on information theory*, vol. 8, no. 1, pp. 21–28, 1962.

[22] R. Tanner, "A recursive approach to low complexity codes," *IEEE Transactions on information theory*, vol. 27, no. 5, pp. 533–547, 1981.

[23] D. J. MacKay and R. M. Neal, "Good codes based on very sparse matrices," in *IMA International Conference on Cryptography and Coding*. Springer, 1995, pp. 100–111.

[24] D. J. MacKay, "Good error-correcting codes based on very sparse matrices," *IEEE transactions on Information Theory*, vol. 45, no. 2, pp. 399–431, 1999.

[25] N. Alon and M. Luby, "A linear time erasure-resilient code with nearly optimal recovery," *IEEE Transactions on Information Theory*, vol. 42, no. 6, pp. 1732–1736, 1996.

[26] J. W. Byers, M. Luby, M. Mitzenmacher, and A. Rege, "A digital fountain approach to reliable distribution of bulk data," *ACM SIGCOMM Computer Communication Review*, vol. 28, no. 4, pp. 56–67, 1998.

[27] X.-Y. Hu, E. Eleftheriou, D.-M. Arnold, and A. Dholakia, "Efficient implementations of the sum-product algorithm for decoding ldpc codes," in *GLOBECOM'01. IEEE Global Telecommunications Conference (Cat. No. 01CH37270)*, vol. 2. IEEE, 2001, pp. 1036–1036E.

[28] T. J. Richardson and R. L. Urbanke, "The capacity of low-density parity-check codes under message-passing decoding," *IEEE Transactions on information theory*, vol. 47, no. 2, pp. 599–618, 2001.

[29] S.-Y. Chung, G. D. Forney, T. J. Richardson, and R. Urbanke, "On the design of low-density parity-check codes within 0.0045 db of the shannon limit," *IEEE Communications letters*, vol. 5, no. 2, pp. 58–60, 2001.

[30] V. Oksman and S. Galli, "G. hn: The new itu-t home networking standard," *IEEE Communications Magazine*, vol. 47, no. 10, pp. 138–145, 2009.

[31] M. Eroz, F.-W. Sun, and L.-N. Lee, "Dvb-s2 low density parity check codes with near shannon limit performance," *International Journal of Satellite Communications and Networking*, vol. 22, no. 3, pp. 269–279, 2004.

[32] Z. Zhang, V. Anantharam, M. J. Wainwright, and B. Nikolic, "An efficient 10gbase-t ethernet ldpc decoder design with low error floors," *IEEE Journal of Solid-State Circuits*, vol. 45, no. 4, pp. 843–855, 2010.

[33] N. Andreadou, C. Assimakopoulos, and F.-N. Pavlidou, "Performance evaluation of ldpc codes on plc channel compared to other coding schemes," in *2007 IEEE International Symposium on Power Line Communications and Its Applications*. IEEE, 2007, pp. 296–301.

[34] N. Andreadou and A. M. Tonello, "Short ldpc codes for nb-plc channel with a differential evolution construction method," in *2013 IEEE 17th International Symposium on Power Line Communications and Its Applications*. IEEE, 2013, pp. 236–241.

[35] Y. Kabalci, I. Develi, and E. Kabalci, "Ldpc coded ofdm systems over broadband indoor power line channels: a performance analysis," in *4th International Conference on Power Engineering, Energy and Electrical Drives*. IEEE, 2013, pp. 1581–1585.

[36] A. Ramzan and M. O. B. Saeed, "Ldpc-coded ofdm-system with bpsk modulation: Performance comparison with uncoded ofdm system," in *2018 3rd International Conference on Control and Robotics Engineering (ICCRE)*. IEEE, 2018, pp. 213–217.

[37] G. A. Al-Rubaye, C. C. Tsimenidis, and M. Johnston, "Non-binary ldpc coded ofdm in impulsive power line channels," in *2015 23rd European Signal Processing Conference (EUSIPCO)*. IEEE, 2015, pp. 1431–1435.

[38] ——, "Low-density parity check coded orthogonal frequency division multiplexing for plc in non-gaussian noise using llrs derived from effective noise probability density functions," *IET Communications*, vol. 11, no. 16, pp. 2425–2432, 2017.

[39] M. C. Davey and D. J. MacKay, "Low density parity check codes over gf (q)," in *1998 Information Theory Workshop (Cat. No. 98EX131)*. IEEE, 1998, pp. 70–71.

[40] D. Declercq and M. Fossorier, "Decoding algorithms for nonbinary ldpc codes over gf (q)," *IEEE transactions on communications*, vol. 55, no. 4, pp. 633–643, 2007.

[41] A. Voicila, D. Declercq, F. Verdier, M. Fossorier, and P. Urard, "Low-complexity decoding for non-binary ldpc codes in high order fields," *IEEE transactions on communications*, vol. 58, no. 5, pp. 1365–1375, 2010.

[42] E. Arikan, "Channel polarization: A method for constructing capacity-achieving codes for symmetric binary-input memoryless channels," *IEEE Transactions on information Theory*, vol. 55, no. 7, pp. 3051–3073, 2009.

[43] H. Vangala, E. Viterbo, and Y. Hong, "A comparative study of polar code constructions for the awgn channel," *arXiv preprint arXiv:1501.02473*, 2015.

[44] E. Arikan, "A performance comparison of polar codes and reed-muller codes," *IEEE Communications Letters*, vol. 12, no. 6, pp. 447–449, 2008.

[45] I. Tal and A. Vardy, "How to construct polar codes," *IEEE Transactions on Information Theory*, vol. 59, no. 10, pp. 6562–6582, 2013.

[46] R. Mori and T. Tanaka, "Performance of polar codes with the construction using density evolution," *IEEE Communications Letters*, vol. 13, no. 7, pp. 519–521, 2009.

[47] Y. Zhang, A. Liu, K. Pan, C. Gong, and S. Yang, "A practical construction method for polar codes," *IEEE Communications Letters*, vol. 18, no. 11, pp. 1871–1874, 2014.

[48] H. Li and J. Yuan, "A practical construction method for polar codes in awgn channels," in *IEEE 2013 Tencon-Spring*. IEEE, 2013, pp. 223–226.

[49] D. Kern, S. Vorköper, and V. Kühn, "A new code construction for polar codes using min-sum density," in *2014 8th International Symposium on Turbo Codes and Iterative Information Processing (ISTC)*. IEEE, 2014, pp. 228–232.

[50] A. Hadi, K. M. Rabie, and E. Alsusa, "Polar codes based ofdm-plc systems in the presence of middleton class-a noise," in *2016 10th International Symposium on Communication Systems, Networks and Digital Signal Processing (CSNDSP)*. IEEE, 2016, pp. 1–6.

[51] L. Jin, Y. Li, B. Li, Z. Wei, and J. Shi, "Performance of polar coding for the power line communications in the presence of impulsive noise," *IET Communications*, vol. 9, no. 17, pp. 2101–2106, 2015.

[52] R. P. Franzin and P. B. Lopes, "A performance comparison between ofdm and fbmc in plc applications," in *2017 IEEE Second Ecuador Technical Chapters Meeting (ETCM)*. IEEE, 2017, pp. 1–6.

[53] M. Lee, R. E. Newman, H. A. Latchman, S. Katar, and L. Yonge, "Homeplug 1.0 powerline communication lans—protocol description and performance results," *International Journal of Communication Systems*, vol. 16, no. 5, pp. 447–473, 2003.

[54] S. A. Aburakhia, E. F. Badran, and D. A. Mohamed, "Distribution of the papr for real-valued ofdm signals," *signal*, vol. 2, p. 2, 2009.

[55] F. H. Juwono, Q. Guo, D. D. Huang, Y. Chen, L. Xu, and K. P. Wong, "On the performance of blanking nonlinearity in real-valued ofdm-based plc," *IEEE Transactions on Smart Grid*, vol. 9, no. 1, pp. 449–457, 2016.

[56] J. Anatory, N. Theethayi, R. Thottappillil, M. M. Kissaka, and N. H. Mvungi, "An experimental validation for broadband power-line communication (bplc) model," *IEEE transactions on power delivery*, vol. 23, no. 3, pp. 1380–1383, 2008.

[57] L. Liu, T. Cheng, and Y. Luo, "Analysis and modeling of multipath for indoor power line channel," in *2008 10th International Conference on Advanced Communication Technology*, vol. 3. IEEE, 2008, pp. 1966–1969.

[58] C. Mulangu, T. Afullo, and N. Ijumba, "Attenuation model for indoor multipath broadband plc channels," in *2012 IEEE-APS Topical Conference on Antennas and Propagation in Wireless Communications (APWC)*. IEEE, 2012, pp. 1084–1087.

[59] A. Papoulis, "The fourier integral and its applications," *Polytechnic Institute of Brooklyn, McCraw-Hill Book Company Inc., USA, ISBN: 67-048447-3*, 1962.

[60] L. T. Berger, A. Schwager, P. Pagani, and D. M. Schneider, "Mimo power line communications," *IEEE Communications Surveys & Tutorials*, vol. 17, no. 1, pp. 106–124, 2014.

[61] A. Schwager, D. Schneider, W. Bäschlin, A. Dilly, and J. Speidel, "Mimo plc: theory, measurements and system setup," in *2011 IEEE International Symposium on Power Line Communications and Its Applications*. IEEE, 2011, pp. 48–53.

[62] S. Kasthala and G. P. Venkatesan, "Estimation of mimo power line communication channel capacity using multi-conductor transmission line theory," in *2016 2nd International Conference on Applied and Theoretical Computing and Communication Technology (iCATccT)*. IEEE, 2016, pp. 787–792.

[63] F. Versolatto and A. M. Tonello, "A mimo plc random channel generator and capacity analysis," in *2011 IEEE International Symposium on Power Line Communications and Its Applications*. IEEE, 2011, pp. 66–71.

[64] B. Nikfar and A. H. Vinck, "Combining techniques performance analysis in spatially correlated mimo-plc systems," in *2013 IEEE 17th International Symposium on Power Line Communications and Its Applications*. IEEE, 2013, pp. 1–6.

[65] R. Hashmat, P. Pagani, A. Zeddam, and T. Chonave, "A channel model for multiple input multiple output in-home power line networks," in *2011 IEEE International Symposium on Power Line Communications and Its Applications*. IEEE, 2011, pp. 35–41.

[66] J. A. Corchado, J. A. Cortés, F. J. Canete, A. Arregui, and L. Díez, "Analysis of the spatial correlation of indoor mimo plc channels," *IEEE Communications Letters*, vol. 21, no. 1, pp. 40–43, 2016.

[67] A. Recioui, "Application of multiple input multiple output power line communication (mimo-plc) to power systems," *Acta Physica Polonica A*, vol. 132, no. 3, pp. 496–499, 2017.

[68] A. Canova, N. Benvenuto, and P. Bisaglia, "Receivers for mimo-plc channels: Throughput comparison," in *ISPLC2010*. IEEE, 2010, pp. 114–119.

[69] M. Almarashli and S. Lindenmeier, "Evaluation of vehicular 4g/5g-mimo antennas via data-rate measurement in an emulated urban test drive," in *2018 48th European Microwave Conference (EuMC)*. IEEE, 2018, pp. 300–303.

[70] D. Schneider, J. Speidel, L. Stadelmeier, and D. Schill, "Precoded spatial multiplexing mimo for inhome power line communications," in *IEEE GLOBECOM 2008-2008 IEEE Global Telecommunications Conference*. IEEE, 2008, pp. 1–5.

[71] R. Hashmat, P. Pagani, A. Zeddam, and T. Chonavel, "Mimo communications for inhome plc networks: Measurements and results up to 100 mhz," in *ISPLC2010*. IEEE, 2010, pp. 120–124.

[72] A. Hadi, E. Alsusa, and K. M. Rabie, "On the construction of polar codes in the middleton class-a channels," in *2020 12th International Symposium on Communication Systems, Networks and Digital Signal Processing (CSNDSP)*. IEEE, 2020, pp. 1–6.

[73] A. Hadi, *Optimisation and Analysis of Polar Codes in Communication Systems*. The University of Manchester (United Kingdom), 2018.

[74] A. Hadi, E. Alsusa, and K. M. Rabie, "A method to enhance the performance of successive cancellation decoding in polar codes," in *2016 10th International Symposium on Communication Systems, Networks and Digital Signal Processing (CSNDSP)*. IEEE, 2016, pp. 1–5.

[75] K. Niu, K. Chen, J. Lin, and Q. Zhang, "Polar codes: Primary concepts and practical decoding algorithms," *IEEE Communications magazine*, vol. 52, no. 7, pp. 192–203, 2014.

[76] Q. Yu, Z. Shi, X. Li, J. Du, J. Zhang, and K. M. Rabie, "On the concatenations of polar codes and non-binary ldpc codes," *IEEE Access*, vol. 6, pp. 65 088–65 097, 2018.

[77] P. Venkateshwari and M. Anbuselvi, "Decoding performance of binary and non-binary ldpc codes for ieee 802.11 n standard," in *2012 International Con-*

ference on Recent Trends in Information Technology. IEEE, 2012, pp. 292–296.

[78] G. A. M. Al-Rubaye, "Coded-ofdm for plc systems in non-gaussian noise channels," Ph.D. dissertation, Newcastle University, 2017.

[79] B. Li, G. Wang, and H.-j. Yang, "A new method of detecting cycles in tanner graph of ldpc codes," in *2009 International Conference on Wireless Communications & Signal Processing.* IEEE, 2009, pp. 1–3.

[80] M. Abdelhedi, F. Tlili, and L. B. H. Slama, "Simulation-based validation of improved bp-based decoding algorithms of ldpc codes," in *2008 3rd International Symposium on Communications, Control and Signal Processing.* IEEE, 2008, pp. 58–61.

[81] S. Zengyou, Z. Jin, and D. Juan, "Research of ldpc decoding based on llr bp algorithm," in *Proceedings of 2011 Cross Strait Quad-Regional Radio Science and Wireless Technology Conference*, vol. 2. IEEE, 2011, pp. 889–892.

[82] W. Zhong-xun, W. Xing-cheng, Y. Xin-qiao, and G. Dong, "A bp decoding algorithm based on nodes residual for ldpc codes," in *2010 IEEE International Conference on Wireless Communications, Networking and Information Security.* IEEE, 2010, pp. 124–127.

[83] X. Zhang, Y. Zhao, and L. Zou, "An efficient impulsive noise mitigation scheme for over-sampled ofdm systems," *IEEE Transactions on Consumer Electronics*, vol. 55, no. 2, pp. 360–365, 2009.

[84] A. Mathur, M. R. Bhatnagar, and B. K. Panigrahi, "Performance evaluation of plc under the combined effect of background and impulsive noises," *IEEE Communications Letters*, vol. 19, no. 7, pp. 1117–1120, 2015.

[85] D. Middleton, "Non-gaussian noise models in signal processing for telecommunications: new methods an results for class a and class b noise models," *IEEE Transactions on Information Theory*, vol. 45, no. 4, pp. 1129–1149, 1999.

[86] ——, "Statistical-physical models of electromagnetic interference," *IEEE transactions on Electromagnetic Compatibility*, no. 3, pp. 106–127, 1977.

[87] ——, "Canonical and quasi-canonical probability models of class a interference," *IEEE Transactions on Electromagnetic Compatibility*, no. 2, pp. 76–106, 1983.

[88] V. B. Balakirsky and A. H. Vinck, "Potential limits on power-line communication over impulsive noise channels," in *Proc. 7th Int. Symp. Power-Line Communications and Its Applications (ISPLC 2003)*. Citeseer, 2003, pp. 32–36.

[89] M. Chitre, J. Potter, and O. S. Heng, "Underwater acoustic channel characterisation for medium-range shallow water communications," in *Oceans' 04 MTS/IEEE Techno-Ocean'04 (IEEE Cat. No. 04CH37600)*, vol. 1. IEEE, 2004, pp. 40–45.

[90] T. H. Tran, D. D. Do, and T. H. Huynh, "Plc impulsive noise in industrial zone: measurement and characterization," *International Journal of Computer and Electrical Engineering*, vol. 5, no. 1, p. 48, 2013.

[91] Z. Mei, "Analysis of low-density parity-check codes on impulsive noise channels," Ph.D. dissertation, Newcastle University, 2017.

[92] G. A. Tsihrintzis and C. L. Nikias, "Performance of optimum and suboptimum receivers in the presence of impulsive noise modeled as an alpha-stable process," *IEEE Transactions on communications*, vol. 43, no. 2/3/4, pp. 904–914, 1995.

[93] Z. Mei, M. Johnston, S. Le Goff, and L. Chen, "Finite length analysis of low-density parity-check codes on impulsive noise channels," *IEEE Access*, vol. 4, pp. 9635–9642, 2016.

[94] S. Elnoubi, S. Elbadawy, and C. Shaban, "Performance of turbo coded ofdm system with comb pilot channel estimation in rayleigh fading channel," in *MILCOM 2008-2008 IEEE Military Communications Conference*. IEEE, 2008, pp. 1–6.

[95] J. Kim, J. Park, and D. Hong, "Performance analysis of channel estimation in ofdm systems," *IEEE Signal Processing Letters*, vol. 12, no. 1, pp. 60–62, 2004.

[96] Z. Xakimjon and A. Bunyod, "Biomedical signals interpolation spline models," in *2019 International Conference on Information Science and Communications Technologies (ICISCT)*. IEEE, 2019, pp. 1–3.

[97] M. M. Mansour, "A parallel pruned bit-reversal interleaver," *IEEE transactions on very large scale integration (VLSI) systems*, vol. 17, no. 8, pp. 1147–1151, 2009.

[98] Y. A. Al-Zahrani, N. K. Al-Mutairi, Y. Al-Hodhayf, and A. Al-Shahrani, "Performance of antenna selection for maximum ratio combining mimo system," in *2011 IEEE 3rd International Conference on Communication Software and Networks*. IEEE, 2011, pp. 642–645.

[99] A. Coskun and C. Candan, "Transmit precoding for flat-fading mimo multiuser systems with maximum ratio combining receivers," *IEEE transactions on vehicular technology*, vol. 60, no. 2, pp. 710–716, 2010.

[100] H. T. Hui, "The performance of the maximum ratio combining method in correlated rician-fading channels for antenna-diversity signal combining," *IEEE transactions on antennas and propagation*, vol. 53, no. 3, pp. 958–964, 2005.

[101] F. A. Dietrich and W. Utschick, "Maximum ratio combining of correlated rayleigh fading channels with imperfect channel knowledge," *IEEE Communications Letters*, vol. 7, no. 9, pp. 419–421, 2003.

[102] Y. Liao, Y. Hua, and Y. Cai, "Deep learning based channel estimation algorithm for fast time-varying mimo-ofdm systems," *IEEE Communications Letters*, vol. 24, no. 3, pp. 572–576, 2019.

[103] R. Lavafi and B. Abolhassani, "A non-iterative channel estimation algorthm for mobile mimo-ofdm systems with comb-type pilots," in *2007 IEEE International Conference on Signal Processing and Communications*. IEEE, 2007, pp. 380–383.

[104] J. Li, L. Song, and C. Liu, "The cubic trigonometric automatic interpolation spline," *IEEE/CAA Journal of Automatica Sinica*, vol. 5, no. 6, pp. 1136–1141, 2017.

[105] Y. Wei, P. Sun, Z. Song, P. Wang, Z. Zeng, and X. Wang, "Fault location of vsc based dc distribution network based on traveling wave differential current with hausdorff distance and cubic spline interpolation," *IEEE Access*, vol. 9, pp. 31 246–31 255, 2021.

[106] H. C. Chui and A. K. Chan, "Lateral mode analysis in semiconductor lasers using a cubic spline approximation of the refractive index profile," *Journal of lightwave technology*, vol. 7, no. 9, pp. 1419–1424, 1989.

[107] S. A. A. Karim, A. Saaban, and V. Skala, "Range-restricted surface interpolation using rational bi-cubic spline functions with 12 parameters," *IEEE Access*, vol. 7, pp. 104 992–105 007, 2019.

[108] D. Petrinovic, "Causal cubic splines: Formulations, interpolation properties and implementations," *IEEE Transactions on Signal Processing*, vol. 56, no. 11, pp. 5442–5453, 2008.

[109] K. Cho and D. Yoon, "On the general ber expression of one-and two-dimensional amplitude modulations," *IEEE Transactions on Communications*, vol. 50, no. 7, pp. 1074–1080, 2002.